Technische Universität München

Fakultät für Medizin

Institut für Pharmakologie und Toxikologie

Generation and characterization of inducible cardiomyocyte-specific Cullin7-deficient mice

Florian Scheufele

Vollständiger Abdruck der von der promotionsführenden Einrichtung der Technischen Universität München zur Erlangung des akademischen Grades eines

Doktors der Medizin (Dr. med.)

genehmigten Dissertation.

Vorsitzender: **Prof. Dr. Ernst J. Rummeny**

Prüfer der Dissertation:

1. **Prof. Dr. Dr. Stefan Engelhardt**
2. **Priv.-Doz. Dr. Antonio Sarikas**

Die Dissertation wurde am 20.03.2017 bei der Technischen Universität München eingereicht und durch die promotionsführende Einrichtung am 10.10.2018 angenommen.

This work is dedicated to my family and friends for infinite support.

1. Abbreviations and definitions

aa	Amino acids
aka	Also known as
Ang-II	Angiotensin II
a.u.	arbitrary units
CF	Cardiofibroblast
CM	Cardiomyocyte
CRL7	Cullin7 E3 ligase
CSA	Cross sectional area
EDV	End-diastolic volume
EF	Ejection fraction
ESV	End-systolic volume
ET-1	Endothelin-1
FS	Fractional shortening
GH	Growth hormone
IGF-1	Insulin like growth factor 1
IGF-1R	Insulin like growth factor 1 receptor
IRS-1	Insulin receptor substrate 1
IRS-2	Insulin receptor substrate 2
LVID	Left ventricular inner diameter
LVPW	Left ventricular posterior wall thickness
MAPK	Mitogen activated protein kinase
MEF	Mouse embryonic fibroblast
n-CM	Non-cardiomyocyte
NRCMs	Neonatal rat cardiomyocytes
PE	Phenylephrine

PI3K	Phosphatidylinositol-3-kinase
TAC	Transverse aortic constriction
Ub	Ubiquitin
UPS	Ubiquitin-proteasome system
α-MHC	α-Myosin heavy chain

SI units are used in the international valid abbreviations.

Gene names, mRNA and cDNA are italicized with the first letter in uppercase. Protein names are not italicized with all letters in uppercase.

CUL7 depleted animals are referred to as $Cul7^{-/-}$ or $Cullin7^{-/-}$. Mice, that are wild type or functional wild type for CUL7, are referred to as $Cul7^{+/+}$ or $Cullin7^{+/+}$. Heterozygosity is indicated by $Cul7^{+/-}$ or $Cullin7^{+/-}$.

2. Summary

The Ubiquitin-proteasome system (UPS) is a selective protein degradation pathway that is critically involved in the pathogenesis of several cardiac disorders. Central to the UPS is the recognition of the substrate by an E3 ubiquitin ligase, a step pivotal for the ubiquitin-mediated degradation of substrate proteins by the 26S proteasome. The Cullin7 E3 ligase (CRL7) consists of the Cullin7 (CUL7) scaffold protein, the SKP1 adaptor, the ROC1 RING finger protein and the substrate receptor FBXW8. We previously identified insulin receptor substrate 1 (IRS-1), a critical mediator of PI3K/Akt and Erk MAPK signaling as a CRL7 substrate.

Thus we thought to investigate the pathophysiological role of CRL7 in the heart and its contribution to cardiac hypertrophy and fibrosis.

Tamoxifen-inducible CM-specific CUL7 knockout mice were generated by crossing $Cul7^{flox/flox}$ and Myh6-Mer-Cre-$MerTg^{(1/0)}$ mice. Depletion of CUL7 was confirmed by immunoblot analyses. Morphological parameters were assessed and cardiac function was analyzed by echocardiographic measurement. CM hypertrophy and interstitial cardiac fibrosis were analyzed by WGA and Sirius Red / Fast Green staining, respectively. Signaling pathways were investigated by immunoblot analyses of $Akt^{P\text{-}Ser473}$ and $Erk^{P\text{-}Thr202/Tyr204}$. Additionally, $Cul7^{flox/flox}$; Myh6-MerCreMer$Tg^{(1/0)}$ mice were subjected to increased afterload by transverse aortic constriction.

Cardiac CUL7 expression in $Cul7^{flox/flox}$; Myh6-MerCreMer$Tg^{(1/0)}$ mice was significantly reduced upon induction by tamoxifen ($p<0.01$). Under basal conditions, cardiac function was increased in CUL7 depleted mice ($p<0.05$) as was cross-sectional area of the cardiomyocytes in these animals ($p<0.05$). Furthermore, Akt-signaling displayed increased activation in cardiomyocytes of CUL7 depleted hearts ($p<0.05$). After transverse aortic constriction, CM-specific CUL7 depletion was associated with amelioration of interstitial cardiac fibrosis ($p<0.05$).

Thus, we provided evidence for a regulatory role of CUL7 in the heart under both physiological and pathological conditions. Under basal conditions depletion of CUL7 resulted in cardiomyocyte hypertrophy and increased cardiac function, while CUL7 deficiency under conditions of increased afterload resulted in amelioration of interstitial cardiac fibrosis. This differential effect on the heart may be mediated by a regulatory effect on IRS-1 downstream Akt-signaling.

3. Introduction

3.1 The Ubiquitin-proteasome system

Turnover of intracellular proteins by the ubiquitin-proteasome system (UPS) is a precisely controlled process that regulates a broad spectrum of fundamental cellular functions, ranging from cell-cycle progression to transcriptional regulation, signal transduction as well as endocytosis and receptor down-regulation (Patrick et al. 2003, Sarikas et al. 2011, Bassermann et al. 2014). The ubiquitination process leading to degradation by the proteasome is executed by a cascade of three enzyme classes, namely E1, E2 and E3. First, the E1 enzyme (also called ubiquitin-activating enzyme) activates ubiquitin (Ub), a highly conserved 76 amino acids (aa) long peptide, under ATP consumption by binding Ub to one of its cysteine residues via a thioester bond. Next, Ub is transferred to a cysteine residue of an E2 enzyme, also called Ub-conjugating enzyme. As a final step Ub is linked by an E3 enzyme to a lysine residue of the substrate protein. The E3 enzyme is central for the specificity of the UPS-mediated protein degradation as it comprises the substrate recognition function. The E3 enzymes can be further divided into two main families, the HECT- and the RING finger-E3 ligases. HECT ligases bind their substrate and the activated Ub simultaneously and thus mediate the transfer of Ub to the substrate. The RING finger-E3 ligases can be further divided into single polypeptide chain RING finger-E3 ligases and multi-subunit RING finger-E3 ligases, the latter comprising a specific substrate recognition subunit protein. Both bind their substrate and the Ub-carrying E2 enzyme and thus catalyze ubiquitination of the substrate (Sarikas et al. 2011). The transfer of Ub to the substrate is repeated multiple times resulting in a poly-ubiquitin chain linking the C-terminus of the previous Ub unit to a specific lysine residue (most commonly Lys48) of the following Ub molecule. This poly-ubiquitin chain attached to the substrate is recognized by the 19S cap-structure of the 26S proteasome leading to transfer of the substrate to the catalytic core of the proteasome at which the subsequent proteolysis takes place. This process guarantees a precisely controlled and highly specific recognition, targeting and degradation of proteins in the cell (Hershko et al. 1998, Bhattacharyya et al. 2014).

3.2 Cullin7 E3 ligase (CRL7)

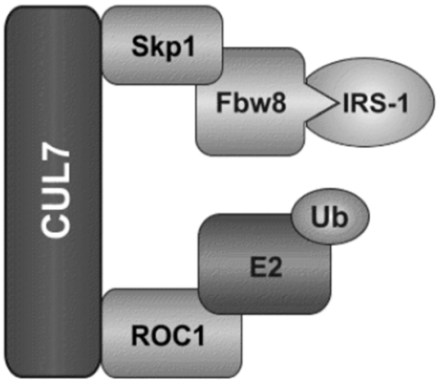

Figure 1: Domaine structure of the Cullin7 E3 ligase. The Cullin7 protein functions as a scaffold protein for the assembly of ROC1, mediating binding of the Ub loaded E2 enzyme and Skp1 mediating binding of Fbx8, the latter functioning as a substrate (e.g. IRS-1) recognition protein. Modified from Sarikas et al. (Sarikas et al. 2011).

Cullin7 (also known as p185, p193 or KIAA0076) is the seventh member of the Cullin-protein family that contribute to the formation of Skp1-Cullin-F-Box protein (SCF) E3 ligases by acting as a molecular scaffold for the assembly of the different components of the E3 ligase. With its C-terminally located conserved Cullin domain, Cullin7 binds to the ROC1 RING finger protein, which itself can bind the Ub-loaded E2 enzymes, e.g. Cdc34 and/or Ubc4/5 (Dias et al. 2002, Sarikas et al. 2008). In its N-terminal part Cullin7 harbors a DOC domain, which is also known from the anaphase-promoting complex (Dias et al. 2002). Additionally, the CPH (conserved protein domain in CUL7, PARC and HERC2) functions as a binding region for p53 (Kaustov et al. 2007). Cullin7 forms an E3 ligase by assembling with the adapter protein Skp1, ROC1 RING finger protein (Rbx1) and WD40 repeat-containing F-box protein Fbxw8 (also called Fbx29 or Fbw6) but interestingly, in contrast to Cullin1 (the prototype of the Cullin-protein family) that can bind Skp1 alone, Cullin7 is only able to bind Skp1 in complex with an F-box protein (Dias et al. 2002, Skaar et al. 2007, Sarikas et al. 2008). Fbxw8 is to date the only known F-box protein binding to Cullin7 (Dias et al. 2002). Cullin7 has also been reported to bind FAP68 (Glomulin), a gene that is linked to glomuvenous malformation (Brouillard et al. 2002, Arai et al. 2003). Furthermore, Cullin7$^{-/-}$ embryos die immediately after birth, placentas show differentiation defects and vascular abnormalities (Arai et al. 2003). Additionally, Cullin7 has been linked to cellular transformation, as it binds Simian virus large T antigen (TAg), and Cullin7 binding-deficient mutants of TAg were unable to induce transformation of primary mouse fibroblasts (Ali et al.

2004). In addition to that, it has been shown that cardiomyocytes of mice expressing a dominant negative mutant of CUL7 are able to re-enter the cell cycle after myocardial infarction and this ameliorates adverse remodeling processes with reduced scar size and preserved cardiac function (Nakajima et al. 2004, Hassink et al. 2009). Furthermore, mutations in *Cul7* have been shown in individuals affected by the 3M-syndrome, an autosomal recessive disease characterized by pre- and postnatal growth retardation (Huber et al. 2005). Similar results were observed in Fbxw8$^{-/-}$ mice that also showed severe pre- and postnatal growth retardation (Tsutsumi et al. 2008). Furthermore, it was shown that Fbxw8, the substrate recognition particle of the Cullin7 E3 ligase (CRL7), could be co-immunoprecipitated with IRS-1 and FBXW8 protein levels reversely correlated with IRS-1 levels, an effect that was abolished upon MG132 treatment. Additionally, MG132 treatment increased the abundance of high molecular weight ubiquitination products in the IRS-1 immunoprecipitates (Xu et al. 2008). Overexpression of either CUL7 or FBXW8 strongly increased the - under basal conditions slow - decay rate of IRS-1 in MCF-7 cells suggesting, together with the interaction between FBXW8 and IRS-1, that CRL7 mediates poly-ubiquitination and subsequent degradation by the proteasome of IRS-1 thereby shortening its half-life (Xu et al. 2008). Ubiquitin-dependent degradation of IRS-1 was proposed to be part of a negative feedback loop involving PI3K/Akt signaling and the downstream components mTORC and S6K, that regulate ubiquitination of IRS-1 by serine phosphorylation (Harrington et al. 2005). Interestingly, treatment of CUL7 or FBXW8 overexpressing MCF-7 cells with rapamycin, an mTORC inhibitor, ameliorated the degradation of IRS-1 significantly (Xu et al. 2008). Furthermore, overexpression of Rheb, an activating G-protein upstream of mTORC and S6K, increased IRS-1 degradation and this effect was even more pronounced when FBXW8 was co-overexpressed in MCF-7 cells (Xu et al. 2008). Additionally, site-directed mutagenesis showed, that the N-terminal part of IRS-1 was crucial for degradation via CRL7. Degradation of IRS-1 was positively linked to phosphorylation within the region of the amino acids 522–574 of IRS1, especially Ser527, which was crucial for proteolysis and the amino acids Ser307 and Ser312 additionally mediated its stability, pointing to the possibility that a certain pattern of phosphorylation at different sites plays in concert and induces conformational changes acting as a degradation signaling site (degron) regulating binding of Fbxw8, ubiquitination and degradation (Mieulet et al. 2008, Xu et al. 2008). Further underlining this, treatment with S6K caused enhanced phosphorylation of Ser307 of IRS-1 and increased efficiency of FBXW8 binding (Xu et al. 2008). In accordance with this, treatment of MCF-7 cells with siRNA directed against *Fbxw8* increased the levels of IRS-1 and similar IRS-1 protein levels were increased by the factor

of 5 in Cul7$^{-/-}$ mouse embryonic fibroblasts (MEF) when compared with Cul7$^{+/+}$ MEFs, while mRNA levels of IRS-1 were equal (Xu et al. 2008). Additionally, treatment of Cul7$^{-/-}$ MEFs with IGF-1 showed an increased activation of the downstream Akt pathway (Akt ^{pS473}) and a sustained activation of Erk MAPK pathway (Erk $^{pT202/Y204}$) in comparison with wild-type MEFs (Xu et al. 2008). Both the Akt (Akt ^{pS473}) and Erk (Erk $^{pT202/Y204}$) activation was also increased under basal conditions (Xu et al. 2008). This activation of Akt and Erk in Cul7$^{-/-}$ MEFs was markedly reduced by knockdown of IRS-1 using siRNA (Xu et al. 2008). Interestingly, amplification of the genomic locus of *Cul7* (6p21.1) has been identified in patients with hepatocellular carcinoma (HCC) developed on the basis of fibrosis in the context of metabolic syndrome but not hepatitis C virus infection alongside with increased fibrosis of the peritumoral region in patients with HCC/MS (Paradis et al. 2013). TBC1D3 is another substrate of CRL7 that has been identified and plays a role in regulating growth factor signaling (Kong et al. 2012). It is a hominoid-specific oncogene, that enhances insulin and IGF-1 signaling by suppression of serine phosphorylation at Ser307 and Ser312 and Ser636/639 of IRS-1. Thereby it interferes with the serine phospho-degron, that is necessary for FBXW8 recognition, ubiquitination and degradation (Wainszelbaum et al. 2012). Mechanistically TBC1D3 activates protein phosphatase 2A (PP2A) which in turn dephosphorylates S6K T389 phosphorylation leading to reduced activation of S6K and thereby phosphorylation of IRS-1 (Wainszelbaum et al. 2012). TBC1D3 has been shown to interact with FBXW8 in response to growth factor stimulation and this process is dependent on phosphorylation of TBC1D3 as phosphatase treatment abolished this interaction, pointing to a degron mechanism similar to that of IRS-1. Furthermore, TBC1D3 is ubiquitinated by CRL7 in response to growth factor stimulation leading to degradation by the proteasome and knockdown of CUL7 by siRNA markedly delayed degradation of TBC1D3 (Wainszelbaum et al. 2012). Recently, we were able to show the importance of CRL7 in insulin signaling in vitro and in vivo. When compared to the *Cul7*$^{+/+}$ mouse embryonic fibroblasts (MEFs), insulin stimulation resulted in enhanced activation and duration of PI3K/Akt signaling (as evidenced by phosphorylation of Akt at S473) in *Cul7*$^{+/-}$ and, to a higher extent, in *Cul7*$^{-/-}$ MEFs (Scheufele et al. 2014). Besides this, there was a higher activation of Erk MAPK pathway (as evidenced by phosphorylation of Erk1/2 at Thr202/Tyr204) observable. Additionally, we investigated the role of CRL7 in another cell system, namely C2C12 myotubes. Upon exposure to insulin, siRNA CUL7-depleted C2C12 cells showed an enhanced phosphorylation of both Akt (Akt ^{pSer473}) and Erk (Erk $^{pThr202/Tyr204}$) when compared to control cells. Furthermore, in the setting of chronic insulin stimulation, which is known to cause a decrease in IRS-1 abundance, we stimulated C2C12 cells for

several hours with insulin under the blockade of protein synthesis by emetine. Insulin stimulation led to a significant reduction of IRS-1 protein abundance, a process which could be partially rescued by inhibition of the proteasome with MG132. Most interestingly, CUL7 depletion resulted in an even more pronounced stabilization of IRS-1. Next, we investigated if CRL7, by influencing insulin signaling, also affected glucose uptake into the cell. Therefore, 2-deoxy-D-(3H)-glucose (2-DOG) uptake assays were performed in CUL7 depleted C2C12 myotubes, that revealed an increased glucose uptake after stimulation with insulin. These in vitro results were also reproducible in vivo as both $Cul7^{+/-}$ and $Fbwx8^{+/-}$ mice exhibited increased stimulation of Akt (Akt ^{pSer473}) after intraperitoneal injection of insulin when compared to control mice. To complete this, the physiological relevance of CRL7 in glucose homeostasis was assessed by insulin tolerance tests (ITT), which showed that both $Cul7^{+/-}$ or $Fbxw8^{+/-}$ mice displayed a 50% increased clearance of blood glucose in response to insulin. Taken together, CRL7 exerts a central role in regulating insulin and IGF signaling by targeting the nodal point of the signaling cascade IRS-1 for ubiquitination and degradation. Thus it displays the opportunity to sensitize insulin signaling by specifically targeting CRL7 thereby reducing insulin-induced degradation of IRS-1 finally leading to an increase in signaling activity, which may have beneficial effects in hyperglycemic conditions (e.g. diabetes mellitus) (Scheufele et al. 2014).

3.3 Different adaptive mechanisms of the heart under physiological and pathophysiological conditions

As other muscle tissues of the body, the heart is capable of reacting to different intensities of workload in order to compensate higher stress and maintain the cardiac function on a sufficient level for the distribution of blood through the body. This cardiac hypertrophy is achieved by enlargement of the cardiomyocytes and thereby the heart itself resulting in a reduction of the wall stress.

There are two types of adaptive cardiac hypertrophy – physiological and pathological hypertrophy. Whereas physiological hypertrophy is a reversible and healthy reaction to elevated workload e.g. through physical exercise or pregnancy, pathological hypertrophy is a detrimental process in response to severe heart damage like volume overload, high blood pressure, valve diseases, myocardial infarction and diseases of the myocardium and endocardium. Initially, the pathological hypertrophy constitutes a compensation mechanism

for the loss of function caused by the underlying disease, but by the time drifts towards decompensation lately ending in heart insufficiency. In comparison to pathological hypertrophy, physiological cardiac hypertrophy is characterized by a balanced increase in ventricular dimensions accompanied by a moderate increase in ventricular wall thickness resulting in improved function of the heart. The pathological hypertrophy can be divided into two main subcategories – concentric and eccentric hypertrophy. The concentric reaction is typically observed in conditions of increased afterload (e.g. aortic stenosis or high blood pressure) and is characterized by an increase of wall thickness and reduction of the ventricular inner radius. On the other hand, eccentric hypertrophy features an increase in ventricular inner diameter and only mild ventricular wall thickening. Similar morphological changes can also be observed on the level of the cardiomyocyte itself, whereas in concentric hypertrophy myocyte width is increased and several myocytes are aligned parallel and in eccentric hypertrophy myocytes are increased in length and are aligned serially. In case of decompensation, both types of pathological hypertrophy can lead to severe dilatation of the ventricle resulting in the breakdown of cardiac function and heart insufficiency in contrast to physiological hypertrophic responses, where this is not observed (Heineke et al. 2006).

Interestingly, along with the morphological differences between physiological and pathological hypertrophy, the cellular signaling pathways involved in the hypertrophy are diverse from each other.

In physiological hypertrophy, thyroid hormones and VEGF, GH, insulin and IGF-1 pathways play a major role in signal transduction (Dorn et al. 2005). Insulin and IGF-1 bind to tyrosine-kinase receptors leading to dimerization and autophosphorylation of the receptor. Thus binding of the adapter molecules IRS-1 and IRS-2 is facilitated leading to activation of PI3K finally causing phosphorylation and activation of Akt (aka protein kinase B). Cardiomyocyte-specific deletion of the insulin receptor (IR) gene resulted in reduced size of the heart, accompanied by a reduction of cardiomyocyte cell size and functional impairment (Belke et al. 2002). Additionally, mice with cardiomyocyte-specific deletion of the IR subjected to aortic banding suffered from more severe impairment of systolic cardiac function, pronounced dilatation of the ventricle and increased cardiac fibrosis, suggesting a protective effect of insulin signaling under conditions of cardiac stress (Hu et al. 2003).

Besides insulin, a key player in physiological hypertrophy is IGF-1 (Zebrowska et al. 2009). IGF-1 is synthesized by the liver and is released upon stimulation via GH. It has been shown that IGF-1 levels are increased in athletes with physiological hypertrophy when compared to athletes without physiological hypertrophy and that IGF-1 serum levels are

significantly elevated following physical exercise compared with resting conditions (Zebrowska et al. 2009). Likewise, GH levels are increased in individuals subjected to exercise (Sutton et al. 1976). Cardiac overexpression of IGF-1 resulted in an increase of cardiac mass, cardiomyocyte size and improved cardiac function with the absence of detrimental interstitial alterations (e.g. fibrosis), accompanied by significant activation of the PI3K(p110α)-Akt pathway (Reiss et al. 1996, Delaughter et al. 1999, McMullen et al. 2004). Additionally, mice harboring a cardiac-specific IGF-1R deletion did not develop physiological hypertrophy following exercise training (Kim et al. 2008). A further central player in physiological hypertrophy is PI3K, as it constitutes a nodal point for the insulin and the IGF-1 signaling pathway. In the PI3K family, class I has the highest relevance for physiological hypertrophy and overexpression of a constitutively active mutant of the catalytic subunit p110α of class I PI3K in the heart resulted in physiological growth, whereas expression of a dominant negative mutant of PI3K resulted in smaller heart size (Shioi et al. 2000, Shiojima et al. 2006). The relevance of class I PI3K in physiological hypertrophy was also shown by muscle-specific deletion of the regulatory subunit p85α in combination with a germline deletion of subunit p85β resulting in reduced heart size and phosphorylation of Akt accompanied by an attenuated exercise-induced physiological hypertrophy (Luo et al. 2005). Additionally, deletion of catalytic PI3K subunit p110α, but not p110β, resulted in reduced Ca^{2+}-current, contractility and insulin signaling in the heart (Lu et al. 2009). Further downstream the signaling pathway Akt exerts a major role in the insulin and IGF-1 pathway. Of the three known isoforms of Akt, Akt1 and Akt2 are expressed in the myocardium (Oudit et al. 2004). Deletion of the Akt1 gene resulted in ameliorated physiological heart hypertrophy in response to exercise and similar results were obtained by overexpression of a dominant negative Akt mutant, whereas expression of a constitutively active Akt mutant increased heart weight of the mice significantly (Shioi et al. 2002, DeBosch et al. 2006). Akt exerts its effects on hypertrophy either by inhibition of GSK3β, with itself is a negative regulator of protein synthesis and by inhibition of FOXO3, that positively mediates activity of FBXO32 and MURF1, both of which are linked to muscle atrophy (Haq et al. 2000, Antos et al. 2002, Skurk et al. 2005).

Taken together, all these results delineate a pivotal role of the insulin/IGF-1 – IRS1 – PI3K – Akt signaling pathway in physiological hypertrophy of the heart as a response to physical exercise stress.

In pathological hypertrophy, which arises from stimuli subtypes like increased afterload or volume overload resulting in concentric or eccentric hypertrophy, respectively, the mitogen-activated protein kinase (MAPK) pathways seem to play an important role. The MAPK

signaling pathways contain three different kinase families, MAP3K, MAP2K and MAPK, that are serially transducing and, because of their cascade-like arrangement, amplifying the signal. One important MAPK family member concerning cardiac hypertrophy is Erk1/2, which is located downstream of a signaling cascade starting with the G-protein Ras. Ras activates MAP3K protein Raf1 through recruitment to the cell membrane which itself phosphorylates and activates MAP2K protein MEK1, that itself activates Erk1/2 by tyrosine and threonine phosphorylation (Shaul et al. 2007). Glennon et al. showed, that depletion of Erk1/2 in cardiomyocytes by antisense oligodeoxynucleotides attenuated the hypertrophic response to phenylephrine (PE) in vitro (Glennon et al. 1996). Similar results were observed in cultured rat cardiomyocytes treated with MEK1 and Raf1 inhibitors that showed ameliorated activation of Erk signaling, protein synthesis and cardiomyocyte cell size upon stimulation via PE or endothelin-1 (ET-1), an effect also reproducible by expression of a dominant negative Raf1 mutant (Yue et al. 2000). Additionally, α-MHC promoter directed cardiac overexpression of an activated MEK1 mutant resulted in activation of the Erk1/2 signaling pathway, increase of cardiomyocyte width and formation of concentric heart hypertrophy in vivo accompanied by increased cardiac performance (Bueno et al. 2000). These findings show, that activation of Erk1/2 plays an important role in the response to stress associated signaling molecules like PE and ET-1 and its activation leads to increased cardiomyocyte width in vitro and formation of concentric hypertrophy of the heart in vivo, both of which characteristics also observed in hypertrophic response to increased afterload.
Interestingly the MEK5 – MAPK Erk5 axis has been shown to be linked to eccentric hypertrophy, as overexpression of an active mutant of MEK5 resulted in elongation and serial alignment of cardiomyocytes resulting in dilatation of the ventricle, finally leading to cardiac death. These effects were reproduced by activation of MEK5 via leukemia inhibitory factor (LIF) and expression of dominant negative mutant of MEK5 was able to block LIF-induced cardiomyocyte elongation (Nicol et al. 2001).

3.4 The role of CRL7 in the heart

In 2001 Pasumarthi and co-workers were able to demonstrate that co-expression of a C-terminally truncated mutant of CUL7 with a p53 mutant in CM was sufficient to block E1A induced apoptosis, exerting a pro-survival function, and to induce a proliferative response (Pasumarthi et al. 2001). As apoptosis is a critical factor involved in remodeling after myocardial infarction (MI), CUL7 may also have an impact on cardiac function after MI.

Nakajima and coworkers created a cardiomyocyte-specific dominant negative mutant of CUL7 by insertion of a premature stop codon resulting in a terminated protein at AA 1152 (α-MHC-1152stop). They were able to detect significant cell cycle induction in the infarct border zone 4 weeks after MI accompanied by an increased DNA synthesis in the infarct border zone and the interventricular septum compared to non-transgenic littermates suggesting a reentry of the generally postmitotic cardiomyocytes into the cell cycle (Nakajima et al. 2004). Concordantly, it was shown that mice expressing a dominant negative CUL7 mutant showed a reduction of infarct size dimensions 4 weeks after permanent left coronary artery ligation and this reduction in MI-expansion positively influenced cardiac function, as systolic (measured by dP/dt_{max}) and diastolic function (measured in LV-isovolumetric relaxation time constant τ) were improved when compared to non-transgenic siblings (Hassink et al. 2009). Surprisingly, the number of apoptotic cardiomyocytes was not different in mice expressing the wild-type or mutated CUL7, implicating that the morphological and functional improvements of Cullin7 inhibition are more likely mediated by an increase in CM number than in a decrease of CM apoptosis rate (Nakajima et al. 2004).

4. Aims and Objectives

Given the pivotal influence of the signaling pathways PI3K/Akt and Erk MAPK in the heart and the regulatory role of CRL7 in controlling these pathways, we sought to determine the role of the CRL7 in the heart.

We first sought to investigate the expression of CUL7 in different types of murine tissue. Therefore, tissue samples from wild-type male mice were collected and expression of the CUL7 protein analyzed by immunoblotting. Next, we investigated the expression of CUL7 in different cell types of the heart. Murine hearts were collected, cardiomyocytes and cardiofibroblasts separated and expression of CUL7 studied by immunoblotting in the respective cell fractions. Next, inducible cardiomyocyte-specific CUL7 depleted mice were generated, by crossing $Cul7^{flox/flox}$ mice with Myh6-Mer-Cre-$Mer^{Tg(1/0)}$ animals. Depletion of CUL7 was validated in whole heart samples as well as cardiomyocyte and cardiofibroblast cell fractions by immunoblotting.

Subsequently, the physical phenotype of those animals was analyzed. Cardiac function was measured by echocardiography, left ventricular fibrosis was analyzed by Sirius Red / Fast Green staining and cross-sectional area of cardiomyocytes was assessed by wheat germ agglutinin staining. Additionally, the impact of cardiomyocyte-specific CUL7 depletion on CM signaling pathways was elucidated by immunoblotting.

Furthermore, we sought to elucidate the role of CRL7 in cardiac disease. To this end, we performed transverse aortic constriction to increase cardiac afterload in CM-specific CUL7 depleted mice. Additionally, we subjected CUL7 depleted NRCMs to phenylephrine-induced cellular hypertrophy.

5. Materials and Methods

5.1. Animals

5.1.1. Mouse breeding

Mice were kept conventionally on a 12 h light and dark cycle in type III cages ('Euronorm'). Special chow for breeding and water were provided ad libitum. As well as different varieties of enrichment, such as nesting material, houses and little sticks for nibbling. Pups were separated at the age of 4 weeks, receiving a punched earmark and the tissue sample was collected for DNA isolation and subsequent genotyping. The animal breeding and any experimental setting were approved and reviewed by the State Government of Bavaria (Germany).

5.1.2. Generation of cardiomyocyte-specific Cul7$^{-/-}$ mice

For the generation of the knockout mice, mice with a floxed *Cul7* allele (Cul7$^{flox/flox}$) were crossed with mice expressing a Cre enzyme flanked by two mutated estrogen receptors under the control of the myosin heavy chain alpha gene promoter Myh6 (Myh6-Mer-Cre-Mer$^{Tg(1/0)}$). Generation of the floxed *Cul7* allele was performed by DeCaprio et al in 2003 (Arai et al. 2003). Briefly, the loxP sites are localized in intron one and intron four resulting in loss of exon two to four in case of recombination mediated by the Cre enzyme. For the generation of the inducible knockout mice, a Cul7$^{flox/+}$ mouse was crossed with a Cul7$^{flox/+}$; Myh6-Mer-Cre-Mer$^{Tg(1/0)}$ mouse which resulted in Cul7$^{flox/flox}$; Myh6-Mer-Cre-Mer$^{Tg(0/0)}$, Cul7$^{+/+}$; Myh6-Mer-Cre-Mer$^{Tg(1/0)}$ and Cul7$^{flox/flox}$; Myh6-Mer-Cre-Mer$^{Tg(1/0)}$. For induction of the recombination male mice were injected intraperitoneally with Tamoxifen (Sigma, Cat. No. T5648-1G) at a dose of 40 mg/kg body weight at the age of 6 weeks using an Omnifix® F Solo syringe (Braun, Cat. No. 9161406V) and Sterican® Insulin G 26 x 1/2" / ø 0,45 x 12 mm cannula (Braun, Cat. No. 4665457) during a short isoflurane anesthesia. The maximum amount of an injectable solution is 200 µl.

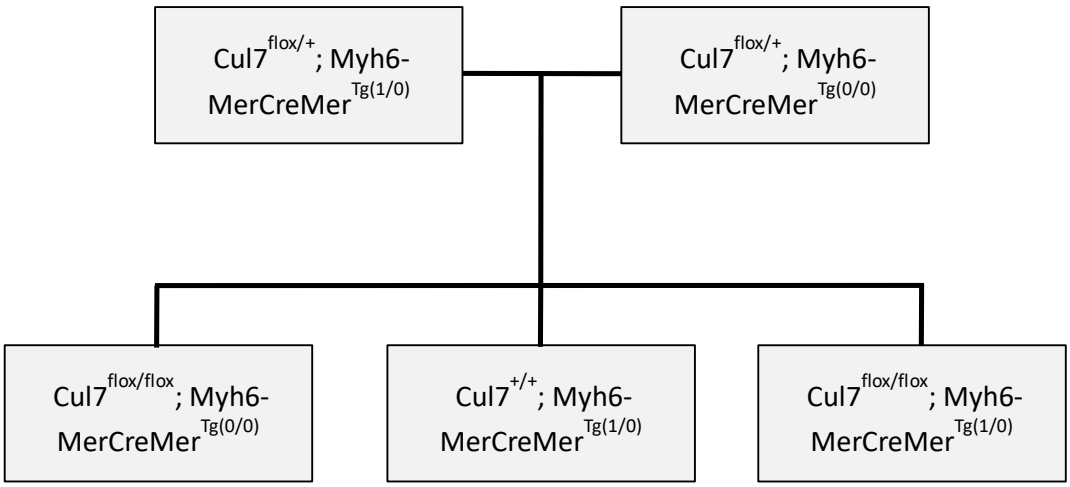

Figure 2: Crossing for the generation of inducible cardiomyocyte-specific CUL7 knockout mice. $Cul7^{flox/+}$; Myh6-$MerCreMer^{Tg(1/0)}$ were crossed with $Cul7^{flox/+}$; Myh6-$MerCreMer^{Tg(0/0)}$ resulting in $Cul7^{flox/flox}$; Myh6-$MerCreMer^{Tg(0/0)}$, $Cul7^{+/+}$; Myh6-$MerCreMer^{Tg(1/0)}$ and $Cul7^{flox/flox}$; Myh6-$MerCreMer^{Tg(1/0)}$ offspring, all at a probability of 1/8. Only relevant genotypes are depicted.

5.1.3. Transverse aortic constriction (TAC) model of increased afterload

Male 8 weeks old mice were anesthetized by inhalation of 4% isoflurane / 96 % oxygen gas mixture and placed in a supine position on a warming platform, which prevents a cool down of the body temperate of the mouse. 60 min before the operation the mice got an injection of buprenorphine (0.1mg/ bodyweight). After the initial phase of anesthesia concentration of isoflurane was reduced to approximately 1 % (2l/min). Subsequently, right thoracotomy was performed at the second intercostal space and the aortic arch exposed. After that, a 27 G cannula was ligated to the aortic arch using a 2/0 nylon suture until blood flow was completely discontinued followed by removal of the cannula, leaving the aorta with a rest lumen of approx. 0.4 mm. Finally, the thorax was closed and the mouse could wake up under constant control in a pre-heated cage. The analgesic procedure was performed every 8 hrs for another approximately 2 days by injecting buprenorphine (0.1mg/ bodyweight) subcutaneously. In each case, this analgesic management was adjusted to the individual pain perception of the mouse. Sham animals were subjected to the same procedure without ligation of the aorta. The total duration of TAC was 4 weeks.

5.2. Molecular biology

5.2.1. DNA isolation

Tissue samples in 1.5 ml microtubes (Sarstedt, Ref. 72.706.400) were put into 500 µl phenol/chloroform lysis-buffer immediately after collection and 2.5 µl Proteinase K (10 mg/dl, AppliChem, A3830,0100) were added. Samples were subsequently incubated at 55°C and 950 rpm in an Eppendorf "Thermomixer compact" (Eppendorf AG, Serial no. 5350YI832147) overnight until complete digestion of the tissue samples.

Phenol/Chloroform lysis-buffer:

Tris	12.1 g
EDTA	1.87 g
NaCl	11.7 g
Aqua dest.	ad 1L

After digestion, 500 µl Phenol/Chloroform/Isoamyl alcohol (Roti® Phenol/Chloroform/Isoamyl alcohol, Roth, Serial no. A156.2) were added directly to the digested tissue samples and the tubes were centrifuged in an Eppendorf centrifuge 5417R (Eppendorf AG, Serial no. 5407YJ028399) at 14000 rpm and room temperature for 10 min. The upper, DNA-containing phase was collected and transferred to a new 1.5 ml tube. 500 µl Isopropanol were subsequently added and the tube converted three times. After 10 min of centrifugation at 4°C and 14000 rpm the supernatant was discharged and 500 µl Ethanol 70 % were added. After 5 min of centrifugation at 4°C and 14000 rpm, the supernatant was discharged and the pellet dried at room temperature with tubes inverted on a cellulose tissue. Dry pellets were dissolved in 50 µl sterile H_2O and DNA samples stored at 4 °C until usage.

5.2.2. PCR

5.2.2.1. Validation of recombination of the floxed *Cul7* allele

To validate recombination of the floxed *Cul7* allele, male mice were injected with tamoxifen to mediate recombination at the age of 6 weeks. After that, cardiomyocytes were isolated as described below. Subsequently, DNA was isolated from these cells and a PCR performed. The forward primer was designed to anneal in intron one and the reverse primer was designed to anneal in intron five. In Case of successful recombination, the distance between the primer annealing sites is reduced resulting in successful amplification of a 300 bps product. By choosing the same PCR conditions as describes below, amplification of the un-recombined product is not feasible using a standard Taq DNA polymerase (Genscript, Cat no. E00007). For internal control primers binding in intron seven were used, which were not affected by the recombination events. After PCR, amplification products were separated on a 2 % agarose gel.

Primer Specifications:

Name	Sequence (5'-3')	GC %	T_m (°C)
SC1	CGAAAGCAGCAACAGCTGTTATTCTGGGTG	50	76.4
SC2	AGACCGCATCCCCCTCCGACACAGTTCTGG	63.3	82.9

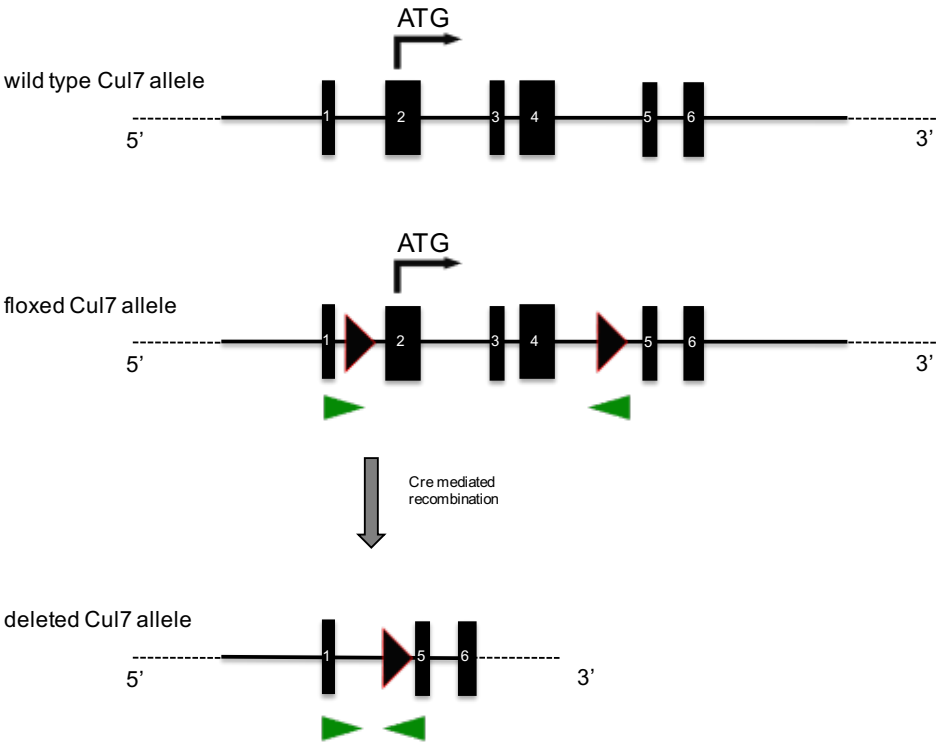

Figure 3: Scheme of the wild type and floxed *Cul7* allele. Upon recombination mediated by the Cre enzyme, exons two to four are deleted, thus reducing the DNA sequence flanked by the recombination screening primers. Vertical black boxes with respective numbers indicate exons. Horizontal black lines indicate introns. Black triangles with red edges indicate loxP-sites. Green triangles indicate primers binding sites for recombination screening.

5.2.2.2. Polymerase chain reaction (PCR) for the *Cul7* allele

The primer sequences for *Cul7* allele genotyping were generously provided by James DeCaprio and coworkers.

The forward primer SC2 and the reverse primer SC1 were designed to align at the first intron of the *Cul7* gene, at which the first loxP site is located, resulting in a 299 bp long amplification product for wild-type mice (loxP site not present) and in a 651 bp long segment for floxed mice (loxP site present).

Primer specifications:

Name	Sequence (5'-3')	GC %	T_m (°C)
SC1	CGAAAGCAGCAACAGCTGTTATTCTGGGTG	50.0	76.4
SC2	AGACCGCATCCCCCTCCGACACAGTTCTGG	63.3	82.9

For the PCR reaction 2.5 µl of 10x Taq Buffer (GenScript, Cat. No. B0005), 0.5 µl 10mM dNTPs (Sigma, Cat. No. 000000011969064001), 1.25 µl 10µM primer SC1 (Sigma Aldrich), 1.25 µl 10µM primer SC2 (Sigma Aldrich), 0.25 µl 5U/µl Taq DNA polymerase (Genscript, Cat no. E00007) and 18.25 µl sterile H_2O were assembled per sample for a mastermix. Subsequently, 24 µl of this mastermix was mixed with 1 µl DNA sample in a 0.5 ml SafeSeal tube (Sarsted, Cat. No. 72.704). All of these procedures were constantly performed on ice.
The PCR program was performed in 0.5 SafeSeal tubes (Sarsted, Cat. No. 72.704) in a Biometra Thermocycler and was designed as the following: step I: pre-denaturation at 94°C for 3 min, step II: denaturation at 94 °C for 30 sec, step III: primer annealing at 68°C for 1 min, step IV: elongation at 72°C for 1 min, step V: final elongation at 72°C for 5 min. Steps II-IV were repeated 37 times followed by cooling at 4 °C until usage.

5.2.2.3. PCR for the Myh6-MerCreMer transgene allele

For Myh6-MerCreMer transgene genotyping, forward primer Cre800 and reverse primer Cre1200 were used for detection of the Cre transgene. As an internal control, forward primer Gabra1F and reverse primer Gabra1R were used, recognizing lacZ-tagged mutant allele Gabra1. All primers were ordered at Sigma Aldrich, Steinheim, Germany. Presence of either the Cre transgene or the internal control resulted in an amplification product with the size of 400 bp and 280 bp, respectively.

Primer specifications:

Name	Sequence (5'-3')	GC %	T_m (°C)
Cre800	GCTGCCACGACCAAGTGACAGCAATG	57.7	77.6
Cre1200	GTAGTTATTCGGATCATCAGCTACAC	42.3	62.7
Gabra1F	AACACACACTGGAGGACTGGCTAGG	56.0	70.3
Gabra1R	CAATGGTAGGCTCACTCTGGGAGATGATA	48.2	71.9

The PCR mastermix was assembled on ice. 1 µl of the DNA-sample was added to 24 µl of PCR mastermix.

PCR mastermix for n=1:

10x Taq Buffer	2.5 µl
Cre800 10µM	1.25 µl
Cre12000 10µM	1.25 µl
Gabra1F 10µM	1.25 µl
Gabra1R 10µM	1.25 µl
dNTPs 10mM	0.5 µl
Taq DNA polymerase	0.25 µl
H_2O	15.75 µl

PCR program for the Myh6-MerCreMer transgene allele:

I:	94°C	5min
II:	94°C	30 sec
III:	58°C	1min
IV:	72°C	30 sec
V:	72°C	5 min
VI:	4°C	pause

Steps II – IV were repeated 29 times.

5.2.2.4. PCR for the $CaV_{1.2}$ transgene allele

For PCR analyzing the presence of the mutated $CaV_{1.2}$ transgene primers VL4, VL8 and VL10 were used. Presence of a mutated CaV1.2 channel was detected by the amplification of a product with 500 bp length while wild-type allele was indicated by a product with 415 bp length.

Primer specifications:

Name	Sequence (5'-3')	GC %	T_m (°C)
VL4	TGGCCCCTAAGCAATGA	52.9	62.9
VL8	AGGGGTGTTCAGAGCAA	52.9	59.3
VL10	CCCCAGCCAATAGAATGCCAA	50.0	69.6

The PCR mastermix was assembled on ice. 1 µl of the DNA sample was added to 24 µl of PCR mastermix. The PCR program was identical as described in section 5.2.2.3.

PCR mastermix for n=1:

10x Taq Buffer	2.5 µl
VL4 10µM	1.25 µl
VL8 10µM	1.25 µl
Vl10 10µM	1.25 µl
dNTPs 10mM	0.5 µl
Taq DNA polymerase	0.25 µl
H2O	17 µl

5.2.2.5. PCR for the CAG-CreERT2 transgene allele

For the presence of the CAG-CreERT2 transgene allele primers TGfwd and TGrev recognizing the transgene and primers INposCfwd and INposCrev serving as an internal control were used. Presence of either the transgene or the internal control resulted in amplification products of 100 bp and 324 bp, respectively.

Primer specifications:

Name	Sequence (5'-3')	GC %	T_m (°C)
TGfwd	GCGGTCTGGCAGTAAAAACTATC	47.8	64.6
TGrev	GTGAAACAGCATTGCTGTCACTT	43.4	65.3
INposCfwd	CTAGGCCACAGAATTGAAAGATCT	41.6	63.5
INposCrev	GTAGGTGGAAATTCTAGCATCATCC	44.0	64.5

The PCR mastermix was assembled on ice. 1 µl of the DNA-sample was added to 24 µl of PCR mastermix.

PCR mastermix for n=1:

10x Taq Buffer	2.5 µl
TGfwd 10µM	1.25 µl
TGrev 10µM	1.25 µl
INposCfwd 10µM	1.25 µl
INposCrev 10µM	1.25 µl
dNTPs 10mM	0.5 µl
Taq DNA polymerase	0.25 µl
H2O	15.75 µl

PCR program for the CAG-CreERT2 transgene allele:

I:	94°C	3min
II:	94°C	30 sec
III:	51.7°C	1min
IV:	72°C	1 min
V:	72°C	2 min
VI:	4°C	pause

Steps II – IV were repeated 35 times.

5.2.2.6. Agarose gel casting

For DNA separation a 2% agarose gel was casted by dissolving 2g of agarose (Roth, Karlsruhe, Serial no. 3810.3) in 100 µl 1x TAE buffer in an Erlenmeyer flask (Fisherbrand, Serial no FB 33132). This mixture was heated in a microwave (Panasonic, Serial no. NN-E245W) at 800W for approximately 3 min until a complete dissolution of the agarose was reached. After cooling under running water, 25 µl 10 mg/ml ethidium bromide (Roth, Serial No. 2218.1) were added and distributed by light pivoting of the flask. After that, the mix was casted using Gel Tray Mini M (PeqLab, Serial No 40-0911-UVT) and gel comb 14 well 1.0mm (PeqLab, Serial no. 40-0911-14C) for the subsequent curing process at room temperature for approx. 30 min.

50x TAE buffer:

Tris base (MW=121.1)	242 g
Glacial acetic acid	57.1 ml
EDTA 0.5 M	100 ml
H_2O	ad 1L

For 1x TAE buffer 20 ml 50x TAE buffer were mixed with 980 ml H_2O.

5.2.2.7. Agarose gel running and analysis

For DNA separation, the cured agarose gel was put in a PeqLab gel electrophoresis system Mini M (PeqLab, serial no. 40-0911) and the chamber was filled with 1x TAE buffer as recommended by the manufacturer. The PCR amplification product was mixed with 5 µl 5x DNA loading buffer and 12.5 µl mix were loaded per gel pocket followed by gel running at 120 V 400mA for 20 min (electrophoresis power supply EPS-301, GE Healthcare Life Science, Serial no. 18-1130-01). Agarose gels were subsequently analyzed using a UV transilluminator MD-25/HD-25 (Wealtec, serial no. 1142003) and the DeVisionG 2.0 software program (Decon Science Tec GmbH, Hohengandern, Germany). Identification of the amplification product length was realized using Quick-Load® 100 bp DNA ladder (New England Biolabs GmbH, Serial no. NEB #N3270) in the flanking lanes of the gel.

5x DNA loading buffer:

EDTA 0.5 M pH 8.0	1.4 ml
Glycerol	3.6 ml
Bromophenol blue	0.01 g
H_2O	7 ml

5.2.3. qPCR

5.2.3.1. RNA preparation from tissue samples

For RNA preparation, tissue samples were shock frozen immediately after preparation in liquid nitrogen. The frozen tissue samples were subsequently mixed with 1 ml peqGOLD TriFast Reagent (PEQLAB, Prod. No. 30-2020) in a 2 ml reaction tube (Sarstedt, Nümbrecht, Ref. 72.695.400) under the fume hood and homogenized using a thurax. After 5 minutes of incubation at room temperature, 0.2 ml chloroform was added to the sample and tubes vortexed for 30 sec. After incubation of 10 min at room temperature, samples were centrifuged for 5 min at 4°C and 12000 g. After centrifugation, the upper RNA-containing phase was transferred to a new tube and 0.5 ml Isopropanol was added to the sample. Samples were then mixed and incubated at 4°C for 10 min. After centrifugation for 10 minutes at 4 °C and 12000 g, the supernatant was discarded and the remnant pellet was washed with 1 ml 75 % ethanol, vortexed and centrifuged for 10 minutes at 4 °C and 12000 g. The ethanol washing step was repeated and, after discarding of the supernatant, pellets were dried at room temperature. Subsequently, pellets were re-suspended in 30 µl RNase free H_2O (Dharmacon. GE lifesciences, Ref. No. B-003000-WB-100) and pellets heated to 55°C for 10 sec under agitation. The RNA-concentration of the samples was subsequently determined using a nano-drop system and tubes were stored at – 80 °C until usage.

5.2.3.2. RNA preparation from cell culture samples

For RNA preparation from cells, the medium was removed and plates washed with Gibco® DPBS 1 x (Life technologies, Prod. No. 14190-940). After that, 1 ml peqGOLD TriFast Reagent (PEQLAB, Prod. No. 30-2020) was added to the plate and cells suspended using a cell scraper (Sarstedt, Ref. 83.1830) under the cell culture hood. Cells were then lysed by pipetting the suspension up and down intensively. After 5 minutes of incubation at room temperature, 0.2 ml chloroform was added to the sample and the tubes were vortexed for 30 sec. After incubation for 10 min at room temperature, the samples were centrifuged for 5 min at 4°C and 12000 g. After centrifugation, the upper RNA-containing phase was transferred to a fresh tube and 0.5 ml Isopropanol (Roth, Cat. No. 200-272-27343.2) was added to the sample. Samples were then mixed and incubated at 4°C for 10 min. After

centrifugation for 10 minutes at 4 °C and 12000 g, the supernatant was discarded and the remnant pellet was washed with 1 ml 75 % ethanol, vortexed and centrifuged for 10 minutes at 4 °C and 12000 g. The ethanol washing step was repeated and, after discarding of the supernatant, pellets were dried at room temperature. Subsequently, the pellets were re-suspended in 30 µl RNase free H_2O (Dharmacon. GE lifesciences, Ref. No. B-003000-WB-100) and heated to 55°C for 10 sec under agitation. The RNA-concentration of the samples was subsequently determined using a nano-drop system and tubes stored at – 80 °C until usage.

5.2.3.3. Reverse transcription

For reverse transcription 250/500 ng RNA in 10 µl H_2O were mixed with 1 µl oligo dT (20 µM) and 1 µl dNTPs 10mM in a 0.5 ml tube on ice. Subsequently, the samples were put in a Biometra Thermocycler for 5 min at 65 °C and 2 min at 4°C. After that, 8 µl reverse transcription mastermix were added and samples cycled for 50 min at 42 °C and 15 min at 70 °C. The generated cDNA samples were stored at - 20°C until usage.

Reverse transcription mastermix:

SuperScript® II Reverse Transcriptase	1 µl
5X first-strand buffer	4 µl
100 mM DTT	2 µl
RNaseOUT™ Ribonuclease Inhibitor	1 µl

5.2.3.4. Quantitative real time PCR

For qPCR analysis, the mastermix was set up on ice and 10.5 µl put in each well of a MicroAmp® Fast 96-Well Reaction Plate (applied biosystems, life technologies, Prod. No.

4346907). After that, 2 µl cDNA were added to the well and the plate was sealed using optical adhesive covers (applied biosystems, Prod. No. 4360954).

qPCR protocol:

I: Taq activation 95°C 10min

II: Denaturation 95°C 15sec

III: Annealing 60°C 60sec

Steps II – III were repeated 40 times.

Melting Curve:

95°C 15sec

60°C 60sec

95°C 15sec

qPCR mastermix n=1:

Forward primer	0.25 µl
Reverse primer	0.25 µl
FastStart SYBR Green Master (Roche, Cat. No. 04913922001)	6.25 µl
H_2O	3.75 µl

qPCR primers were designed using the Basic Local Alignment Search Tool (BLAST) (www.ncbi.nlm.nih.gov/blast/) and Primer3web version 4.0.0 (http://primer3.ut.ee/). Primer sequences were designed to bridge introns in order to rule out DNA contamination.

qPCR primer characteristics:

Name	Sequence (5'-3')	GC %	T_m (°C)
Cul7 Full length forward	CTCTCCTTCACACGGTCCA	57.8	64.1
Cul7 Full length reverse	GCATGAGCAAGTTCACAACC	50.0	63.4
Cul7 Exon 19_20 forward	CTGTGCTGAGGCTCCCTTT	57.8	64.5
Cul7 Exon 19_20 reverse	ACTGTGCCAGCATCTCCATT	50.0	64.7
Cul7 Exon 1_2 forward	TCCCTAGCTCTGCAAAGGAC	55.0	63.4
Cul7 Exon 1_2 reverse	GCACCCTGAATTCCCTGTAT	50.0	62.7
Cul7 Exon 22_23 forward	GTCTGCCAAATGCTCAACC	52.6	63.3
Cul7 Exon 22_23 reverse	GCCTCTGTGGCTCTTTCTCT	55.0	62.7
RPL32 forward	ACATCGGTTATGGGAGCAAC	50.0	58.0
RPL32 reverse	GGGATTGGTGACTCTGATGG	55.0	57.7
ANP forward	GCTTCCAGGCCATATTGGAG	55.0	58.4
ANP reverse	GGGGGCATGACCTCATCTT	57.9	59.1
β-MHC forward	GCAGCTCCTTCGTTGCCGGT	65.0	65.8
β-MHC reverse	TACAGCCCGGGGAGCATCGT	65.0	65.7
GAPDH (rat)	TGACAACTCCCTCAAGATTGTCA	43.5	59.6

forward			
GAPDH (rat) reverse	GGCATGGACTGTGGTCATGA	55.0	60.0

If not indicated differently primers target mouse cDNA.

5.2.4. Protein isolation

5.2.4.1. Protein sample preparation from murine tissue

For protein sample preparation from murine tissue, tissue samples were isolated immediately after preparation. Subsequently, the tissue was put in a 1.8 ml cryotube (Sarstedt, Nümbrecht, Ref. 72.379) and frozen in liquid nitrogen. Samples were then either frozen and stored at – 80°C or protein samples were prepared as described in the following. The samples, stored on ice, were mixed with ice-cold lysis buffer “Cell Signaling” in a 2 ml Eppendorf tube (Sarsted, Ref. 72.695.400). Subsequently, samples were homogenized using an ultrathurax until complete dissociation of the tissue. To avoid contamination, the thurax was cleaned intensively by using water and 0.5 M NaOH. After that, lysates were incubated in an ultrasonic bath for 5 min. If necessary, 10% of total volume of 5% Benzonase (Sigma, Serial No. E1014-5KU) was added and incubated for 10 min at room temperature. After that, lysates were centrifuged in an Eppendorf centrifuge 5417R (Eppendorf, Serial no. 5407YJ028399) at 14000 rpm and 4 °C for 10 min. The supernatant was transferred to a new 1.5 ml Eppendorf tube and stored at – 80°C until usage.

Lysis buffer “Cell Signaling”

Tris pH 7.5	20 mM
NaCl	150 mM
EDTA	1 mM
EGTA	1 mM
Triton-X-100	1 % vol.
Natriumpyrophosphate	2.5 mM
Na_3VO_4	1 mM

For phosphatase inhibition, a phosphatase inhibitor mix was added to the lysis buffer. For a total volume of 10 ml lysis buffer the mix was set up as shown below:

Lysis buffer	9482 µl
DTT (1M)	10 µl
NaF (500mM)	250 µl
Na_3VO_4 (100mM)	100 µl
PAO (40mM)	100 µl
PMSF (200mM)	50 µl
Leupeptin (25mg/ml)	4 µl
Antipain (25mg/ml)	4 µl

5.2.4.2. Protein sample preparation from cultured cells

For protein sample preparation from cultured cells, the medium was removed from the cells under the cell culture hood. Subsequently, dishes were put on ice and washed with ice-cold Gibco™ DPBS (life technologies, Serial No. 14190-144). DPBS was removed and lysis buffer added to the cells in respect of the cell density and aimed protein concentration. Cells were then scraped off the dish with a cell scraper (Sarstedt, Nümbrecht, Ref. 83.1830), transferred to a 1.5 ml Eppendorf tube (Sarsted, Nümbrecht, Ref. 72.706.400) and incubated for 10 min on ice. After that, samples were centrifuged in an Eppendorf centrifuge 5417R (Eppendorf AG, Hamburg, Serial no. 5407YJ028399) at 14000 rpm and 4 °C for 10 min. The supernatant was transferred to a fresh 1.5 ml Eppendorf tube and samples stored at – 80°C until usage.

5.2.4.3. Quantification of sample protein concentration

For determination of the sample protein concentration, a Bradford assay was performed. Bio-Rad Protein Assay Dye Reagent Concentrate (BIO RAD, Bio-Rad Cat.No. 500-0006) was diluted 1 : 5 with H_2O. Subsequently, 1000 µl of the diluted dye were mixed with 2 µl of protein sample in a 1.5 ml tube and mixed by converting. 200 µl of this mixture were pipetted in triplicates into a 96 well plate and the absorbance at 595 nm was measured. The

protein concentration was then calculated by plotting against a straight line obtained by absorbance values of albumin samples BSA (AppliChem, Cat.No. A6588.0100) of known concentration. If the sample was out of the linear range of the Bradford assay (2 µg/ml to 120 µg/ml), the samples were diluted with lysis buffer and the assay was repeated.

5.2.5. Immunoblotting

5.2.5.1. Casting of the SDS gel

For SDS-gel casting a Mini-PROTEAN® Tetra Cell Casting Stand (BIO RAD, Ref. No. 1658050) was used. Glass plates and combs (1mm) were cleaned with ethanol and dried at room temperature. Stacking gel (upper gel) and separation gel (lower gel) were prepared separately in a 50 ml falcon tube (Sarstedt, Nümbrecht, Ref. 62.548.004) without the addition of APS (Roth Karlsruhe, Serial No. 9592.3) and TEMED (BIO RAD, Cat.No.1610801). After assembly of the casting system, APS and TEMED were added to the separation gel, components mixed by pivoting of the flask and the mixture was carefully pipetted between the glass plates with approx. 2 cm space on top, which was subsequently filled with H_2O. The separation gel polymerized at room temperature for 30 min. After polymerization of the separation gel, H_2O was removed and, after addition of APS and TEMED, the stacking gel mix was carefully pipetted on top of the lower gel and a comb was placed between the glass plates after removal of trapped air. After polymerization of 30 min at room temperature, the gels were stored at 4°C covered with wet tissues in a plastic bag.

<u>Separating gel 8 %:</u>

30% Acrylamid + 0.8 Bis	3000 µl
4x Lower buffer	2850 µl
H_2O	3525 µl
Glycerol 80 %	1875 µl
APS 10 %	54 µl
TEMED	9 µl

Separating gel 12 %:

30% Acrylamid + 0.8 Bis	4500 µl
4x Lower buffer	2850 µl
H_2O	2025 µl
Glycerol 80 %	1875 µl
APS 10 %	54 µl
TEMED	9 µl

Stacking gel:

30% Acrylamid + 0.8 Bis	250 µl
4x Upper buffer	625 µl
H_2O	1600 µl
APS 10 %	24 µl
TEMED	3 µl

4x Lower buffer:

Tris/HCl	182 g
SDS 10%	40 ml
H_2O	ad 1000 ml
Adjust with HCl	pH 8.8

4 x Upper buffer:

Tris/HCl	61 g
SDS 10%	40 ml
H_2O	ad 1000 ml
Adjust with HCl	pH 6.7

5.2.5.2. Protein sample denaturation

An appropriate volume of protein samples for the aimed protein amount was mixed with 4x LAEMMLI loading buffer and mixed by pipetting. Subsequently, samples were denaturized in an Eppendorf "Thermomixer compact" (Eppendorf AG, Hamburg, Serial no. 5350YI832147) at 97 °C for 5 min. After samples have cooled down, they were centrifuged 5 seconds at 14000 rpm in an Eppendorf centrifuge 5417R (Eppendorf AG, Hamburg, Serial no. 5407YJ028399) at room temperature. After that, samples were either loaded or stored at - 20 °C for later usage.

4x LAEMMLI loading buffer:

Final concentration:	Stock of 7.5ml
TrisCL 200mM (pH 6.8)	TrisCL 1M (pH 6.8) 1.5ml
DTT 400mM	DTT 1M 3ml
SDS 8%	SDS 0.6g
Bromophenol blue 0.4%	Bromophenol blue 0.03g
Glycerol 50%	Glycerol 3ml

5.2.5.3. SDS-PAGE

For the SDS-PAGE, casted gels were placed in a BIO RAD running chamber (BIO RAD, Ref No. 1658001) and chambers were filled with SDS-PAGE running buffer up to the recommended filling level. The respective volume of denaturized protein samples mixed with 4x LAEMMLI loading buffer was loaded using loading tips (BIO RAD, Ref No 2239915) and protein lanes were flanked with protein marker Precision Plus Protein™ Standards (BIO RAD, Cat. No.: #161-0373) with 4 µl in the first lane and 2 µl in the last lane for running height determination. Subsequently, the gels were run at 30 mA per gel and 400 V for 1 h at room temperature.

10x SDS running buffer:

Tris/Cl	30 g

Glycin	144 g
SDS	15 g
H_2O	ad 1000 ml

5.2.5.4. Western blotting

For blotting PVDF Immobilon® Transfer Membranes Immobilon®-P (Millipore, Cat. No.: IPVH00010) were incubated in methanol (Sigma, Serial No. 322415-18L) under agitation for 2 minutes. Blotting chambers were filled with transfer buffer and a frozen cool pack (-20°C) was placed in the chamber. The SDS gel was rinsed with transfer buffer, placed on the PVDF membrane and put in the blotting casket. After that, blotting was performed at 375 mA for 2 h and membranes were blocked in 5 % BSA in PBST overnight at 4°C under agitation.

10x Transfer buffer:

Tris/Cl 1M pH 8.3	225 ml
Glycin	101.34 g
H_2O	ad 900 ml

For 1x Transfer buffer, 100ml 10x stock was mixed with 100 ml methanol and filled up to 1000ml with H_2O.
After blocking overnight in 5 % BSA in PBST 0.05 % Tween, membranes were washed 5 min in PBST 0.05 % Tween under agitation. Subsequently, membranes were incubated with the first antibody for 2 h at room temperature under agitation. First antibodies were diluted in 10 ml PBST 0.05 % Tween with 0.5 g BSA and 100 µl 2 % sodium acid. After incubation of the first antibody, membranes were washed four times for 5 min in PBST 0.05 % Tween under agitation at room temperature and subsequently incubated with the second antibody for one hour at room temperature. Second antibodies were diluted in 10 ml PBST 0.05 % Tween. After that, membranes were washed four times for 5 min in PBST 0.05 % Tween under agitation. For detection Pierce ® ECL 2 Western Blotting Substrate (Thermo Scientific, Rockford, USA; Prod # 80196) was used. According to the manufacturer's protocol "Solution A" was mixed with "Solution B" in the proportion 40 : 1 in a 15 ml falcon

tube (Sarstedt, Nümbrecht, Ref. 62.554.001). PBST 0.05 % Tween was carefully removed with a tissue wipe, membrane covered with detection solution and incubation performed at room temperature for 2 min. After that, redundant detection solution was absorbed with a tissue wipe and membrane placed between plastic sheets. Chemiluminescence signal detection was performed in Fujifilm LAS 4000 multipurpose CCD camera system (GE Healthcare Life sciences, Product code: 28-9558-10) according to the manufacturer's protocol. Quantification of signal intensity was realized using MultiGauge Software (Fujifilm).

1st antibodies:

Name	Company	Prod. No.	Species	Dilution
Monoclonal Anti-Cul7 Clone Ab38	Sigma	C1743	Mouse	1 : 5000
HSP 90 (F-8) sc-13119	Santa Cruz Biotechnology	H2312	Mouse	1 : 10000
Anti-IRS1	Millipore	LBC1863297	Rabbit	1 : 1000
P-IRS1 (S302) Rabbit Ab	Cell Signalling	2384S	Rabbit	1 : 1000
Akt Rabbit Ab	Cell Signalling	9272S	Rabbit	1 : 1000
P-Akt (S473) Rabbit Ab	Cell Signalling	9271S	Rabbit	1 : 1000
p44/42 MAPK (Erk1/2) (L34F12) mouse mAb	Cell Signalling	4696S	Mouse	1 : 1000
P-p44/42 MAPK (T202/Y204) Rabbit Ab	Cell Signalling	9101S	Rabbit	1 : 1000

S6 Ribosomal Protein (5G10) Rabbit mAb	Cell Signalling	2217	Rabbit	1 : 1000
P-S6 Ribosomal Protein (S235/236) Rabbit Ab	Cell Signalling	2211S	Rabbit	1 : 1000

Characteristics of 2nd antibodies:

Name	Manufacturer	Prod. No.	Source	Dilution
Anti-mouse IgG, HRP-linked Ab	Cell Signalling	7076S	Horse	1 : 10000
Anti-rabbit IgG, HRP-linked Ab	Cell Signalling	7074S	Goat	1 : 10000

5.2.5.5. Stripping of the PVDF immunoblot membranes

For consecutive detection of phosphorylated proteins and their total protein levels, membranes were stripped after detection of the phosphorylated protein. Therefore, stripping buffer was heated to 50 °C in a water bath and membranes incubated 2 x 20 min in hot stripping buffer under constant agitation. After that, membranes were washed three times with PBST 0.05 % Tween and blocked with 5 % BSA blocking solution as described above.

Stripping buffer:

Glycin (Roth, Cat. No. 200-272-2)	15g
SDS (Serva, Cat. No. 20783.02)	1 g
HCl (Roth, Serial No. 4625.2)	ad pH 2.0

5.2.6. Histology

5.2.6.1. Paraffin fixation of tissue samples

After preparation of the murine heart, a 1mm axial slice of the ventricles was isolated and subsequently put in 4 % PFA fixation solution for 24h under agitation. After incubation slides were cut with a thickness of 6 μm.

5.2.6.2. Hematoxylin and Eosin staining

For Hematoxylin and Eosin staining of cardiac paraffin-embedded sections, deparaffinization and rehydration of the sections was performed by consecutive incubation in 100 % toluol for 2 x 10 min, 100 % ethanol for 2 x 5 min, 90 % ethanol for 5 min, 70 % ethanol for 5 min, 50 % ethanol for 5 min and water for 5 min. After that, the sections were incubated in “Hematoxylin 2 solution” (ThermoScientific, Cat. No. 7231) for 2 min. Subsequently, the slides were rinsed with water followed by washing for 30 sec and 2 min. After that “Clarifier 2” (ThermoScientific, Cat. No. 7402) was incubated for 10 sec followed by washing with water for 60 sec. Subsequent incubation of “Bluing Reagent”

(ThermoScientific, Cat. No. 7301) for 30-60 sec was followed by washing with water for 60 sec. Counterstaining with Eosin solution was performed using 0.1 % Eosin solution for 1 min followed by washing with water for 10 sec, 80 % ethanol for 10 – 30 sec, 100 % ethanol for 1 min and 100 % toluol for 3 min. After that, the sections were covered with DEPEX (Serva, Cat. No. 18243), sealed with a 24 x 50 mm coverslip (Roth, Cat. No. 1871) and dried at room temperature overnight.

Eosin 0.1 % solution:

Eosin Y Solution aqueous (Sigma, Cat. No. HT110216-500ml)	20 ml
dd H_2O	80 ml
Acetic acid glacial	1 drop

5.2.6.3. Fast Green / Sirius Red staining

For Fast Green / Sirius Red staining of cardiac paraffin-embedded sections, deparaffinization and rehydration of the sections was performed by consecutive incubation in 100 % toluol for 2 x 10 min, 100 % ethanol for 2 x 5 min, 90 % ethanol for 5 min, 70 % ethanol for 5 min, 50 % ethanol for 5 min and water for 5 min. After that, the sections were incubated with preheated Bouin's solution for 1 hour at 58 °C and subsequently washed with water for 10 min until disappearance of the yellow color of the sections. After that, the sections were incubated in 0.1 % Fast Green solution at room temperature for 30 min. After rinsing with acetic acid 1 % for 60 sec and water for 5 min, sections were incubated in 0.1 % Sirius Red solution at room temperature for 30 min. Dehydration was performed by consecutive incubation in 70 % ethanol for 10 sec, 100 % ethanol for 60 sec and 100 % toluol for 3 min. After that sections were covered with DEPEX (Serva, Cat. No. 18243), sealed with a 24 x 50 mm coverslip (Roth, Cat. No. 1871) and dried at room temperature overnight.

Fast Green solution 0.1 %:

Fast Green FCF	500 mg
(Sigma, Cat. No. F7252-5G)	
ddH_2O	500 ml

Sirius Red solution 0.1 %:

Direct Red 80	50 mg
(Sigma, Cat. No. 365548-5G)	
ddH2O	15 ml
Filter solution	
Piric acid-saturated solution 1.3 %	485 ml
(Sigma, Cat. No. P6744-1GA)	

Acetic acid solution 1 %:

Acetic acid glacial	1 ml
(Roth, Cat. No. 3738.1)	
ddH2O	99 ml

5.2.6.4. Wheat germ agglutinin staining

For wheat germ agglutinin (WGA) staining of cardiac paraffin-embedded sections, deparaffinization was performed by consecutive incubation of sections in xylene for 2 x 4 min, 100 % ethanol for 2 min, 90 % ethanol for 2 min, 70 % ethanol for 2 min, 50 % ethanol for 2 min, H_2O for 1 min and PBS for 1 min. After that, the sections were incubated in 10 mM sodium citrate buffer and heated in the microwave for 4 min at 800 W followed by rinsing with PBS. Subsequently, hydrophobic barrier lines were drawn around the sections using a PAP PEN (Sigma, Cat. No. Z377821-1EA). WGA staining solution (Alexa Fluor® 647 conjugate, Life Technologies / Molecular Probes, Cat. No. W32466) was diluted 1 : 100 in PBS and incubated on the sections for 1.5 h at room temperature in a dark, humid incubation chamber followed by two-fold washing with PBS. After that, SYTOX® Green dye (Life Technologies / Molecular Probes, Cat. No. S7020) was diluted in PBS 1 : 1000 and incubated for 10 min in a dark, humid incubation chamber at room temperature followed by three-fold washing with PBS. Subsequently, sections were covered with Aquatex (Merck, Cat. No. 1.08562.0050), sealed with a 24 x 50 mm coverslip (Roth, Cat. No. 1871) and dried at room temperature for 1 h in the dark. After that, the sections were stored at 4°C in the dark until usage not exceeding one week.

<u>Sodium citrate buffer 10 mM:</u>

Tri sodium citrate (dihydrate)	2.94 g
(Roth, Cat. No. 3580.1)	
ddH_2O	1000 ml
HCl	ad pH 6.0
Tween 20	0.5 ml
(AppliChem, Cat. No. A4974,0250)	
Storage at 4 °C	

5.2.7. Cell culture

5.2.7.1. Preparation of adult cardiomyocytes and non-cardiomyocytes

For isolation of adult mouse cardiomyocytes and non-cardiomyocytes the mouse was heparinized by intraperitoneal injection of heparin (Ratiopharm) and after 5 min anesthetized by injection of 600 – 700 µl of avertin. After thoracotomy and isolation of the heart, the ascending aorta was tied to the plastic cannula of a perfusion system (Julabo, type 13, pump type EC-BRÜ-PU; Amersham Bioscience, type P1) using a stereo microscope. After manual filling of the heart with a syringe and perfusion buffer, the heart was perfused with pre-warmed perfusion buffer for 3 min at a constant flow of 4 x 10 ml/h. Subsequently, the hearts were perfused with digestion buffer for 5 min with a constant flow of 4 x 10 ml/h until the cardiac tissue adopted a pale color and soft and flaccid consistency. Then the atria were removed and the heart transferred into a beaker containing 2.5 ml digestion buffer followed by cutting the tissue in small pieces and shearing with an Omifix-F1 1ml syringe (Braun, Cat. No. 9161406) until complete dissolution of the heart. After addition of 2.5 ml P1 stop buffer, shearing was continued for another 3 min and cell solution filtered through a 100 µm cell strainer (Falcon® 100µm Cell Strainer (Corning, Ref. No. 352360; BD falcon, 100 µm pore size) into a 50 ml falcon. After that, the cell suspension was transferred to a fresh 15 ml tube and cells sedimented for 10 min in a 37°C warm water bath. The supernatant was carefully removed, centrifuged at 55 x g for 1 min and transferred to a new 15 ml tube for non-cardiomyocyte isolation. For subsequent cardiomyocyte isolation, the sediment from the 10 min sedimentation step and the pellet from the centrifugation are pooled in 10 ml of pre-warmed P2 stop buffer and transferred to a 25 ml flask. Calcium reconstitution was performed by addition of 50 µl CaCl 10 mM, then 50 µl CaCl 10 mM after 4 min incubation, 100 µl CaCl 10 mM after 4 min incubation, 30 µl CaCl 100 mM after 4 min incubation and 50 µl CaCl 100 mM after 4 min incubation. After that, sedimentation in a 15 ml falcon was performed for 10 min in the 37 °C water bath followed by centrifugation of the supernatant at 55 x g for 1 min. The sediment and the pellet were then pooled in 3 ml pre-warmed plating medium and seeded on a laminin-coated 6 cm plate and incubated for 1 h at 37 °C and 5 % CO_2. Laminin coating was performed by incubation of 333 µl laminin (BD Bioscience, Cat. No. 354232, 1mg) solution with 1200 µl DPBS for 1h at 37 °C. For isolation of the non-cardiomyocytes, the non-cardiomyocytes containing supernatant from the cardiomyocyte

isolation was centrifuged for 5 min at 1200 rpm. After discard of the supernatant, the residual non-cardiomyocyte pellet was dissolved in 5 ml 5 % AMCF plating/culture medium on a 6 cm cell culture dish and incubated at 37 °C and 1 % CO_2 for 1 h. After plating for 1 h, both the cardiomyocytes containing dishes and the non-cardiomyocytes containing dishes were rinsed carefully with DPBS and frozen at – 80°C until usage.

Perfusion buffer stock (1X):

NaCl	6.6 g
(Sigma, Cat. No. S9625)	
KCl	0.35 g
(Sigma, Cat. No. P4504)	
KH_2PO_4	0.082 g
(Sigma, Cat. No. P5379)	
Na_2HPO_4	0.085 g
(Sigma, Cat. No. S0876)	
$MgSO_4$ x $7H_2O$	0.3 g
(Sigma, Cat. No. M9397)	
Phenol Red	0.012 g
(Sigma, Cat. No. P5530)	
$NaHCO_3$	1.01 g
(Sigma, Cat. No. S5761)	
$KHCO_3$	1.01 g
(Sigma, Cat. No. P9144)	
Hepes buffer 1 M	10 ml
(Sigma, Cat. No. H0887)	

Taurine	3.75 g
(Sigma, Cat. No. T0625)	
Purified H_2O	ad 1 l
Filter with 0.22 μm filter	
(Corning, Cat. No. 430624)	
Store at 4 °C	

Perfusion buffer:

Perfusion buffer stock (1X)	490 ml
BDM (500 mM)	10 ml
(Sigma, Cat. No. B0753)	
Glucose 5 %	10 ml
(Sigma, Cat. No. G7528)	

Digestion buffer:

Perfusion buffer	50 ml
Collagenase type 2 (280 U/mg)	107 mg
(Worthington, Ref. No. LS004174)	
$CaCl_2$ 100 mM	15 μl

P1 stop buffer:

Perfusion buffer	9 ml
FCS	1 ml
(PAN Biotech, Cat. No. 3302-P282905)	

$CaCl_2$ 10 mM	12.5 µl

P2 stop buffer:

Perfusion buffer	47.5 ml
FCS	1 ml
(PAN Biotech, Cat. No. 3302-P282905)	
$CaCl_2$ 10 mM	62.5 µl

AMCM plating medium:

MEM	45.5 ml
(Gibco, Cat. No. 21575)	
FCS	2.5 ml
(PAN Biotech, Cat. No. 3302-P282905)	
BDM (500 mM)	1 ml
(Sigma, Cat. No. B0753)	
Penicillin/Streptomycin	0.5 ml
(Pan Biotech, Cat. No. P06-07100)	
L-Glutamine (200 mM)	0.5 ml
(Pan Biotech, Cat. No. P04-80100)	

AMCF incomplete medium:

MEM	10.8 g
(Gibco, Cat. No. 21575)	
Vitamin B12	1 ml

NaHCO3	350 mg
(Merck, Cat. No. 6329)	
H2O	ad 1 l
pH	adjust to 7.3
sterile filtering	
store at 4 °C	
AMCF 5 % medium:	
FCS	25 ml
Penicillin/Streptomycin	5 ml
(Pan Biotech, Cat. No. P06-07100)	
Incomplete medium	ad 500 ml

5.2.7.2. Preparation of neonatal rat cardiomyocytes (NRCMs)

For the preparation of neonatal rat cardiomyocytes, newborn rats are cleaned with 70 % ethanol, decapitated, thorax opened, heart isolated and put in a 50 ml falcon tube (Sarstedt, Nümbrecht, Ref. 62.548.004) containing 15 ml CBFHH buffer on ice. Subsequently, the atria of the heart were removed in a 10 cm cell culture dish containing CBFHH medium on ice and cleaned hearts transferred to a fresh 6 cm well containing CBFHH. After pressing out the residual blood from the ventricles, the heart was carefully transferred to a fresh, empty 6 cm dish and was cut into small pieces. After that, a 10 ml pre-warmed trypsin solution was added to the hearts and two autoclaved beakers, containing a magnetic stirrer, were filled each with 5 ml of the solution. Subsequently, 10 ml trypsin solution were added and, after stirring for 15 min, the supernatant was discarded and the trypsin step was repeated. After that, 15 ml trypsin solution were added, cells stirred for 10 min and pipetted up and down for 10 times using a mouth pipette (BD, Cat. No. 357550). After that, the supernatant was transferred to fresh tubes willed with pre-warmed 7.5 ml FCS. Consecutively, the tubes were centrifuged at 800 g and room temperature for 10 min, supernatant discarded and 10 ml of

pre-warmed preplating medium were added. After that, the solution was put onto a cell strainer with 40 μm pores (BD, Cat. No. 352340) and the filtrate was diluted with warm preplating medium, transferred to fresh 10 cm plates and incubated at 37 °C and 1 % CO_2 for 1 h in a cell incubator. For coating of the plates, polylysine was incubated on the dishes at room temperature for 1 h. After incubation plates were rinsed with PBS and put in the incubator for pre-warming. The cell suspension was subsequently collected in a 50 ml tube and 10 μl of the suspension were mixed with 10 μl trypan blue for consecutive cell counting in the cell counter. For culture, the cells are then seeded in culture medium in the desired density and incubated at 37 °C and 1 % CO_2.

NaCl stock solution:

NaCl	20 g
(AplliChem, Cat. No. A1371,5000)	
H_2O	ad 100 ml

Store at 4 °C

KCl stock solution:

KCl	4 g
(AplliChem, Cat. No. A3582,1000)	
H_2O	ad 100 ml

Store at 4 °C

$MgSO_4$ x $7H_2O$ stock solution:

$MgSO_4$ x $7H_2O$	2 g
(Merck, Cat. No. A105086840)	
H_2O	ad 100 ml

Store at 4 °C

KH_2PO_4 stock solution:

KH_2PO_4	600 mg
(Roth, Cat. No. 3904.1)	
H_2O	ad 100 ml

Store at 4 °C

$Na_2HPO_4 \times 7H_2O$ stock solution:

$Na_2HPO_4 \times 7H_2O$	900 mg
(Merck, Cat. No. K33946475716)	
H2O	ad 100 ml

Store at 4 °C

Calcium and bicarbonate free Hanks with Hepes (CBFHH):

NaCl stock	40 ml
KCl stock	10 ml
$MgSO_4 \times 7H_2O$ stock	10 ml
KH_2PO_4 stock	10 ml
$Na_2HPO_4 \times 7H_2O$ stock	10 ml
HEPES	4.76 g
(AppliChem, Cat. No. A1069,1000)	
Glucose	1 g
(Merck, Cat. No. 8342)	

H_2O	ad 1 l
ph ad 7.30 with NaOH	
sterile filtering	
Penicillin/Streptomycin	5 ml
(Pan Biotech, Cat. No. P06-07100)	

DNase:

DNase	100 mg
(Sigma, Cat. No. DN-25-100MG)	
NaCl 0.9 %	50 ml
Sterile filtering	
Store at – 20 °C	

Vitamin B12:

Vitamin B12	100 mg
(Sigma, Cat. No. V-2876-100MG)	
H_2O	50 ml
Sterile filtering	
Store at – 20 °C	

Bromdesoxyuridin (BrdU):

BrdU	230 mg
(Sigma, Cat. No. B5002-1G)	
H_2O	74.8 ml

Sterile filtering

Store at – 20 °C

Trypsin solution:

Difco Trypsin 250	320 mg
(BD, Cat. No. 212540-100G)	
PAN Trypsin	80 mg
(PAN, Cat. No. P10-025025P)	
CBFHH	198 ml
DNase	2 ml

Sterile filtering

NRCM medium incomplete:

MEM	10.8 g
(Sigma, Cat. No. M1018-10L)	
Vitamin B12	1 ml
$NaHCO_3$	350 mg
(Merck, Cat. No. 6329)	
H_2O	ad 1 l

pH adjust to 7.3

sterile filtering

store at 4 °C

NRCM culture medium FCS 5 %:

FCS	25 ml
(PAN Biotech, Cat. No. P30-3302)	
Penicillin/Streptomycin	5 ml
BrdU	5 ml
NCRM medium incomplete	ad 500 ml

Store at 4 °C

NRCM culture medium FCS 1 %:

FCS	5 ml
Penicillin/Streptomycin	5 ml
BrdU	5 ml
NCRM medium incomplete	ad 500 ml

Store at 4 °C

NRCM culture medium FCS 1 % (w/o BrdU):

FCS	5 ml
Penicillin/Streptomycin	5 ml
NCRM medium incomplete	ad 500 ml

Store at 4 °C

Preplating Medium FCS 5 %:

FCS	25 ml
Penicillin/Streptomycin	5 ml

NCRM medium incomplete	ad 500 ml

Store at 4 °C

Polylysin:

Polylysin	5 mg
(Sigma, Cat. No. P6407-5MG)	
PBS	200 ml
(PAN Biotech, Cat. No. P04-36500)	

Store at 4 °C

Trypan Blue:

Trypan Blue	50 mg
(AppliChem, Cat. No. A0668,0025)	
NaCl 0.9 %	10 ml

5.2.7.3. siRNA knockdown of *Cul7* in NRCM

Depletion of protein abundance in cells by siRNA interference is a common mechanism to elucidate its target protein function. After transfection of the siRNA molecule, it targets its complementary mRNA strain in the cell, which after formation of the RISC complex is degraded resulting in the reduction of mRNA translation and thus protein abundance. For knockdown of *Cul7* in NRCMs ON-TARGET plus SMART pool (Thermo Scientific, Cat. No. L-05471-01-0005) siRNA was used. As a negative control, ON-TARGET plus non-targeting pool (Thermo Scientific, Cat. No. D-001810-10-20) was used. For a final concentration of 20 μM, the siRNA was diluted in 4/5 of the respective amount of RNase free water (life technologies, gibco, Cat. No. 10977-035) and 1/5 of 5 X siRNA Buffer (Thermo Scientific, Cat. No. B-002000-UB-100).

Characteristics of siRNA:

Name	Target Name	Target Sequence	Molecular weight	Ext. Coeff.
ON-TARGET plus SMART pool siRNA J-054741-09, Cul7	Cullin7	CCGAAGU CCUGGUA GGGCA	13474.9 (g/mol)	356712 (L/mol cm)
ON-TARGET plus SMART pool siRNA J-054741-10, Cul7	Cullin7	GCCACAA GAUGCUG GGCGA	13 747.9 (g/mol)	351995 (L/mol cm)
ON-TARGET plus SMART pool siRNA J-054741-11, Cul7	Cullin7	CAGAGGA GUUGCAG CGUCA	13 459.9 (g/mol)	357958 (L/mol cm)
ON-TARGET plus SMART pool siRNA J-054741-12, Cul7	Cullin7	CUACAGA GCCUGAA CGUCU	13 444.8 (g/mol)	367125 (L/mol cm)
ON-TARGET plus Non-targeting pool	Negative control	-	-	-

For knockdown verification, 600 000 NRCMs were seeded on a 12 well plate in 2 ml of 5 % FCS NRCM medium and incubated at 1 % CO_2 and 37 °C for 20 h. After that, 50 pmol of siRNA / non targeting control were diluted in 250 µl OptiMEM I serum-reduced medium (Invitrogen, Cat. No. 31985-047) in one tube and 2.5 µl Lipofectamine 2000 (Invitrogen, Cat. No. 11668-027) mixed with 247.5 µl OptiMEM I in a separate tube. After 5 min of incubation at room temperature, the siRNA mix / non-targeting mix was added to the Lipofectamine 2000 mix and incubated for 20 min at room temperature. During this incubation time, the medium on the NRCM cells was changed twice to 500 µl 5 % FCS NRCM medium w/o PS. Subsequently, 500 µl of the transfection mix was added to the cells and incubation continued for 5 h at 1 % CO_2 and 37 °C. After incubation, the medium was changed to 1 % FCS NRCM medium 1 % P/S and the culture was continued for 48 h at 1 % CO_2 and 37 °C. 1 % FCS medium was used for higher RNA yield and better viability. After 48 h, the RNA was isolated as described above and qPCR for Cul7 and GAPDH was performed.

5.2.7.4. Hypertrophy assay of neonatal rat cardiomyocytes

For assessment of hypertrophy of NRCM in response to (R)-(-)-phenylephrine hydrochloride (Sigma, Cat. No. P6126) under conditions of presence or absence of CUL7, 50000 NRCM per well were seeded in a 96 well plate (IBDI, Cat. No. 89606) and incubated for 20 h at 37°C and 1 % CO_2 in 1 % FCS NRCM medium. The transfection was performed as described above in respect of down-scaling to the surface area of the cell culture dish, also resulting in a final siRNA / negative control concentration of 50 nM per dish. Additionally, a mock control containing only Lipofectamine 2000 was included. After incubation for 5 h, the medium was changed to 0.1 % FCS NRCM 1 % P/S medium and the culture was continued for 48 h at 37 °C and 1 % CO_2. For basal conditions medium was replaced after 48 h with 0.1 % FCS NRCM medium and incubation continued for 48 h, while for stimulation conditions the medium was changed to 0.1 % FCS NRCM medium containing (R)-(-)-phenylephrine hydrochloride (Sigma, Cat. No. P6126) at a final concentration of 50 mM. After that, the plates were washed with PBS and 75 µl 4 % PFA was added to each well followed by incubation for 5 min at room temperature. After threefold rinsing with PBS, the cells were stored in PBS at 4°C. For staining of the cells, a permeabilization was achieved by incubation with 50 µl of 0.2 % Triton-X solution for 5 min. After threefold washing with PBS, 75 µl of 1 : 1000 anti-alpha-actinin antibody (Sigma, Cat. No. A7811, Clone EA-53)

were added and incubation was continued for 30 min at 37 °C in a humid chamber. Subsequently, the cells were washed threefold with PBS, 75 µl of 1 : 400 secondary antibody goat anti-mouse IgG (H+L), Alexa 488 (Invitrogen, Cat. No. A11029) and 75 µl of 4',6-diamindino-2-phenylindole dihydrochloride (DAPI) (Sigma, Cat. no. D9542) 1 : 200 were added and incubation was continued for 30 min at 37 °C in a dark humid chamber. After washing with PBS, 75 µl Glycerol were added, plates sealed with sealing tape (Sarstedt Cat.-no. 95.1995) and stored at 4 °C in the dark. For positive area analysis pictures were taken using fluorescence microscopy and analyzed with the Metamorph software.

5.3. Physical characterization of animals

5.3.1. Phenotyping

For phenotyping, mice were sacrificed at the desired age by cervical dislocation. Mice were weighted using a scale. After thoracotomy heart was removed and heart weight determined using a precision scale. After removal of the atria, the ventricle weight was determined. Lung weight was also determined after cleaning the lungs from blood clots. For measurement of the tibia length, tibias were digested in Phenol/Chloroform digestion buffer containing Proteinase K 10mg/ml (AppliChem, A3830,0100) as described above. After removal of all residual tissue, the length was determined using a precision sliding caliper.

5.3.2. Echocardiographic evaluation of cardiac function

For evaluation of cardiac function, mice were anesthetized using 1 % isoflurane applied with a facial mask. Mice were then placed on a warming pad in supine position and cardiac function was assessed using the Vevo 770 ultrasonic machine (VisualSonics, FUJIFILM). First, the left ventricle was focused in the long axis with the aorta being in the horizontal level of the cavity of the left ventricle in B-Mode. Then after switching to the short axis with focusing on the papillary muscles, the movements of the left ventricle are assessed in M-Mode. Diastolic and systolic dimensions were measured and fractional shortening (FS)

calculated by the ratio of the difference of the end-diastolic diameter (EDD) and the end-systolic diameter (ESD) with the end-diastolic diameter (EDD).

$$FS = \frac{EDD - ESD}{EDD} \times 100\%$$

5.3.3. Timeline of experimental design

For characterization under basal conditions, mice were injected on five consecutive days with tamoxifen intraperitoneally as described above. Assessment of cardiac function was performed in intervals of two weeks. Finally, animals were sacrificed at the age of 14 weeks to perform phenotyping and histological investigation (Timeline A).
For assessment of the impact of increased afterload, TAC was performed at the age of 8 weeks and subsequently, characterization was performed by echocardiography, phenotyping and histological investigation (Timeline B).

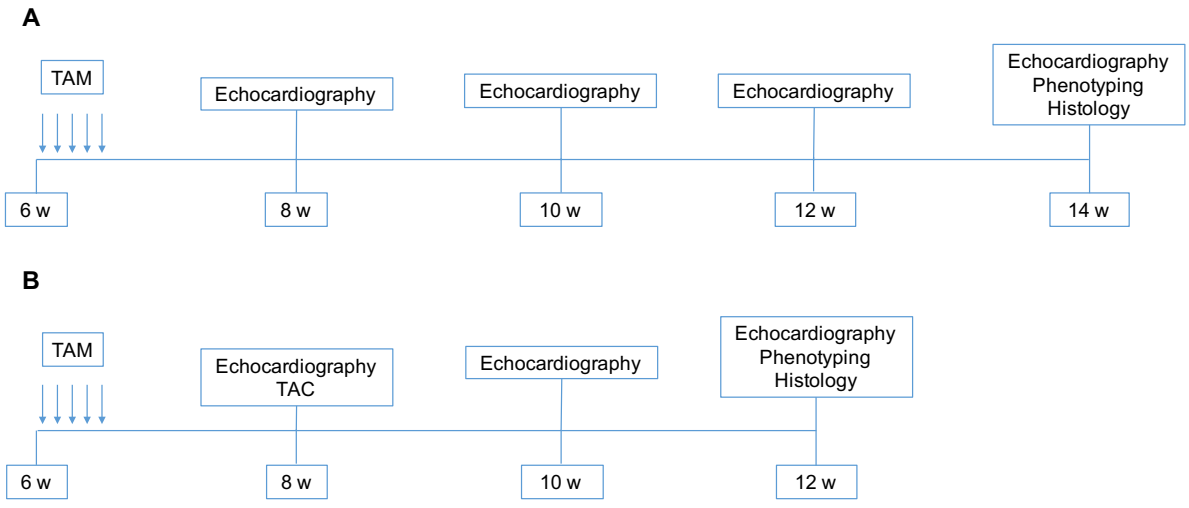

Figure 4: Experimental timeline for the characterization under basal conditions (A) and under conditions of increased afterload by TAC (B).

5.3.4. Statistics

The presented data is depicted as the mean ± standard deviation (SD) if not indicated otherwise. Statistical testing was performed using Prism (Version 6, GraphPad Software, Inc., California). For comparison of two means, student's t-test (2-tailed) was used. For the comparison of multiple means, the ANOVA test (Bonferroni correction) was used. A p-value of <0.05 was considered as statistically significant.

6. Results

6.1. Expression of the Cullin7 protein in different murine tissues

To investigate the expression of the Cullin7 protein in different types of murine tissue, samples were isolated from male wild-type C57BL/6 mice at the age of 8 weeks. Therefore, heart, skeletal muscle (M. gastrocnemius), smooth muscle (urinary bladder), pancreas, lung, liver, kidney, adipose tissue, testis, brain and spleen were isolated, lysed and subsequently immunoblot against CUL7 was performed.

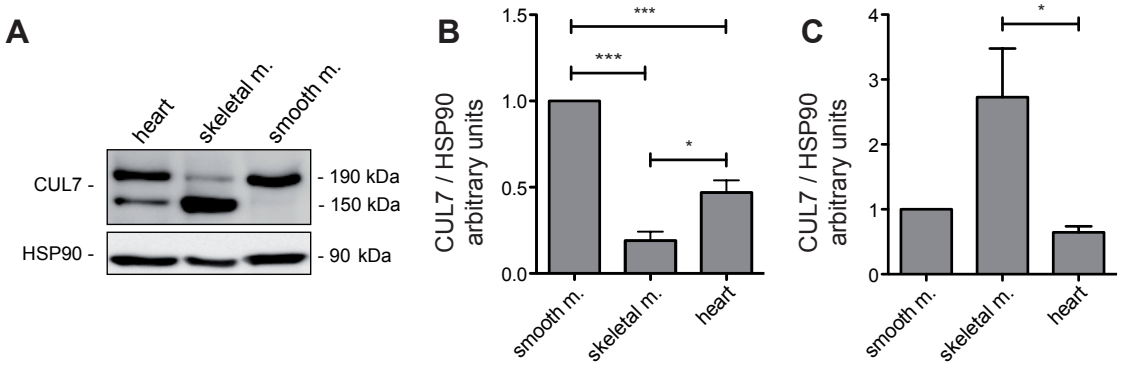

Figure 5: Expression of the Cullin7 protein in different types of muscle tissues.

Immunoblot directed against CUL7 and HSP90 as a loading control. Representative picture of an immunoblot against CUL7 in heart, skeletal muscle and smooth muscle in wild type mice (Fig.5 A). Quantification of protein abundance of CUL7 at 190 kDa; N=3 (Fig. 5 B). Quantification of CUL7 protein abundance at 190 kDa and 150 kDa; N=3 (Fig. 5 C).

Figure 5 shows the expression of CUL7 in different types of muscle tissue. At the expected migration front of the Cullin7 protein of 190 kDa, a high protein abundance in the cardiac muscle and the smooth muscle was evident, while the abundance in skeletal muscle tissue was reduced (0.47 ± 0.12 vs. 1 ± 0, vs. 0.19 ± 0.09; n=3). The inclusion of a hypothetic

isoform at 150 kDa resulted in higher CUL7 expression in skeletal muscle when compared to smooth muscle and heart muscle, respectively (2.72 ± 1.3 vs. 1 ± 0 vs. 0.64 ± 0.16; n=3). Furthermore, for both, the cardiac muscle and for skeletal muscle there was a strong band at the migration height of 150 kDa, which was not evident in smooth muscle tissue. When comparing to other tissue samples, there was a robust expression of CUL7 in all parenchymatous organs and the brain (Fig. 6). Interestingly, none of these tissues showed a prominent band at the height of 150 kDa as observed in heart muscle and skeletal muscle. In conclusion, CUL7 was robustly expressed ubiquitously in all murine tissues exanimated. Furthermore, we raised evidence for a tissue-specific isoform of the CUL7 protein with expression restricted to striated muscle tissue.

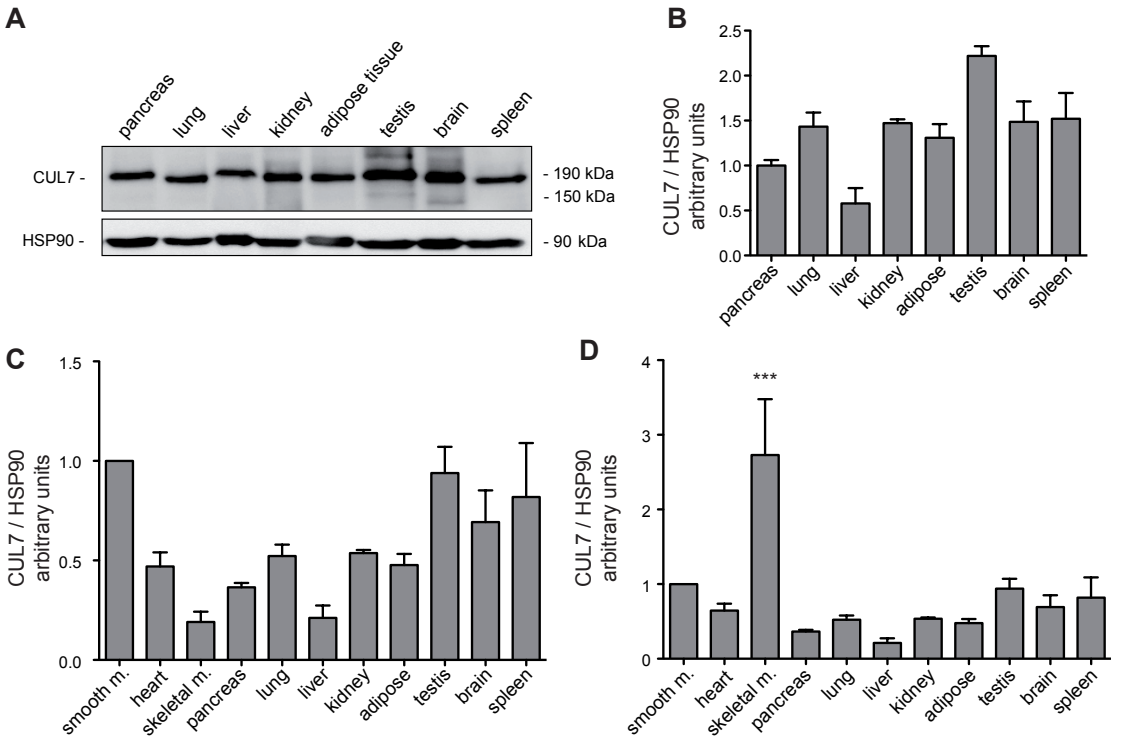

Figure 6: Expression of CUL7 in different parenchymatous tissues.

Representative immunoblot directed against CUL7 and HSP90 as a loading control (Fig. 6 A). Quantification of CUL7 abundance in parenchymatous tissue (Fig. 6 B). Quantification of protein abundance of CUL7 at 190 kDa

(Fig. 6 C). Quantification of CUL7 protein abundance at 190 kDa and 150 kDa (Fig. 6 D). N=3. Statistics: ANOVA. ***: p<0.001.

To further elucidate the expression of CUL7 in cardiac muscle tissue, cardiomyocytes were isolated from male wild-type C57BL/6 mice at the age of 8 weeks and protein expression studied in comparison to the non-cardiomyocyte cell fraction. CUL7 was expressed in both the cardiomyocyte cell fraction and the non-cardiomyocyte cell fraction. Quantification revealed an equal expression level in both cell fractions (1.00 ± 0.40 vs. 1.16 ± 0.45; n=6; p=0.53). Interestingly, the additional band for CUL7 at 150 kDa was only detectable in the cardiomyocyte cell fraction and not in the non-cardiomyocyte cell fraction, further underlining its restricted expression to striated muscle cells, in this case, cardiomyocytes in the cardiac tissue.

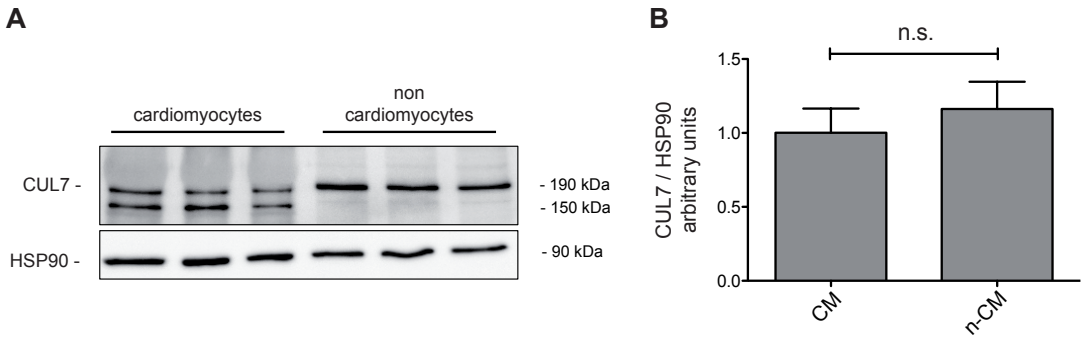

Figure 7: Expression of CUL7 in different cell fractions in cardiac tissue.

CUL7 expression in cardiomyocytes (Fig. 7 A; lane 1-3) and non-cardiomyocytes (n-CM, e.g. fibroblasts) (Fig. 7 A; lane 4-6) Quantification of CUL7 abundance (Fig. 7 B). N=6. Representative picture shown. Statistics: t-test.

Taken together, the CUL7 protein was expressed robustly in all analyzed types of murine tissue, with exception of the cardiac tissue and skeletal muscle, the latter showing only weak expression at 190 kDa but a strong protein abundance at 150 kDa. In the heart, those signals at 190 kDa and 150 kDa are more equally distributed. When differentiating CUL7 protein expression in cardiomyocytes and non-cardiomyocytes the two distinct signals were

only present in the CM cell fraction supporting evidence for the existence of a tissue-specific CUL7 isoform restricted to striated muscle tissue as shown in skeletal muscle as well as cardiomyocytes.

6.2. Depletion of CUL7 in cardiomyocytes

To validate recombination events reflecting Cre-loxP mediated deletion of Exons 2 to 4 of the *Cul7* gene, genomic DNA was isolated from purified cardiomyocytes of male transgenic mice 3 weeks after Tamoxifen injection and PCR for recombination was performed as described above. An amplification product was only detectable in $Cul7^{flox/flox}$; Myh6-$MerCreMer^{Tg(1/0)}$ animals, whereas in DNA obtained from $Cul7^{+/+}$; Myh6-$MerCreMer^{Tg(1/0)}$ and $Cul7^{flox/flox}$; Myh6-$MerCreMer^{Tg(0/0)}$ sufficient amplification was not evident.

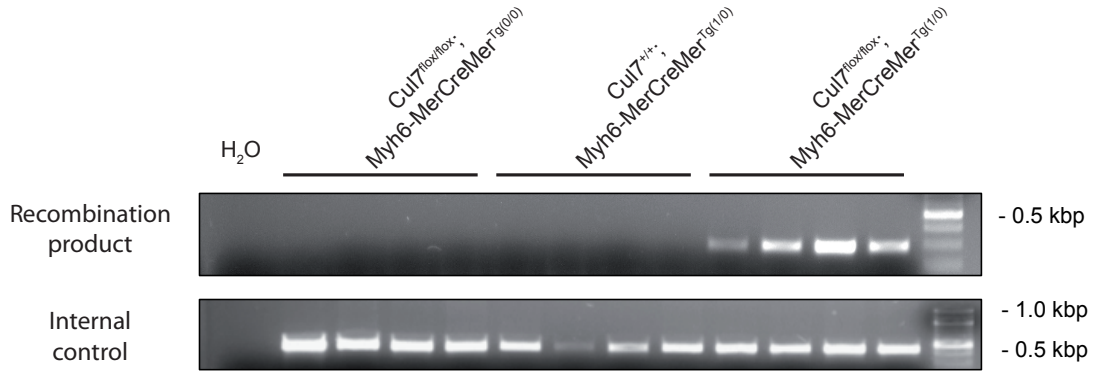

Figure 8: Validation of Cre-loxP mediated gene recombination via PCR.

Agarose gel for PCR directed against recombination sites after tamoxifen injection in DNA samples from isolated cardiomyocytes.

For verification of CUL7 depletion in cardiac tissue, male transgenic mice were injected with Tamoxifen at a dose of 40 mg/kg body weight intraperitoneally at 6 weeks of age, and hearts were isolated at the age of 12 weeks. Subsequently, whole heart tissue lysates were prepared and CUL7 expression was assessed by immunoblotting. The CUL7 abundance in

the hearts isolated from Cul7$^{flox/flox}$; Myh6-MerCreMer$^{Tg(1/0)}$ animals was significantly reduced to 0.287 ± 0.11 (n=4; p<0.01) when compared to the respective Cul7$^{+/+}$; Myh6-MerCreMer$^{Tg(1/0)}$ control animals with 1.00 ± 0.35 (n=4) (Fig. 9).

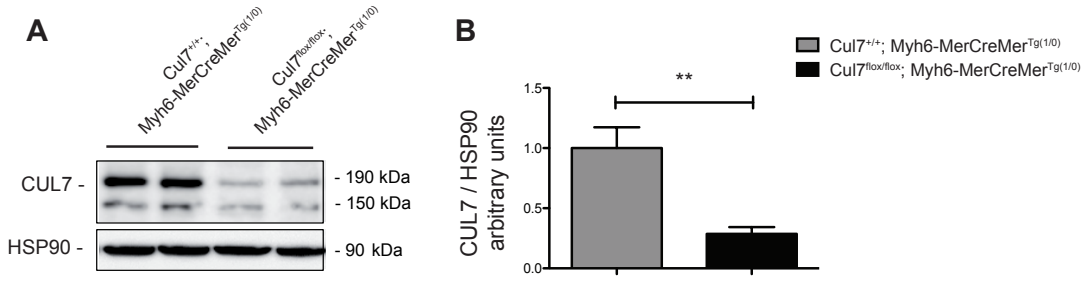

Figure 9: Expression of the CUL7 in whole heart samples after induction of CUL7 depletion.

Immunoblot against the CUL7 in whole hearts from Cul7$^{flox/flox}$; Myh6-MerCreMer$^{Tg(1/0)}$ mice and respective controls (Fig. 9 A). Quantification of CUL7 abundance (Fig. 9 B). N=4. Representative immunoblot depicted. Statistics: t-test, *: p<0.05, **: p<0.01.

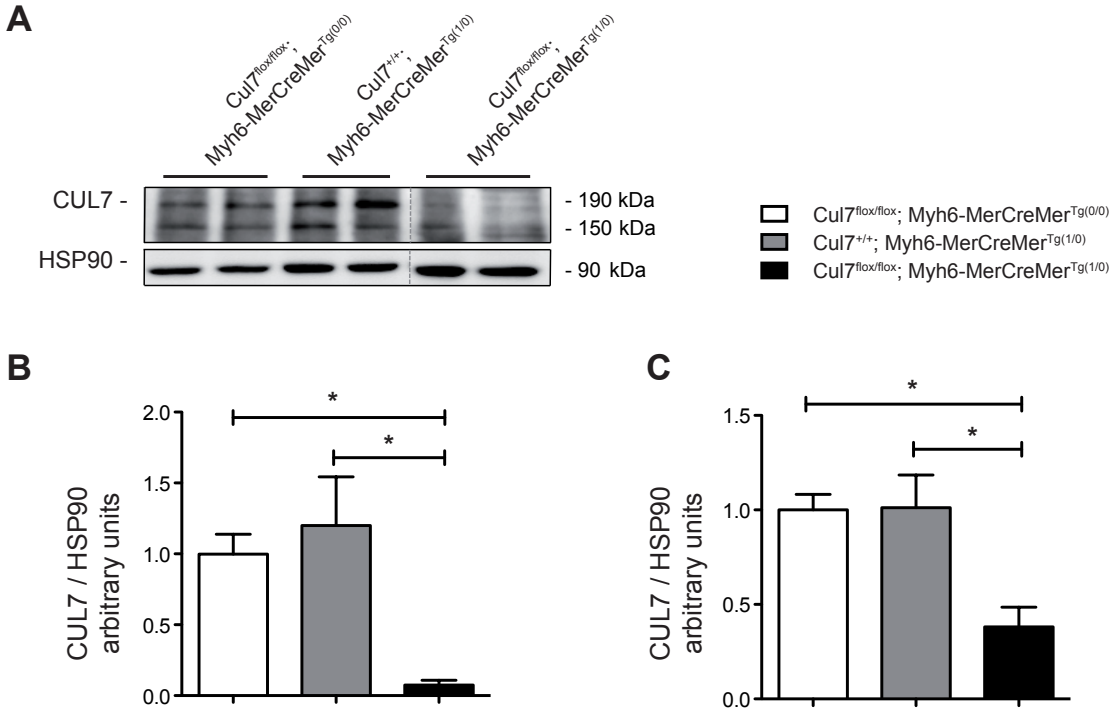

Figure 10: Expression of the CUL7 in the cardiomyocyte cell fraction after induction of recombination.

Immunoblot of CUL7 expression in cardiomyocytes of Cul7$^{flox/flox}$; Myh6-MerCreMer$^{Tg(1/0)}$ animals compared with respective Cul7$^{flox/flox}$; Myh6-MerCreMer$^{Tg(0/0)}$ and Cul7$^{+/+}$; Myh6-MerCreMer$^{Tg(1/0)}$ controls (Fig. 10 A). Quantification of protein abundance of CUL7 at 190 kDa (Fig. 10 B). Quantification of CUL7 protein abundance at 190 kDa and 150 kDa (Fig. 10 C). Representative immunoblot shown. N=4. Statistics: ANOVA, *: $p<0.05$.

To get a more detailed picture of the CUL7 depletion, the expression of CUL7 was evaluated in the cardiomyocyte and the non-cardiomyocyte cell fraction of the heart. The CUL7 protein expression in cardiomyocytes isolated from Cul7$^{flox/flox}$; Myh6-MerCreMer$^{Tg(1/0)}$ hearts was found to be significantly reduced to 0.075 ± 0.07 compared to both the cardiomyocytes of Cul7$^{+/+}$; Myh6-MerCreMer$^{Tg(1/0)}$ (1.2 ± 0.69; $p<0.05$) and Cul7$^{flox/flox}$; Myh6-MerCreMer$^{Tg(0/0)}$ control animals (1.0 ± 0.28; $p<0.05$) (Fig. 10). In contrast to this, CUL7 expression was unchanged in the non-cardiomyocyte cell fraction in Cul7$^{flox/flox}$; Myh6-MerCreMer$^{Tg(1/0)}$ mice (1.16 ± 0.12) when compared to Cul7$^{+/+}$; Myh6-MerCreMer$^{Tg(1/0)}$ (1.40 ± 0.19) or Cul7$^{flox/flox}$; Myh6-MerCreMer$^{Tg(0/0)}$ controls (1.00 ± 0.22), respectively (Fig. 11). Furthermore, not only the band at 190 kDa reflecting the by now described Cullin7 protein was reduced in depleted animals in comparison to respective controls, but also the signal at

150 kDa was significantly reduced in the cardiomyocyte cell fraction of Cul7$^{flox/flox}$; Myh6-MerCreMer$^{Tg(1/0)}$ mice hearts to 0.38 ± 0.21 ($p<0.05$) when compared to Cul7$^{+/+}$; Myh6-MerCreMer$^{Tg(1/0)}$ (1.01 ± 0.35) and Cul7$^{flox/flox}$; Myh6-MerCreMer$^{Tg(0/0)}$ controls (1.00 ± 0.17), further supporting the existence of a CUL7 protein isoform.

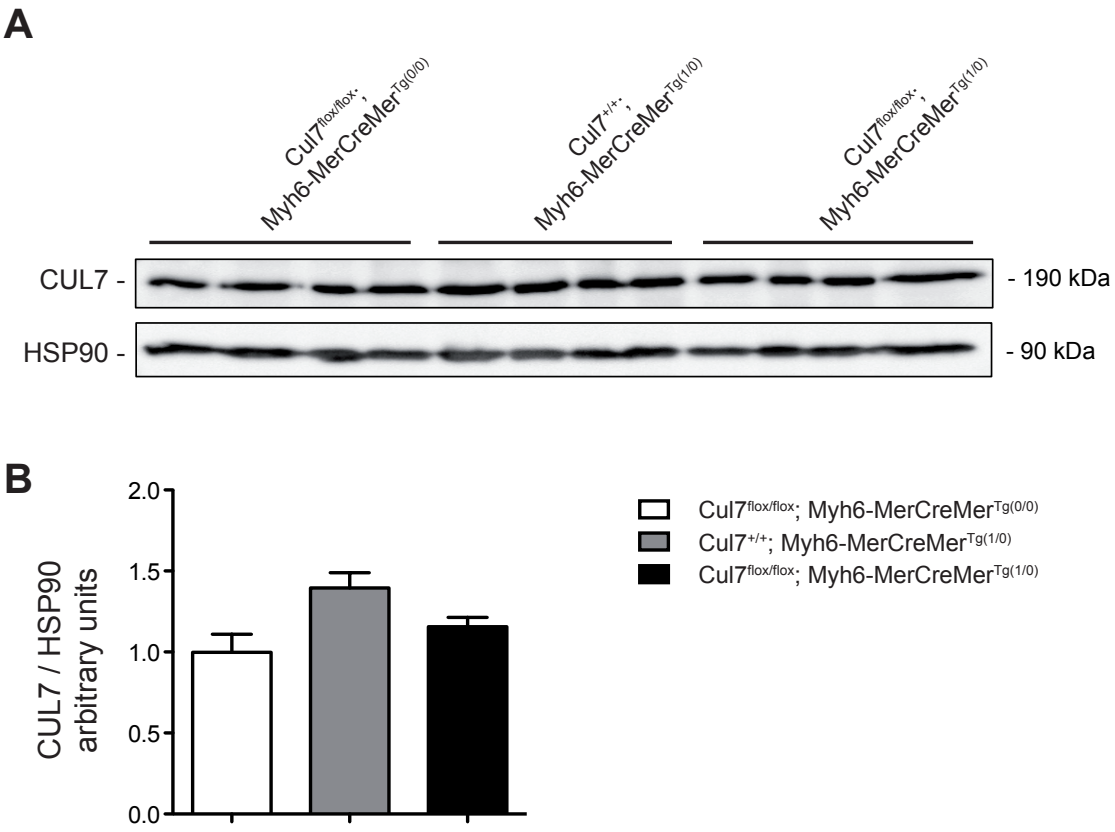

Figure 11: Expression of CUL7 in the non-cardiomyocyte cell fraction after induction of recombination.

Immunoblot of the CUL7 protein expression in non-cardiomyocytes in Cul7$^{flox/flox}$; Myh6-MerCreMer$^{Tg(1/0)}$ animals compared with respective Cul7$^{flox/flox}$; Myh6-MerCreMer$^{Tg(0/0)}$ and Cul7$^{+/+}$; Myh6-MerCreMer$^{Tg(1/0)}$ controls (Fig. 11 A). Quantification of protein abundance of CUL7 at 190 kDa (Fig. 11 B). Representative immunoblot shown. N=4. Statistics: ANOVA, *: $p<0.05$.

In conclusion, CUL7 depletion was sufficiently mediated by intraperitoneal injection of tamoxifen at a dose of 40 mg/kg bodyweight in Cul7$^{flox/flox}$; Myh6-MerCreMer$^{Tg(1/0)}$ animals compared to respective control animals. Additionally, this reduction was specifically observed in the cardiomyocyte cell fraction of the heart and the protein expression in non-cardiomyocytes remained unchanged. Furthermore, depletion of the additional CUL7 signal

in the immunoblot at 150 kDa raised evidence for the existence of at not yet described tissue-specific CUL7 isoform.

6.3. Phenotyping of Cullin7$^{-/-}$ mice under basal conditions

To assess the impact of the cardiomyocyte-specific depletion of the *Cul7* gene, mice were examined at the age of 14 weeks, corresponding to a duration of CUL7 depletion of 8 weeks. Therefore, the mice were sacrificed and heart weight, ventricular weight, lung weight, tibia length and body weight measured. At this time point no significant difference in heart weight / tibia length, ventricular weight / tibia length, lung weight / tibia length or body weight between the different genotypes was detectable (Fig. 12).

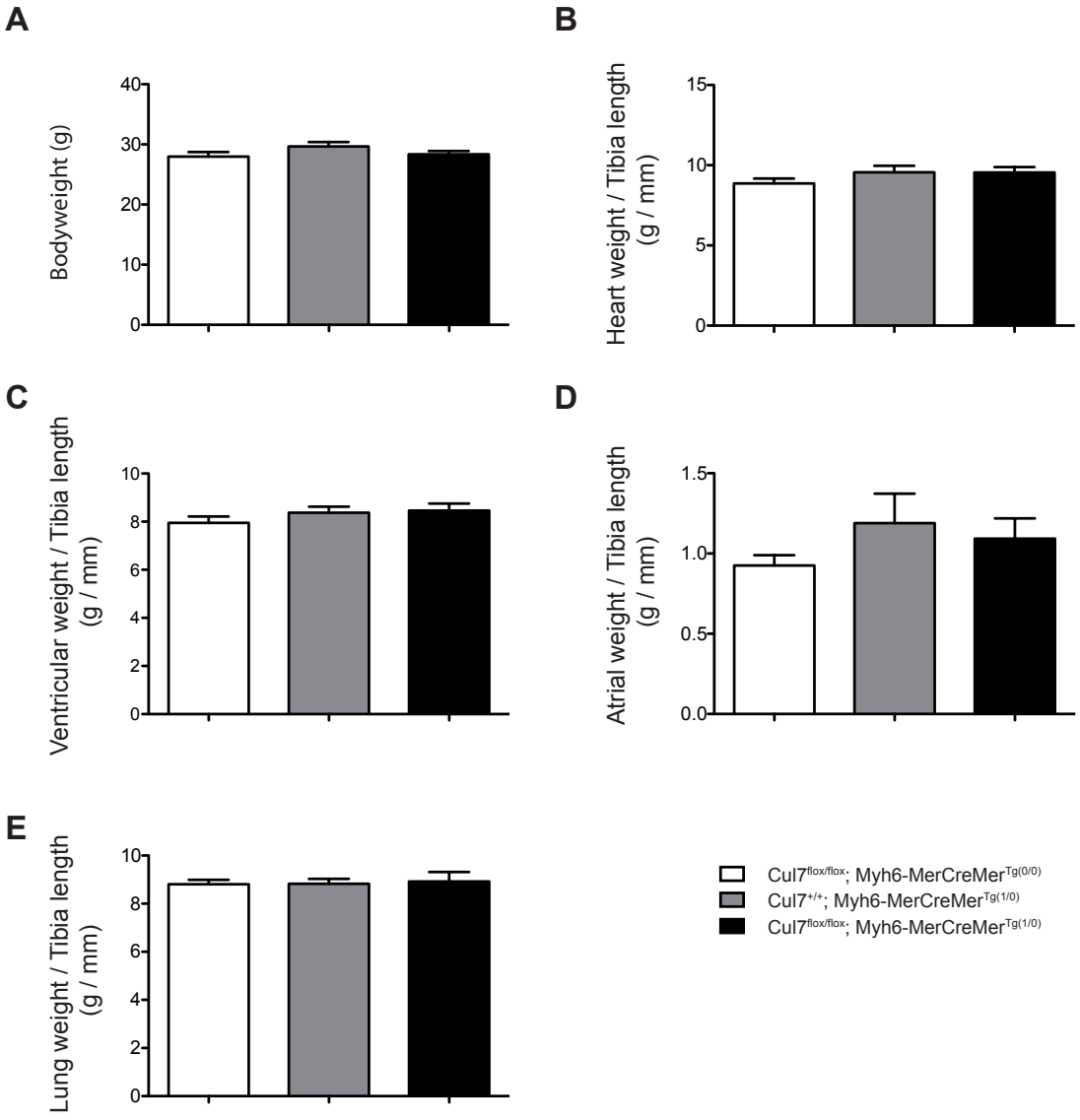

Figure 12: Phenotyping of Cullin7$^{-/-}$ mice under basal conditions.

Phenotypical characterization at the age of 14 weeks, corresponding to a CUL7 depletion duration of 8 weeks by assessment of body weight (Fig, 12 A), heart weight / tibia length (Fig. 12 B), ventricular weight / tibia length (Fig. 12 C), atrial weight / tibia length (Fig. 12 D) and lung weight / tibia length (Fig. 12 E). N=7-8. Statistics: ANOVA.

6.4. Cardiac function of Cullin7$^{-/-}$ mice under basal conditions

To assess the impact of the cardiomyocyte-specific inducible depletion of the CUL7 protein on cardiac function, echocardiographic evaluation was performed at the age of 8, 10, 12 and 14 weeks corresponding to a CUL7 depletion duration of 2, 4, 6 and 8 weeks, respectively. At the age of 8 weeks no significant difference in fractional shortening (16.4 ± 3.9 % vs. 17.3 ± 5.0 %) or ejection fraction (34.6 ± 7.5 % vs. 36.0 ± 9.6 %) was detectable between Cul7$^{+/+}$; Myh6-MerCreMer$^{Tg(1/0)}$ and Cul7$^{flox/flox}$; Myh6-MerCreMer$^{Tg(1/0)}$ animals, both of which displaying a marked depression of EF and FS. With increasing time of CM-specific CUL7 depletion, at the age of 10 weeks, there was an increase in both the ejection fraction (51.1 ± 3.8 % vs. 43.2 ± 8.4 %) and the fractional shortening (25.7 ± 2.3 % vs. 21.2 ± 4.8 %) in Cul7$^{flox/flox}$; Myh6-MerCreMer$^{Tg(1/0)}$ mice when compared to Cul7$^{+/+}$; Myh6-MerCreMer$^{Tg(1/0)}$ controls, reaching statistical significance at 12 weeks of age (EF: 51.8 ± 5.3 % vs. 41.4 ± 7.9 %, $p<0.05$; FS: 26.3 ± 3.2 % vs. 20.3 ± 4.9 %, $p<0.05$) (Fig. 13 C, Fig. 14 C).

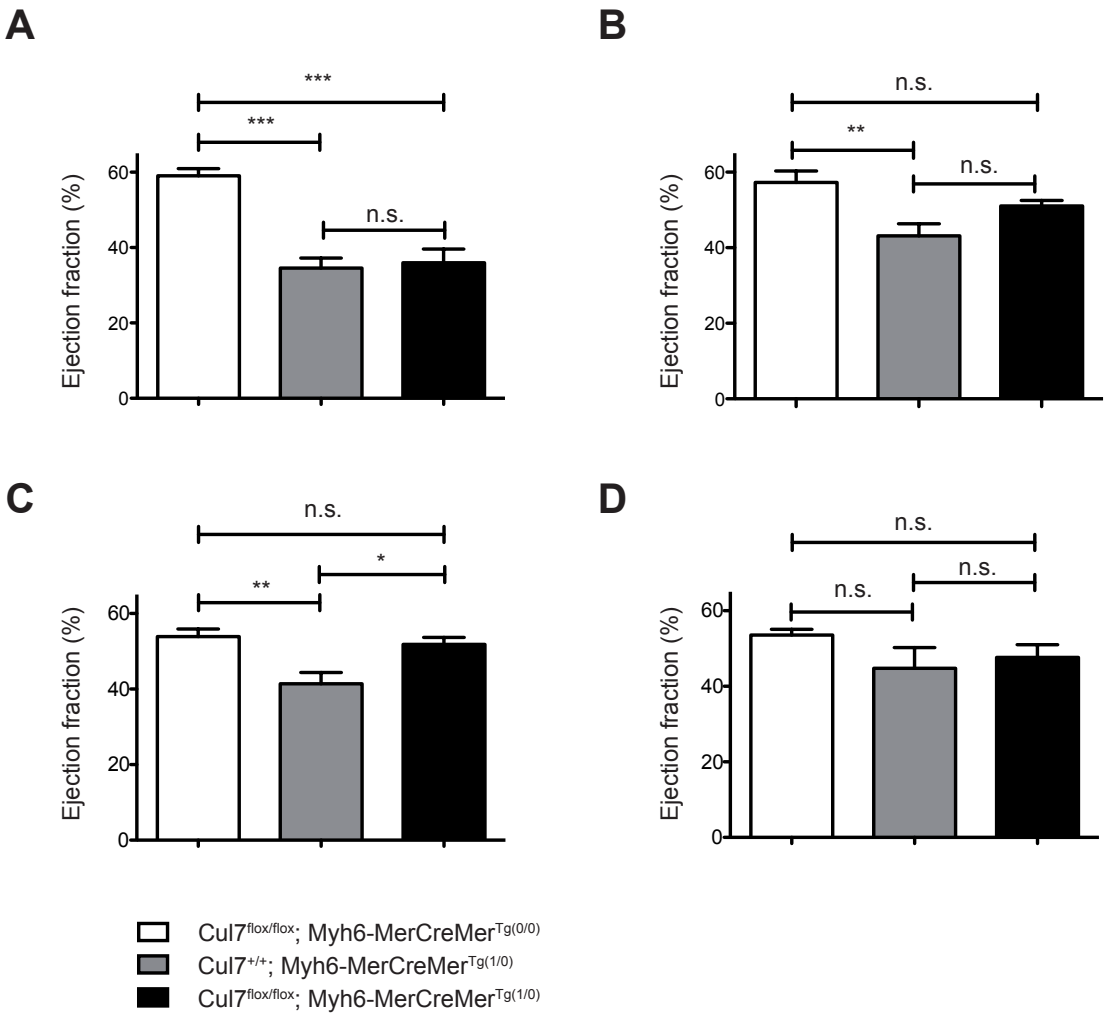

Figure 13: Ejection Fraction (EF) under basal conditions.

Echocardiographic assessment of ejection fraction at the age of 8 (Fig. 13 A), 10 (Fig. 13 B), 12 (Fig. 13 C), 14 (Fig. 13 D), corresponding to a duration of CUL7 depletion of 2, 4, 6 and 8 weeks, respectively. N=4-9. Statistics: ANOVA, *: $p<0.05$, **: $p<0.01$.

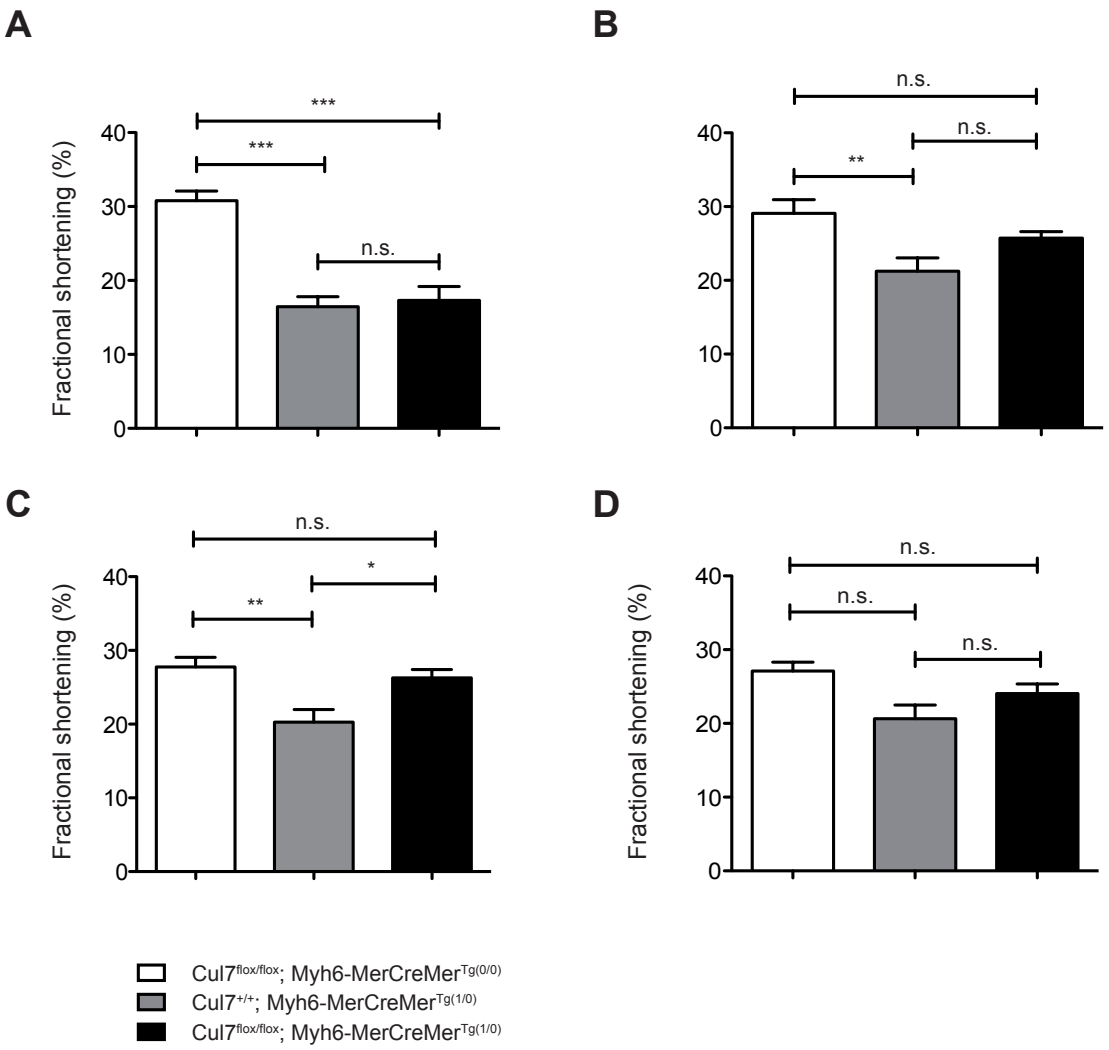

Figure 14: Fractional shortening (FS) under basal conditions.

Echocardiographic assessment of fractional shortening at the age of 8 (Fig. 14 A), 10 (Fig. 14 B), 12 (Fig. 14 C), 14 (Fig. 14 D), corresponding to a duration of CUL7 depletion of 2, 4, 6 and 8 weeks, respectively. N=4-9. Statistics: ANOVA, *: $p<0.05$, **: $p<0.01$.

To further analyze cardiac function, end-systolic volumes were measured at different time points. At the age of 8 weeks, Cul7$^{+/+}$; Myh6-MerCreMer$^{Tg(1/0)}$ (58.7 μl) and Cul7$^{flox/flox}$; Myh6-MerCreMer$^{Tg(1/0)}$ animals (57.5 μl) showed a significantly increased end-systolic volume when compared to respective Cul7$^{flox/flox}$; Myh6-MerCreMer$^{Tg(0/0)}$ controls (24.2 μl, $p<0.001$) (Fig. 15 A). At the age of 10 weeks and 12 weeks corresponding to CUL7 depletion of 4 weeks and 6 weeks, end-systolic volume of Cul7$^{flox/flox}$; Myh6-MerCreMer$^{Tg(1/0)}$ animals had

normalized and did not show significant difference when compared to Cul7$^{flox/flox}$; Myh6-MerCreMer$^{Tg(0/0)}$ controls, whereas Cul7$^{+/+}$; Myh6-MerCreMer$^{Tg(1/0)}$ end-systolic volumes were still markedly increased at the respective time points (Fig. 15 B, C).

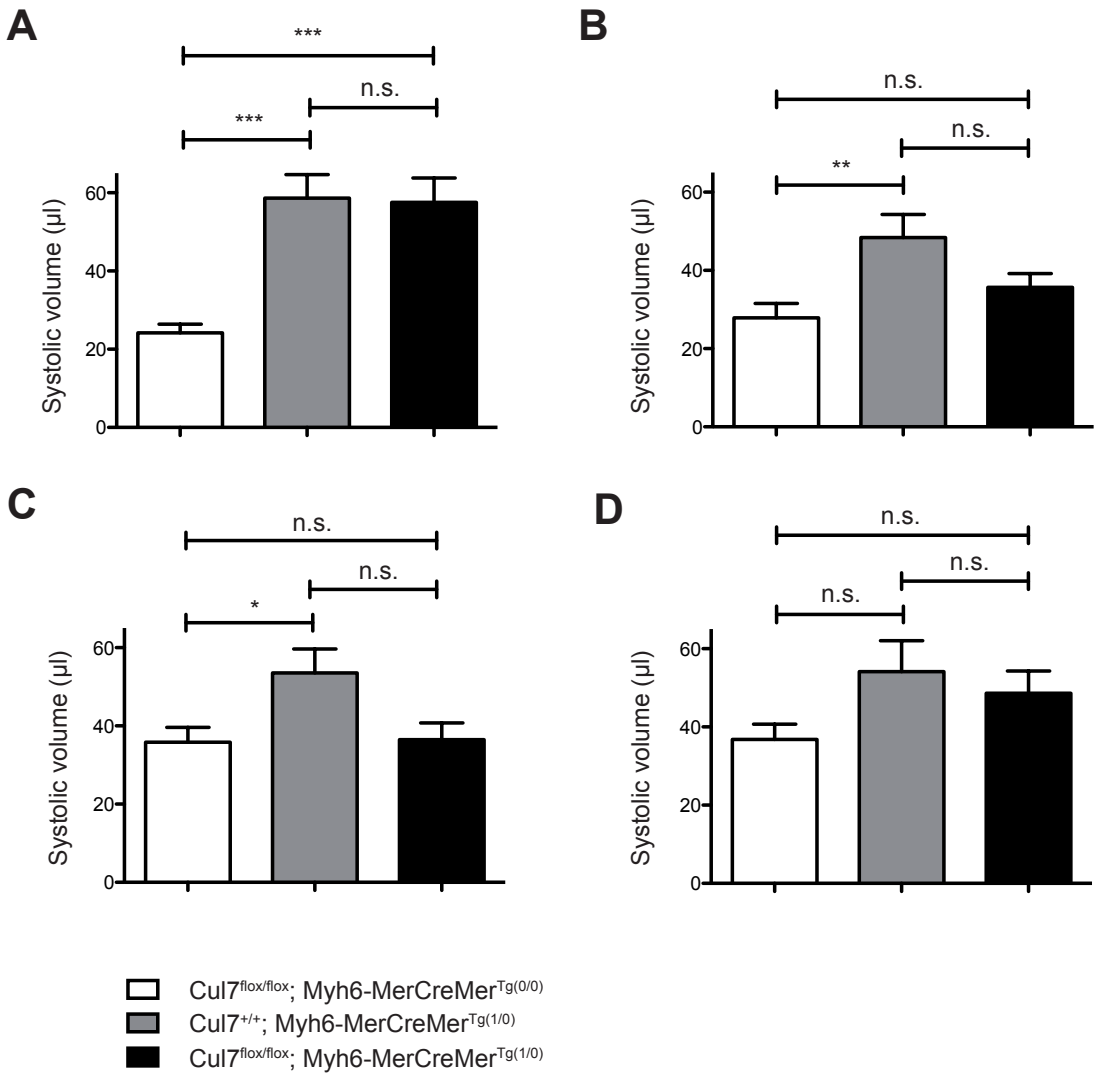

Figure 15: End-systolic volume (ESV) under basal conditions.

Echocardiographic assessment of end-systolic volume (ESV) at the age of 8 (Fig. 15 A), 10 (Fig. 15 B), 12 (Fig. 15 C), 14 (Fig. 15 D), corresponding to a duration of CUL7 depletion of 2, 4, 6 and 8 weeks, respectively. N=4-9. Statistics: ANOVA, *: p<0.05, **: p<0.01.

To evaluate diastolic function, end-diastolic volumes were measured at different time points. At 8 weeks of age, end-diastolic volume was significantly increased in both Cul7$^{+/+}$; Myh6-MerCreMer$^{Tg(1/0)}$ (88.2 μl) and Cul7$^{flox/flox}$; Myh6-MerCreMer$^{Tg(1/0)}$ animals (88.7 μl), when compared to Cul7$^{flox/flox}$; Myh6-MerCreMer$^{Tg(0/0)}$ controls (58.9 μl, $p<0.001$) (Fig. 16 A). At 10 weeks of age end-diastolic volume of Cul7$^{flox/flox}$; Myh6-MerCreMer$^{Tg(1/0)}$ animals was normalized and did not show any significant difference compared to Cul7$^{flox/flox}$; Myh6-MerCreMer$^{Tg(0/0)}$ controls, whereas Cul7$^{+/+}$; Myh6-MerCreMer$^{Tg(1/0)}$ animals still showed markedly increased end-diastolic volumes (Fig. 16 B). At 12 and 14 weeks no differences in end-diastolic volume between the respective groups were found (Fig. 16 C, D).

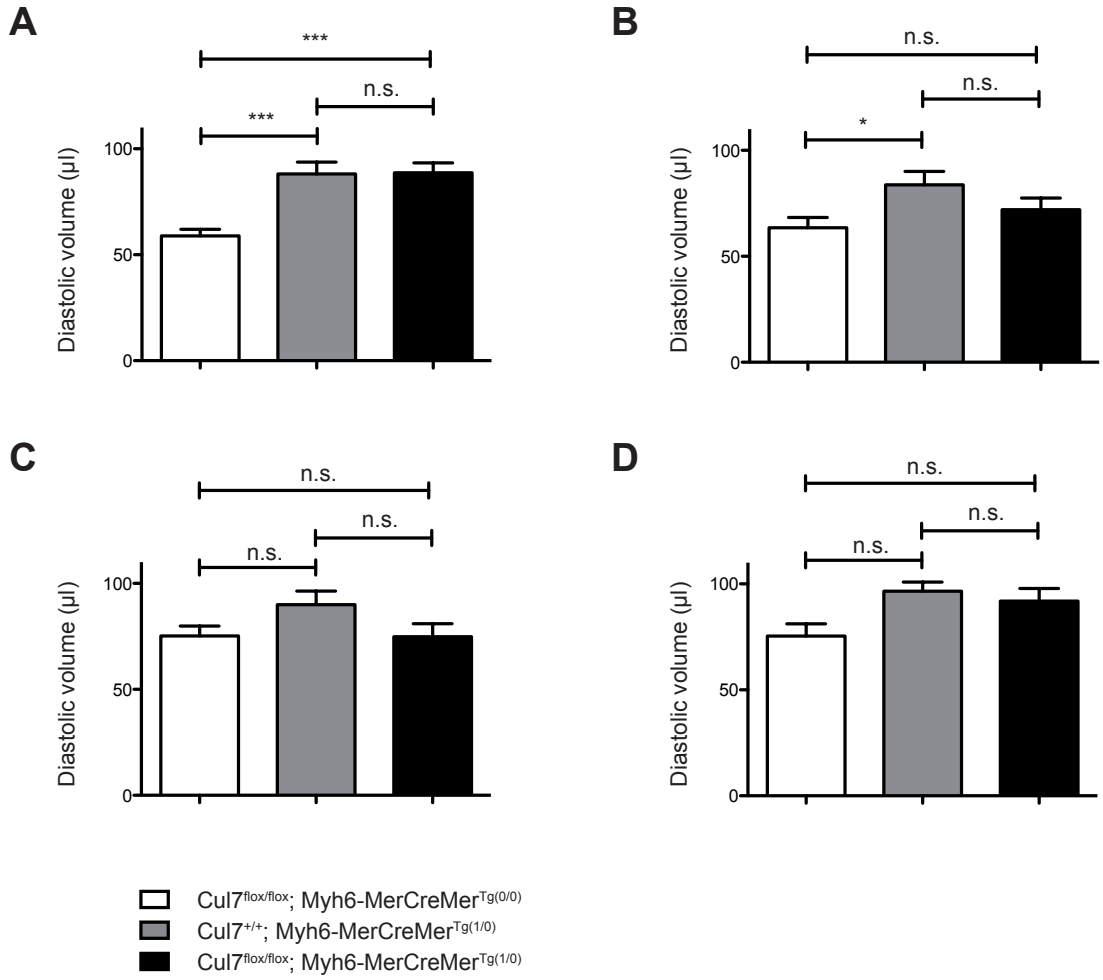

Figure 16: End-diastolic volume (EDV).

Echocardiographic assessment of end-diastolic volume (EDV) at the age of 8 (Fig. 16 A), 10 (Fig. 16 B), 12 (Fig. 16 C), 14 (Fig. 16 D), corresponding to a duration of CUL7 depletion of 2, 4, 6 and 8 weeks, respectively. N=4-9. Statistics: ANOVA, *: $p<0.05$, **: $p<0.01$.

To measure the effects of CUL7 depletion on cardiac hypertrophy and ventricle geometry, left ventricular posterior wall thickness was assessed in systole and diastole at the above-mentioned time points. Neither systolic or diastolic left ventricular posterior wall thickness showed any significant difference at 8 weeks, 10 weeks, 12 weeks and 14 weeks of age, corresponding to 2 weeks, 4 weeks, 6 weeks and 8 weeks of CUL7 depletion (Fig. 17, 18).

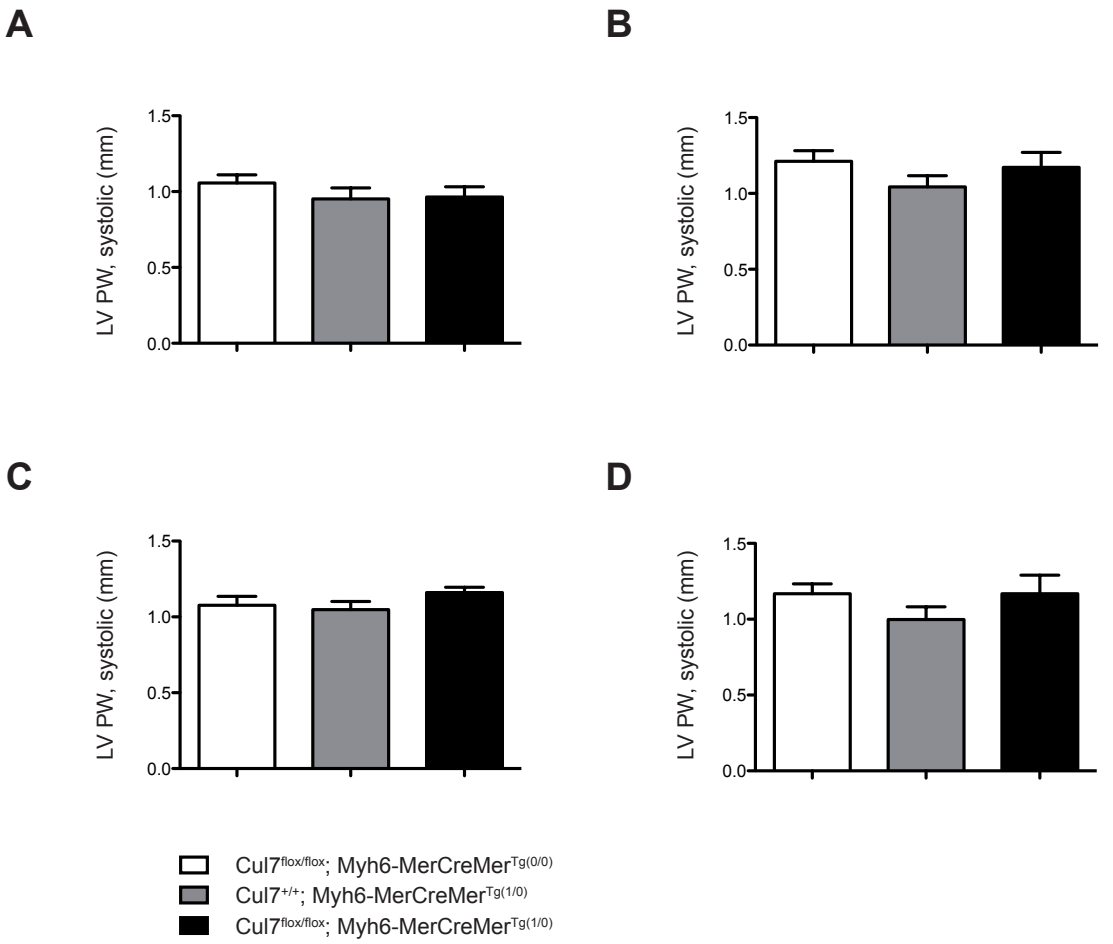

Figure 17: Systolic left ventricular posterior wall thickness (LVPW, systolic) under basal conditions.

Echocardiographic assessment of systolic left ventricular posterior wall thickness (LVPW, systolic) at the age of 8 (Fig. 17 A), 10 (Fig. 17 B), 12 (Fig. 17 C), 14 (Fig. 17 D), corresponding to a duration of CUL7 depletion of 2, 4, 6 and 8 weeks, respectively. N=4-9. Statistics: ANOVA, *: $p<0.05$, **: $p<0.01$.

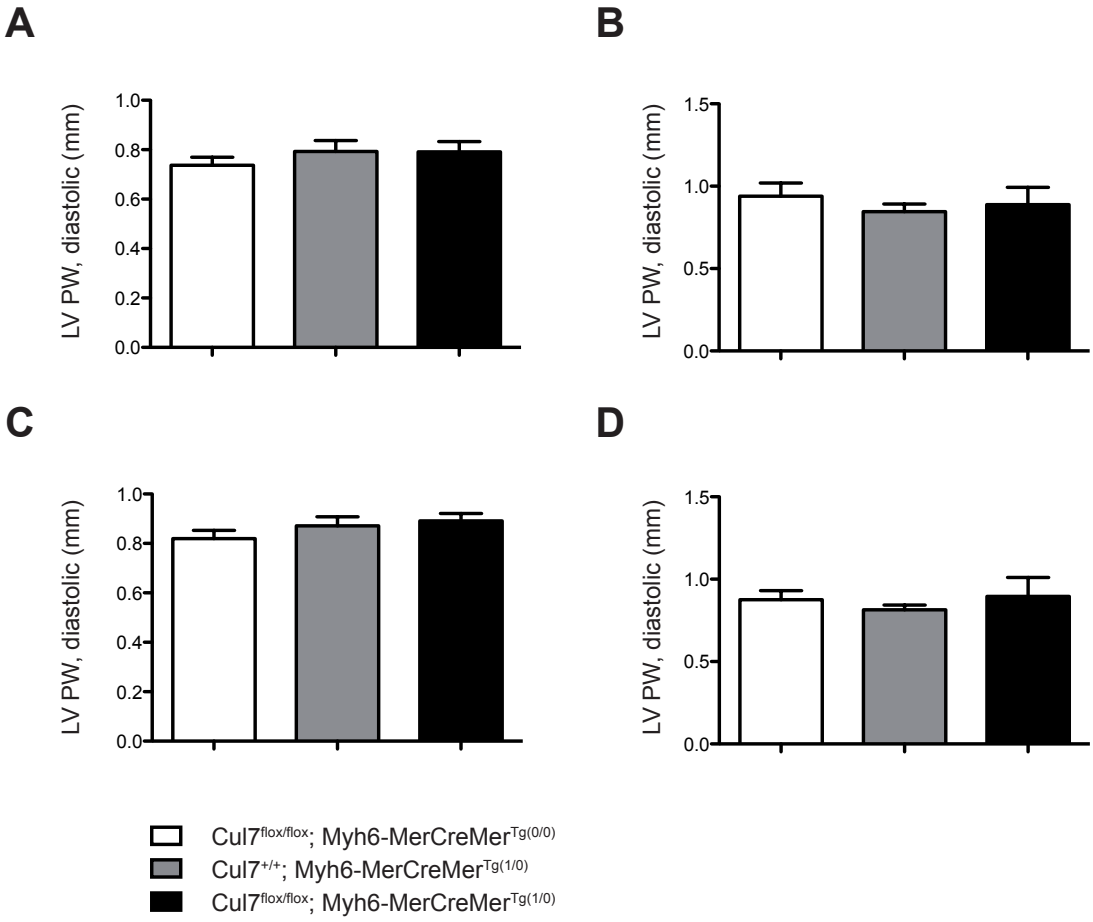

Figure 18: Diastolic left ventricular posterior wall thickness (LVPW, diastolic) under basal conditions.

Echocardiographic assessment of diastolic left ventricular posterior wall thickness (LVPW, diastolic) at the age of 8 (Fig. 18 A), 10 (Fig. 18 B), 12 (Fig. 18 C), 14 (Fig. 18 D), corresponding to a duration of CUL7 depletion of 2, 4, 6 and 8 weeks, respectively. N=4-9. Statistics: ANOVA, *: $p<0.05$, **: $p<0.01$.

In conclusion depletion of CUL7 in cardiomyocytes resulted in a significant improvement of EF and FS when comparing Cul7$^{flox/flox}$; Myh6-MerCreMer$^{Tg(1/0)}$ animals with Cul7$^{+/+}$; Myh6-MerCreMer$^{Tg(1/0)}$ controls, although this effect was temporarily limited. Cre-carrying animals, Cul7$^{flox/flox}$; Myh6-MerCreMer$^{Tg(1/0)}$ and Cul7$^{+/+}$; Myh6-MerCreMer$^{Tg(1/0)}$, both showed depression of cardiac function after induction of recombination when compared to Cul7$^{flox/flox}$; Myh6-MerCreMer$^{Tg(0/0)}$ non-Cre carrying controls. Systolic LVPW was increased by trend in

Cul7$^{flox/flox}$; Myh6-MerCreMer$^{Tg(1/0)}$ in comparison to respective controls, pointing towards hypertrophy of the left ventricular myocardium.

6.5. Impact of the CUL7 depletion on cardiomyocyte hypertrophy under basal conditions

With increased systolic left ventricular posterior wall thickness in Cul7$^{flox/flox}$; Myh6-MerCreMer$^{Tg(1/0)}$ animals when compared to Cul7$^{+/+}$; Myh6-MerCreMer$^{Tg(1/0)}$ we thought to determine the impact of the CM-specific CUL7 depletion on cellular cardiomyocyte hypertrophy by assessment of cardiomyocyte cross-sectional area using a wheat germ agglutinin staining assay. Therefore, hearts of 14 weeks old mice were collected and subjected to preparation procedure and staining as described above. Analysis of cross-sectional area revealed an increase in cardiomyocyte cell size in the hearts of Cul7$^{flox/flox}$; Myh6-MerCreMer$^{Tg(1/0)}$ mice (610 μm^2 ± 199 μm^2) compared to Cul7$^{+/+}$; Myh6-MerCreMer$^{Tg(1/0)}$ (483 μm^2 ± 115 μm^2, $p<0.05$) and Cul7$^{flox/flox}$; Myh6-MerCreMer$^{Tg(0/0)}$ control animals (445 μm^2 ± 129 μm^2, $p<0.01$) (Fig. 19 B). Interestingly, hypertrophy of the ventricular septum was even more pronounced (651 μm^2 ± 149 μm^2 vs. 439 μm^2 ± 82 μm^2 vs. 446 μm^2 ± 140 μm^2, $p<0.05$) (Fig. 19 C).

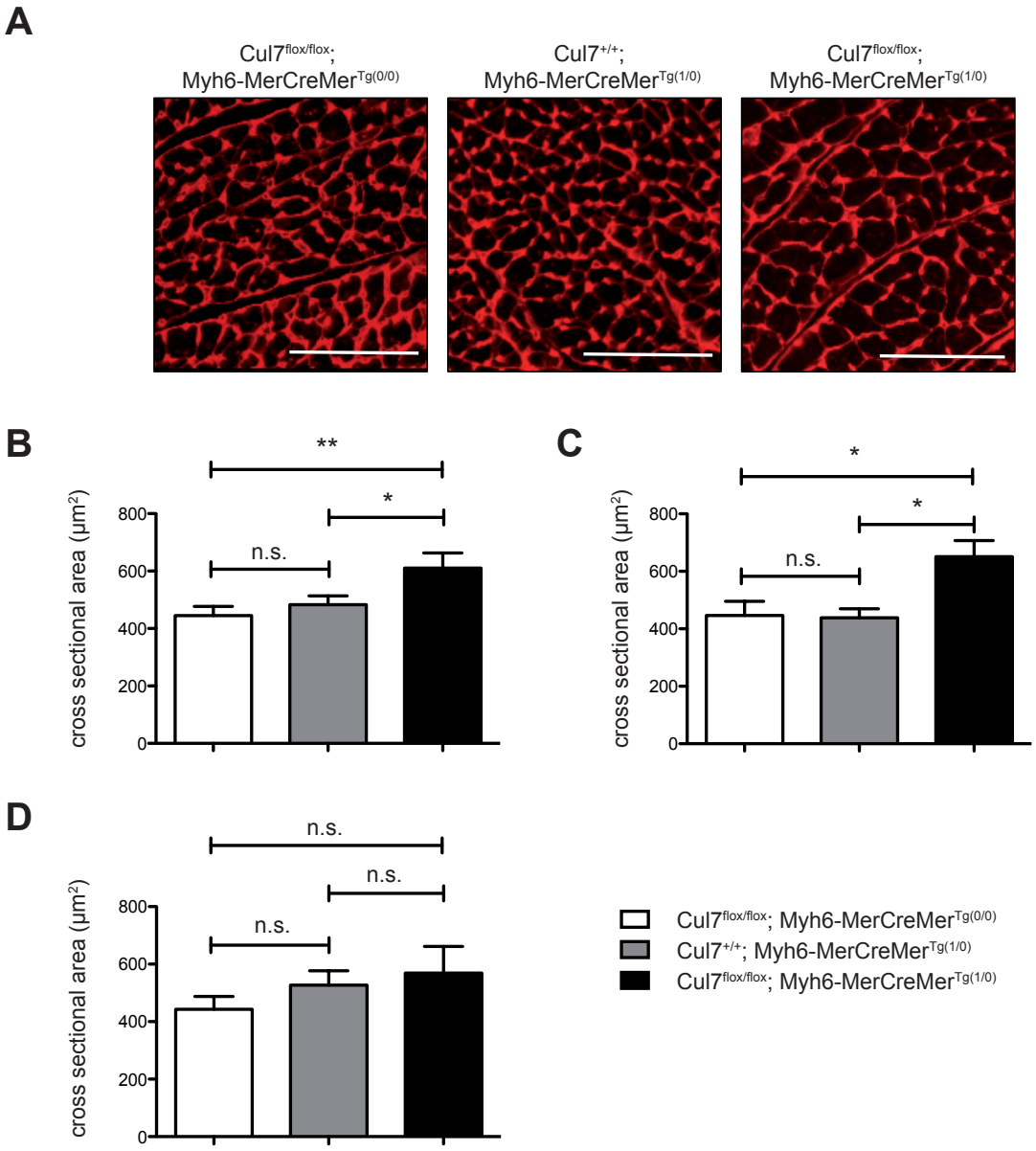

Figure 19: Cross sectional area of cardiomyocytes under basal conditions.

Cardiomyocyte cross sectional area assessed by wheat germ agglutinin (WGA) staining of hearts from 14 weeks old mice under basal conditions. N=7-8. Analysis of left ventricle (Fig. 19 B), septum (Fig. 19 C) and lateral wall (Fig. 19 D). Representative pictures shown. Scale bar = 100 µm. Statistics. ANOVA. *: $p<0.05$, **: $p<0.01$.

6.6. Impact of CUL7 depletion on cardiac left ventricular fibrosis under basal conditions

To evaluate the influence of CUL7 deletion on left ventricular cardiac fibrosis, the hearts of 14 weeks old mice were subjected to Sirius Red / Fast Green staining as described above. When comparing collagen positive area of the left ventricle in relation to total left ventricular area both $Cul7^{+/+}$; Myh6-$MerCreMer^{Tg(1/0)}$ and $Cul7^{flox/flox}$; Myh6-$MerCreMer^{Tg(1/0)}$ mice showed a significant increase in left ventricular fibrosis in comparison to $Cul7^{flox/flox}$; Myh6-$MerCreMer^{Tg(0/0)}$ control animals. Whereas left ventricular fibrosis in $Cul7^{flox/flox}$; Myh6-$MerCreMer^{Tg(0/0)}$ animals was 2.2 % ± 0.52 %, $Cul7^{+/+}$; Myh6-$MerCreMer^{Tg(1/0)}$ displayed a significantly increased ventricular fibrosis of 9.2 % ± 4.72 % ($p<0.01$) as did $Cul7^{flox/flox}$; Myh6-$MerCreMer^{Tg(1/0)}$ animals with a fibrotic area of 7.2 % ± 3.29 % ($p<0.05$). Interestingly, left ventricular fibrosis in $Cul7^{flox/flox}$; Myh6-$MerCreMer^{Tg(1/0)}$ animals was ameliorated by trend in comparison to $Cul7^{+/+}$; Myh6-$MerCreMer^{Tg(1/0)}$ animals (confidence interval $Cul7^{+/+}$; Myh6-$MerCreMer^{Tg(1/0)}$ vs. $Cul7^{flox/flox}$; Myh6-$MerCreMer^{Tg(1/0)}$; 95 % CI = -2.663 to 6.452) (Fig. 20).

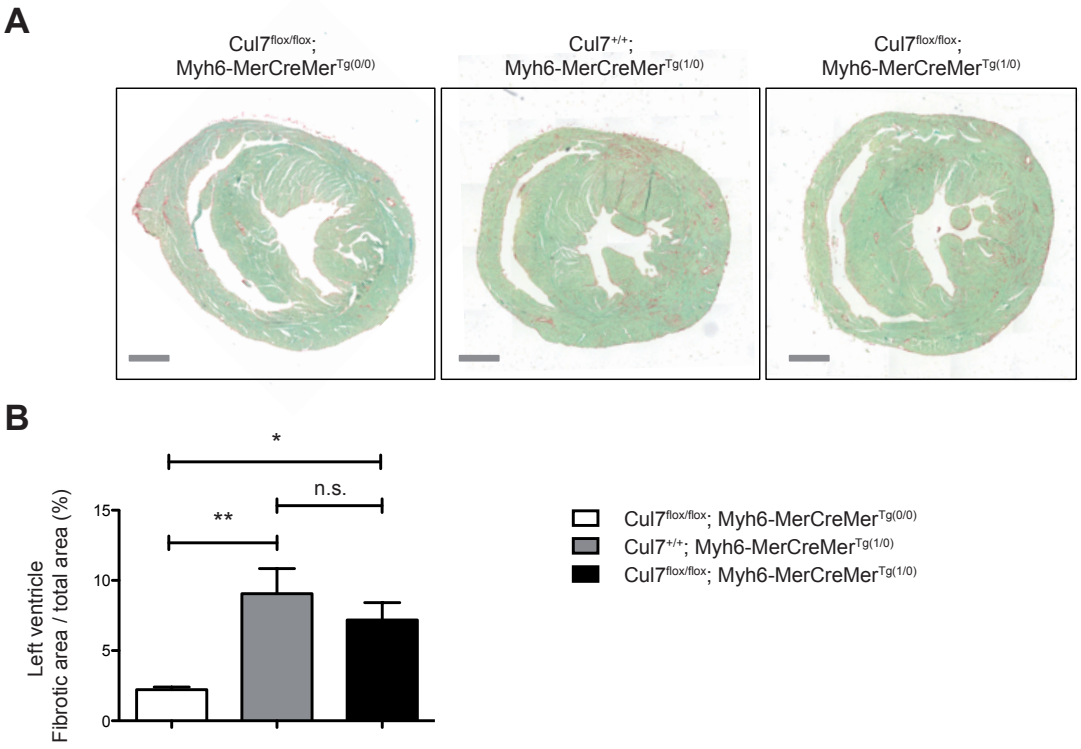

Figure 20: Left ventricular fibrosis under basal conditions.

Left ventricular interstitial fibrosis assessed by Sirius red / Fast green staining of hearts of 14 weeks old mice under basal conditions. N=7-8. Representative pictures shown. N-numbers as indicated. Statistics: ANOVA, *: $p<0.05$, **: $p<0.01$. Scale bar: 1 mm.

6.7. Impact of CUL7 depletion on downstream insulin- / IGF1-receptor signaling under basal conditions

As CUL7 has been shown to play an important role in IRS-1 mediated tyrosine kinase receptor signaling, we thought to investigate the impact of cardiomyocyte-specific depletion of CUL7 on insulin and IGF1 receptor pathways. Therefore, cardiomyocytes were isolated from hearts of 10 weeks old animals under basal conditions and immunoblots directed against Akt, Erk1/2 and IRS-1 were performed. Phosphorylated proteins were normalized to their respective total protein amounts. In the cardiomyocyte cell fraction isolated from Cul7$^{flox/flox}$; Myh6-MerCreMer$^{Tg(1/0)}$ mice hearts, the activation of the Akt signaling pathway, assessed as the ratio of phospho-Akt / total-Akt, was significantly increased by the factor of 1.5 ± 0.5 ($p<0.05$) when compared to cardiomyocytes isolated from Cul7$^{+/+}$; Myh6-

MerCreMer$^{Tg(1/0)}$ control animals (1.00 ± 0.24). On the other hand, there was no significant alteration of the activation of the Erk MAPK pathway or a change in total abundance of the IRS-1 protein (Fig. 21).

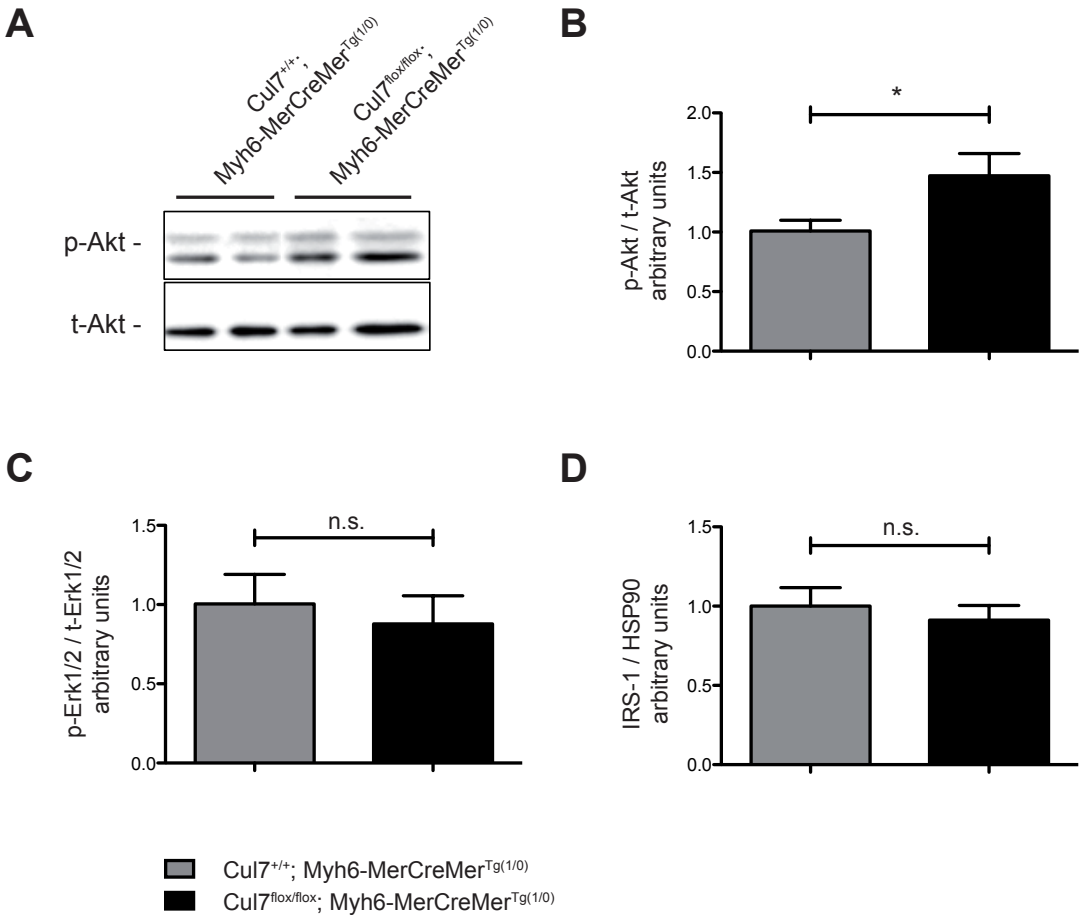

Figure 21: Downstream signaling of IRS-1 dependent tyrosine kinase receptors in the cardiomyocyte cell fraction under basal conditions.

Immunoblots from lysates prepared from isolated cardiomyocyte cells directed against p-Akt and t-Akt (Fig. 21 A). Quantification of p-Akt / t-Akt ratio 4 weeks after induction of CUL7 depletion (Fig. 21 B). Quantification of p-Erk1/2 / t-Erk1/2 ratio 4 weeks after induction of CUL7 depletion (Fig. 21 C). Quantification of IRS1 / HSP90 ratio 4 weeks after induction of CUL7 depletion (Fig. 21 D). N=7. Representative immunoblot shown. Statistics: t-test; *: $p<0.05$.

Taken together CM-specific CUL7 depletion under basal conditions induced hypertrophy of left ventricular cardiomyocytes in hearts of $Cul7^{flox/flox}$; Myh6-$MerCreMer^{Tg(1/0)}$ animals, as evidenced by increased cross-sectional area. Furthermore, it resulted in an increased activation of the Akt signaling pathway, evidenced by increased p-Akt / t-Akt ratios under basal conditions. Additionally, there was evidence for a mild attenuation of left ventricular fibrosis in $Cul7^{flox/flox}$; Myh6-$MerCreMer^{Tg(1/0)}$ when compared to $Cul7^{+/+}$; Myh6-$MerCreMer^{Tg(1/0)}$ mice.

6.8. Impact of transverse aortic constriction on *Cul7* mRNA expression

To evaluate the impact of increased afterload by transverse aortic constriction (TAC) on *Cul7* in cardiomyocytes, wild-type C57BL/6 mice were subjected to 4 and 6 weeks of transverse aortic constriction followed by the isolation of cardiomyocytes and *Cul7* mRNA quantification by qPCR. To verify the effect of TAC on the heart, the abundance of *Anp* mRNA was measured. For both, 4 weeks and 6 weeks of transverse aortic constriction the level of *Anp* mRNA was increased significantly by the factor of 6.8 ± 3.29 ($p<0.05$) and 5.6 ± 5.06 ($p<0.05$), respectively (Fig. 22 B, D). The *Cul7* mRNA abundance showed a trend towards an up-regulation by the factor of 1.2 ± 0.30 ($p = 0.27$) and 1.4 ± 0.36 ($p = 0.07$), although statistical significance was not reached (Fig. 22 A, C).

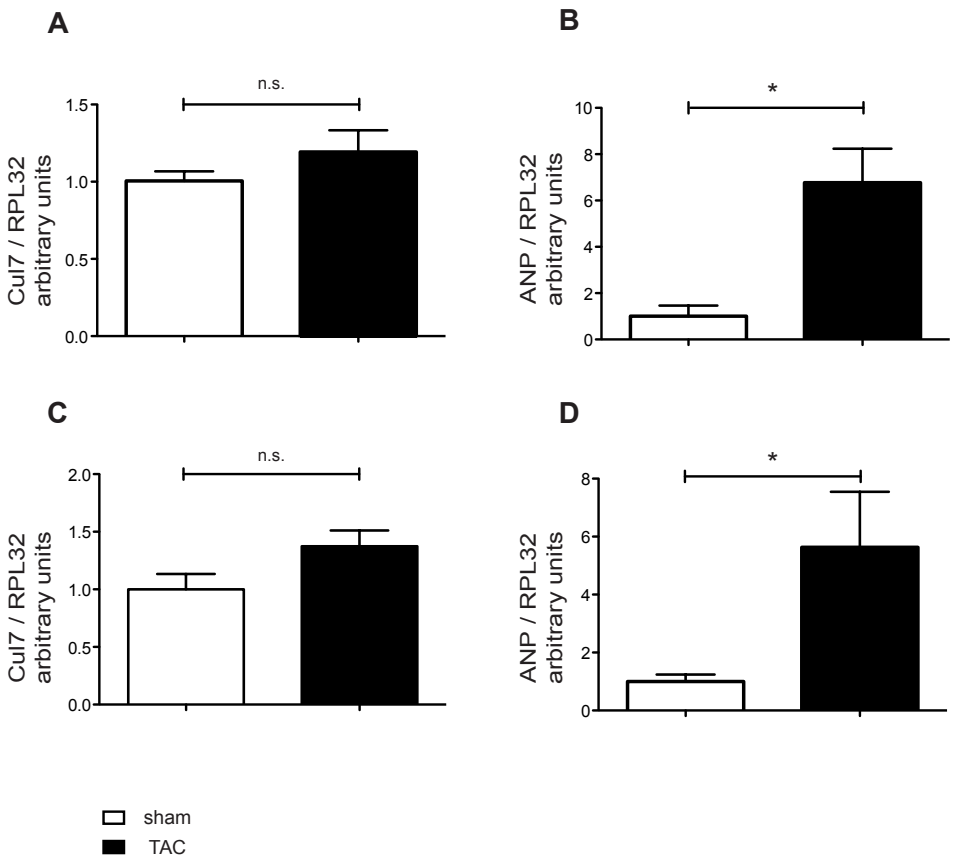

Figure 22: Regulation of *Cul7* mRNA under conditions of increased afterload (TAC).

Abundance of *Cul7* mRNA after four weeks of transverse aortic constriction (Fig. 22 A). Abundance of *Anp* mRNA after four weeks of transverse aortic constriction (Fig. 22 B). Abundance of *Cul7* mRNA after six weeks of transverse aortic constriction (Fig. 22 C). Abundance of *Anp* mRNA after six weeks of transverse aortic constriction (Fig. 22 D). Cul7 and *Anp* mRNA values were normalized to *Rpl32* mRNA vales. N=4-7. Statistics: t-test; *: $p<0.05$.

6.9. Knockdown of the CUL7 protein under conditions of increased afterload

To evaluate the efficiency of the CUL7 knockdown under conditions of increased afterload, whole heart samples were obtained from the left ventricles of mice after the animals had undergone 4 weeks of transverse aortic constriction or a respective sham operation. Subsequently, immunoblotting against CUL7 and HSP90 as a loading control was performed for assessment of protein abundance.

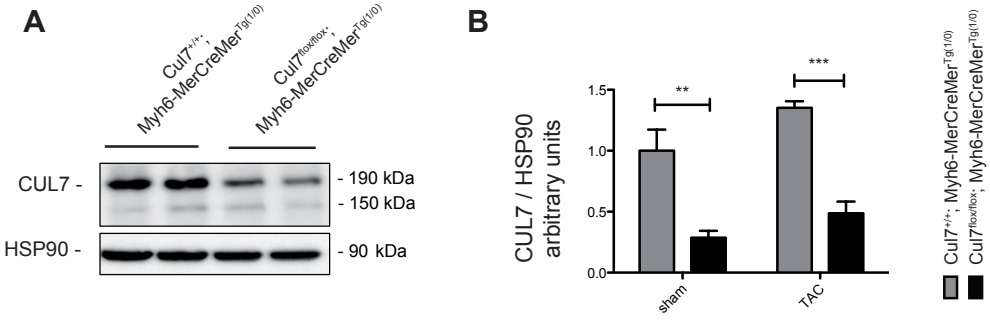

Figure 23: Expression of CUL7 under conditions of increased afterload.

CUL7 expression in whole heart samples after four weeks of increased afterload (Fig. 23 A). Quantification CUL7 expression after four weeks of increased afterload (Fig. 23 B, lanes 3,4) and after respective sham conditions (Fig. 23 B, lanes 1,2). N=4. Representative immunoblot shown. Statistics: t-test; **: p<0.01, ***: p<0.001.

After transverse aortic constriction for 4 weeks, expression of CUL7 was increased by trend in Cul7$^{+/+}$; Myh6-MerCreMer$^{Tg(1/0)}$ when compared to respective sham group (1.35 $\pm$ 0.11 vs. 1.00 $\pm$ 0.35; p=0.1) as wells as in Cul7$^{flox/flox}$; Myh6-MerCreMer$^{Tg(1/0)}$ animals (0.29 ± 0.11 vs. 0.49 ± 0.20; p=0.12) (Fig. 23 B). Importantly, CUL7 expression was significantly reduced in whole hearts of Cul7$^{flox/flox}$; Myh6-MerCreMer$^{Tg(1/0)}$ mice (0.49 ± 0.20) in comparison to Cul7$^{+/+}$; Myh6-MerCreMer$^{Tg(1/0)}$ controls (1.35 ± 0.11) to 35.5 % rest abundance of CUL7 (p<0.001).

In conclusion increased cardiac afterload by transverse aortic constriction up-regulated CUL7 abundance, both on mRNA and protein level, although statistical significance was not reached. Most importantly, depletion of the CUL7 was sufficiently achieved under conditions of increased afterload.

6.10. Impact of CUL7 depletion on the phenotype under conditions of increased afterload

To assess the impact of the cardiomyocyte-specific depletion of CUL7 on the phenotype of the mice under conditions of increased afterload, animals were subjected to transverse aortic constriction for 4 weeks and subsequently, mice heart weight, ventricular weight, atrial weight, lung weight, body weight and tibia length were measured. Heart weight / tibia length ratios were significantly increased in $Cul7^{flox/flox}$; Myh6-$MerCreMer^{Tg(1/0)}$, $Cul7^{flox/flox}$; Myh6-$MerCreMer^{Tg(0/0)}$ and $Cul7^{+/+}$; Myh6-$MerCreMer^{Tg(1/0)}$ animals, when comparing TAC mice to their respective sham-operated controls. In the TAC group there was no difference between $Cul7^{flox/flox}$; Myh6-$MerCreMer^{Tg(1/0)}$, $Cul7^{flox/flox}$; Myh6-$MerCreMer^{Tg(0/0)}$ and $Cul7^{+/+}$; Myh6-$MerCreMer^{Tg(1/0)}$ mice detectable (Fig. 24 A). Concordantly, left ventricular weight / tibia length ratios were increased in the TAC group when compared to their respective sham-operated group, whereas no difference between the different genotypes was detectable (Fig. 24 B). Atrial weight / tibia length ratios were also increased in all TAC animals when compared to their respective sham-operated control. Atrial weight / tibia length ratio was significantly increased in $Cul7^{flox/flox}$; Myh6-$MerCreMer^{Tg(1/0)}$ animals subjected to transverse aortic constriction in comparison to $Cul7^{flox/flox}$; Myh6-$MerCreMer^{Tg(0/0)}$ animals but not $Cul7^{+/+}$; Myh6-$MerCreMer^{Tg(1/0)}$ controls under conditions of increased afterload (Fig. 24 C). Furthermore lung weight / tibia length ratios were increased in TAC-operated animals when compared to the sham group, reaching significance for $Cul7^{+/+}$; Myh6-$MerCreMer^{Tg(1/0)}$ and $Cul7^{flox/flox}$; Myh6-$MerCreMer^{Tg(1/0)}$ mice and a trend for $Cul7^{flox/flox}$; Myh6-$MerCreMer^{Tg(0/0)}$ animals (95 % CI: -13.39 to 4.41). Lung weight / tibia length ratios were markedly increased in $Cul7^{+/+}$; Myh6-$MerCreMer^{Tg(1/0)}$ and $Cul7^{flox/flox}$; Myh6-$MerCreMer^{Tg(1/0)}$ mice after aortic constriction for 4 weeks when compared to respective $Cul7^{flox/flox}$; Myh6-$MerCreMer^{Tg(0/0)}$ controls, whereas there was no significant difference between the first two genotypes (Fig. 24 D). Bodyweight was unaffected at any time point or in respect of TAC or sham operation (Fig. 24 E).

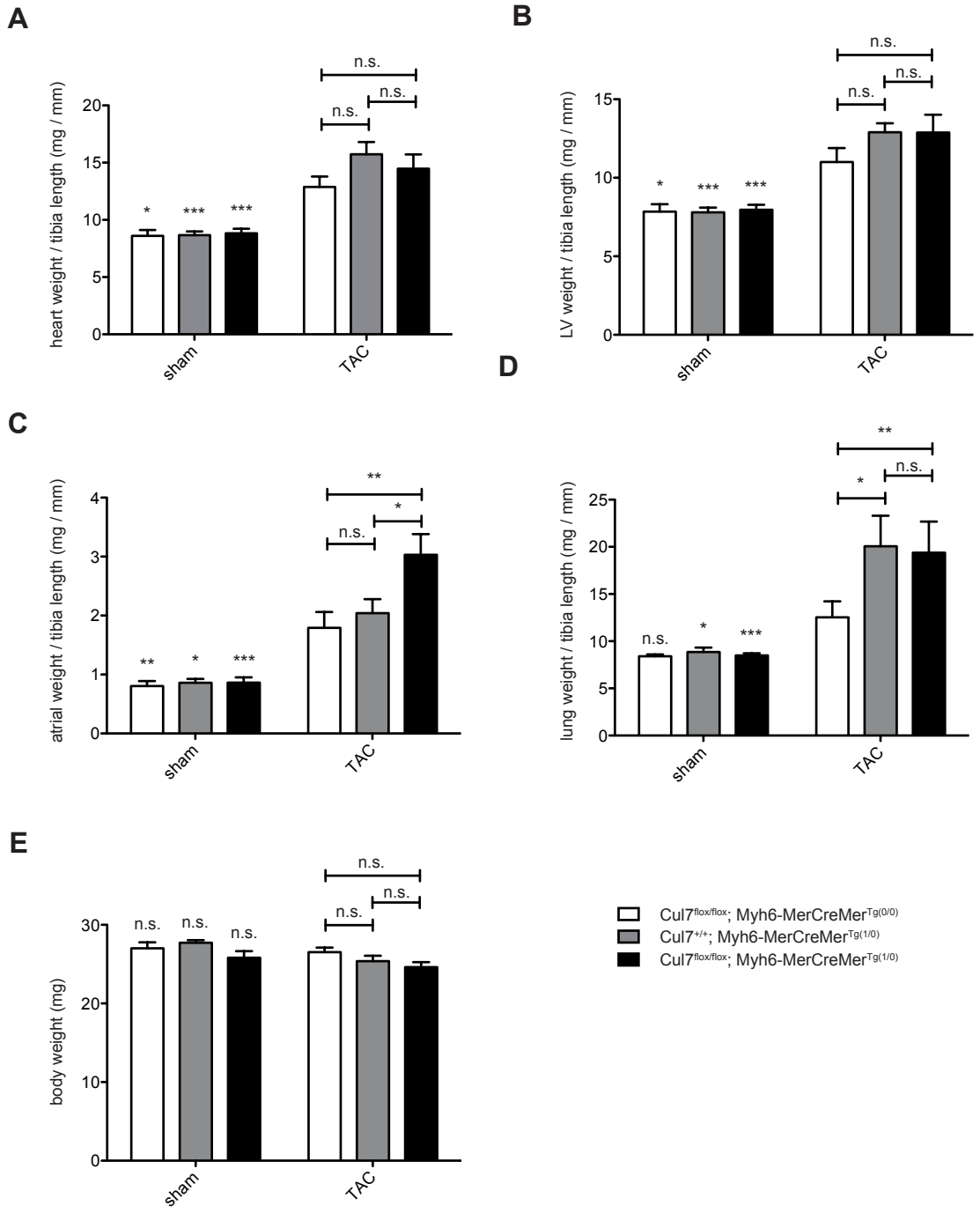

Figure 24: Phenotyping of CUL7 depleted mice under conditions of increased afterload.

Phenotypical characterization after four weeks of transverse aortic constriction and respective sham period by assessment of heart weight / tibia length (Fig, 24 A), left ventricular (LV) weight / tibia length (Fig. 24 B), atrial weight / tibia length (Fig. 24 C), lung weight / tibia length (Fig. 24 D) and bodyweight (Fig. 24 E). N=7-9. Statistics: ANOVA, *: p<0.05, **: p<0.01, ***: p<0.001.

6.11. Impact of CM-specific CUL7 depletion on cardiac function under conditions of increased afterload

To evaluate the impact of increased afterload induced by transverse aortic constriction on functional performance of the hearts of cardiomyocyte-specific CUL7 depleted mice in comparison to respective controls, echocardiography was performed at baseline before TAC operation, after 2 weeks and 4 weeks of increased afterload, respectively and ejection fraction, fractional shortening, left ventricular end-diastolic inner diameter (LVID, diastolic) and left ventricular end-systolic inner diameter (LVID, systolic) were measured. Ejection fraction was compromised at baseline due to transient cardio-depression in Cre-carrying animals in comparison to non-Cre carrying controls, with EF of 40 % and 42% in $Cul7^{flox/flox}$; Myh6-$MerCreMer^{Tg(1/0)}$ and $Cul7^{+/+}$; Myh6-$MerCreMer^{Tg(1/0)}$ mice when compared to 58 % in $Cul7^{flox/flox}$; Myh6-$MerCreMer^{Tg(0/0)}$ controls ($p<0.01$, $p<0.05$) (Fig. 25 A). After 2 weeks of transverse aortic constriction there was a significant decrease in ejection fraction for all genotypes comparing the TAC-group with its respective sham group, with EF of 52 % and 40 % for the sham and TAC-group in $Cul7^{flox/flox}$; Myh6-$MerCreMer^{Tg(0/0)}$ animals ($p<0.05$), 48 % and 33 % for $Cul7^{+/+}$; Myh6-$MerCreMer^{Tg(1/0)}$ mice ($p<0.05$) and 50 % and 29 % for $Cul7^{flox/flox}$; Myh6-$MerCreMer^{Tg(1/0)}$ animals ($p<0.01$). When comparing the TAC animals among themselves, there was no significant difference (Fig. 25 B). After 4 weeks of transverse aortic constriction the cardiac function in the TAC-group was further compromised with EF of 35 %, 27 % and 24 % for $Cul7^{flox/flox}$; Myh6-$MerCreMer^{Tg(0/0)}$, $Cul7^{+/+}$; Myh6-$MerCreMer^{Tg(1/0)}$ and $Cul7^{flox/flox}$; Myh6-$MerCreMer^{Tg(1/0)}$ mice, respectively in comparison to 57 %, 51 % and 53 % in their respective sham groups ($p<0.01$, $p<0.001$). There was no significant difference detectable between the different genotypes under conditions of increased afterload (Fig. 25 C).

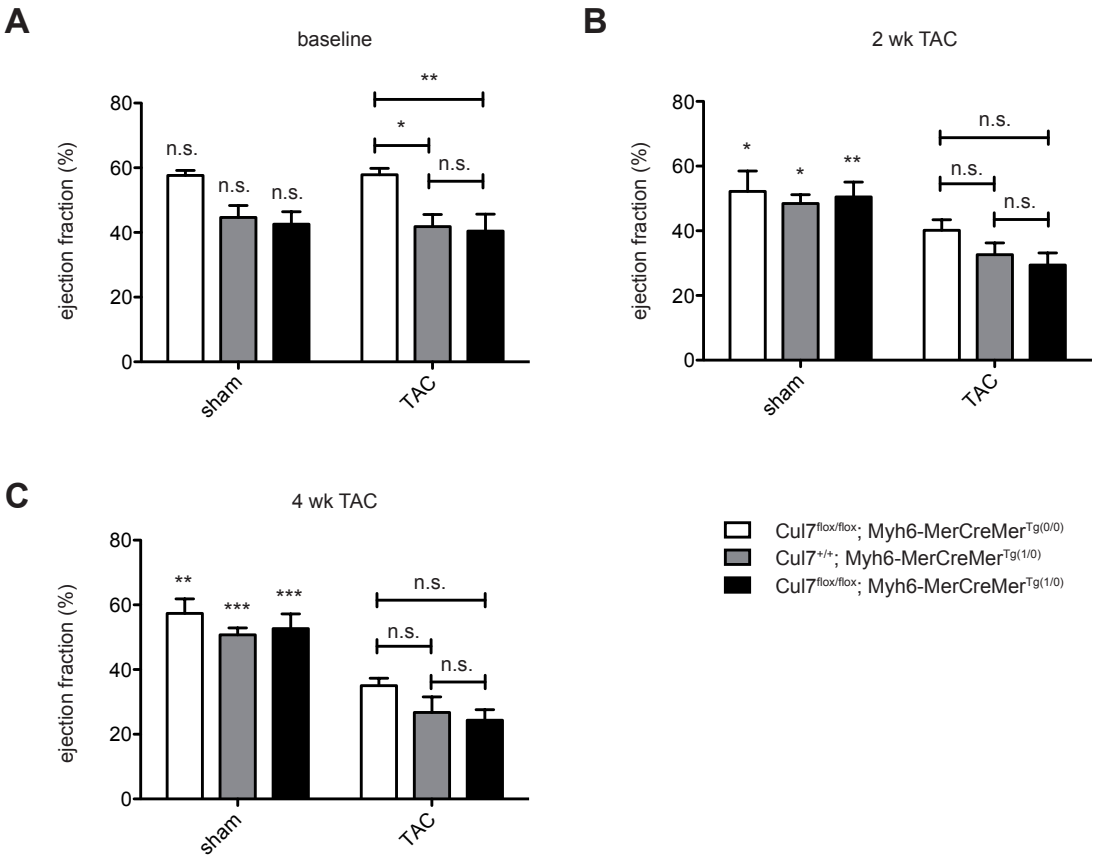

Figure 25: Ejection fraction (EF) under conditions of increased afterload.

Echocardiographic assessment of ejection fraction (EF) after transverse aortic constriction (TAC) and respective sham period at baseline (Fig. 25 A), after two weeks of transverse aortic constriction (Fig. 25 B) and after 4 weeks of aortic constriction (Fig. 25 C). Sham animals are shown in lanes 1-3, TAC animals in lanes 4-5, respectively. N=7-9. Statistics: ANOVA, *: $p<0.05$, **: $p<0.01$.

At baseline, there was no difference in fractional shortening (FS) between the sham group and the TAC-operated group when comparing animals with the same genotype. Simultaneously, at baseline, FS was significantly decreased in Cul7$^{+/+}$; Myh6-MerCreMer$^{Tg(1/0)}$ (20 %) and Cul7$^{flox/flox}$; Myh6-MerCreMer$^{Tg(1/0)}$ mice (19 %) in comparison to Cul7$^{flox/flox}$; Myh6-MerCreMer$^{Tg(0/0)}$ controls (30 %, $p<0.01$, $p<0.001$) (Fig. 26 A). After two weeks of transverse aortic constriction, animals showed a markedly decrease in FS when compared to their isogenic sham-operated controls (Fig. 26 B). After 4 weeks of increased afterload, TAC animals also showed a significantly depressed FS in respect of the sham

group. FS in Cul7$^{+/+}$; Myh6-MerCreMer$^{Tg(1/0)}$ and Cul7$^{flox/flox}$; Myh6-MerCreMer$^{Tg(1/0)}$ animals was reduced when compared to Cul7$^{flox/flox}$; Myh6-MerCreMer$^{Tg(0/0)}$ controls, but did not reach significance (Fig. 26 C).

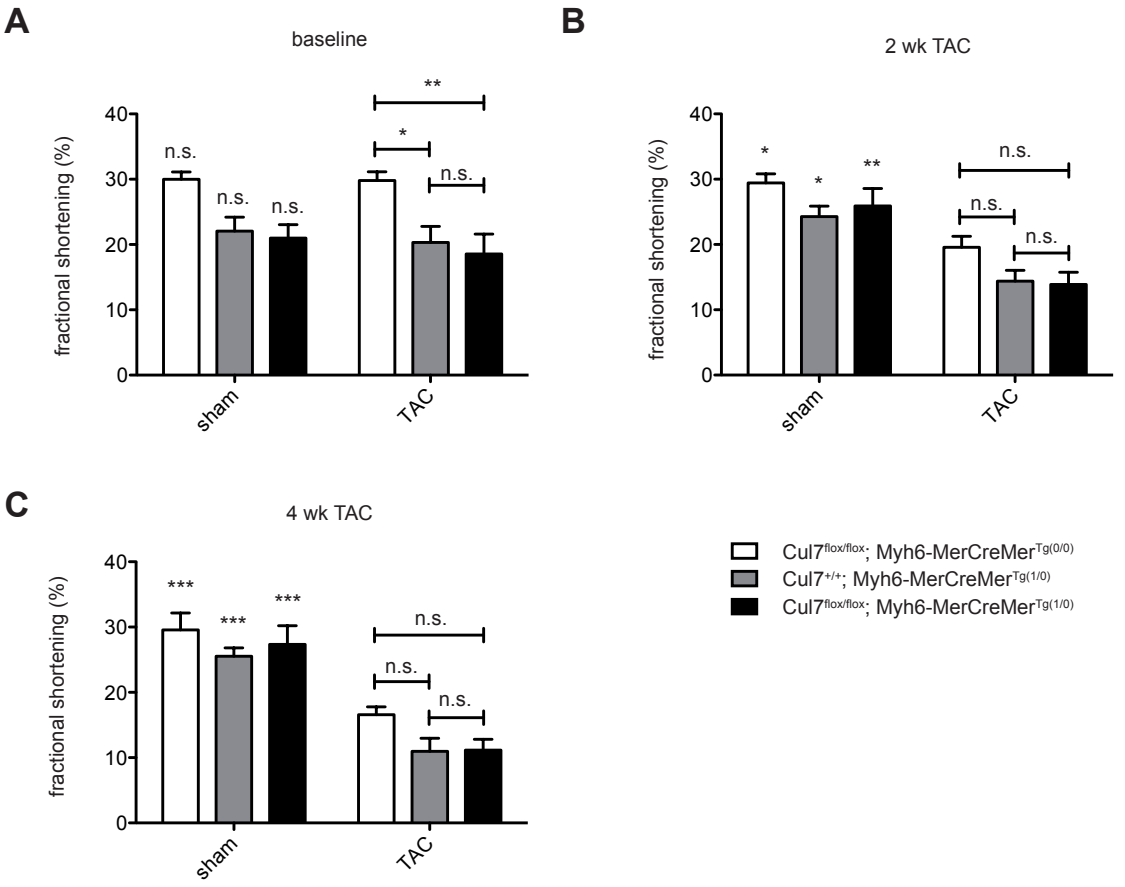

Figure 26: Fractional shortening (FS) under conditions of increased afterload.

Echocardiographic assessment of fractional shortening (FS) after transverse aortic constriction (TAC) and respective sham period at baseline (Fig. 26 A), after two weeks of transverse aortic constriction (Fig. 26 B) and after 4 weeks of aortic constriction (Fig. 26 C). Sham animals are shown in lanes 1-3, TAC animals in lanes 4-5, respectively. N=7-9. Statistics: ANOVA, *: $p<0.05$, **: $p<0.01$.

Left ventricular end-diastolic inner diameter (LVID, diastolic) showed an increase at baseline in Cul7$^{+/+}$; Myh6-MerCreMer$^{Tg(1/0)}$ and Cul7$^{flox/flox}$; Myh6-MerCreMer$^{Tg(1/0)}$ animals that reached significance in the TAC group (Fig. 27, A, lanes 4-6). There was no significant difference between the sham-operated and the TAC group at baseline. After 2 weeks of TAC, there was no alteration in LVID, diastolic when comparing isogenic sham and TAC animals. LVID, diastolic was markedly increased in Cul7$^{+/+}$; Myh6-MerCreMer$^{Tg(1/0)}$ and Cul7$^{flox/flox}$; Myh6-MerCreMer$^{Tg(1/0)}$ animals in comparison to Cul7$^{flox/flox}$; Myh6-MerCreMer$^{Tg(0/0)}$ controls, whereas those animals did not show any difference between each other (Fig. 27 B). After 4 weeks of TAC, Cul7$^{+/+}$; Myh6-MerCreMer$^{Tg(1/0)}$ animals showed a significantly increased LVID, diastolic, when compared to their respective sham animals, while there was no difference between sham and TAC-operated Cul7$^{flox/flox}$; Myh6-MerCreMer$^{Tg(0/0)}$ or Cul7$^{flox/flox}$; Myh6-MerCreMer$^{Tg(1/0)}$ mice. Within the TAC group Cul7$^{+/+}$; Myh6-MerCreMer$^{Tg(1/0)}$ animals showed an increased LVID, diastolic when compared to Cul7$^{flox/flox}$; Myh6-MerCreMer$^{Tg(0/0)}$ controls, whereas the other differences did not reach significance.

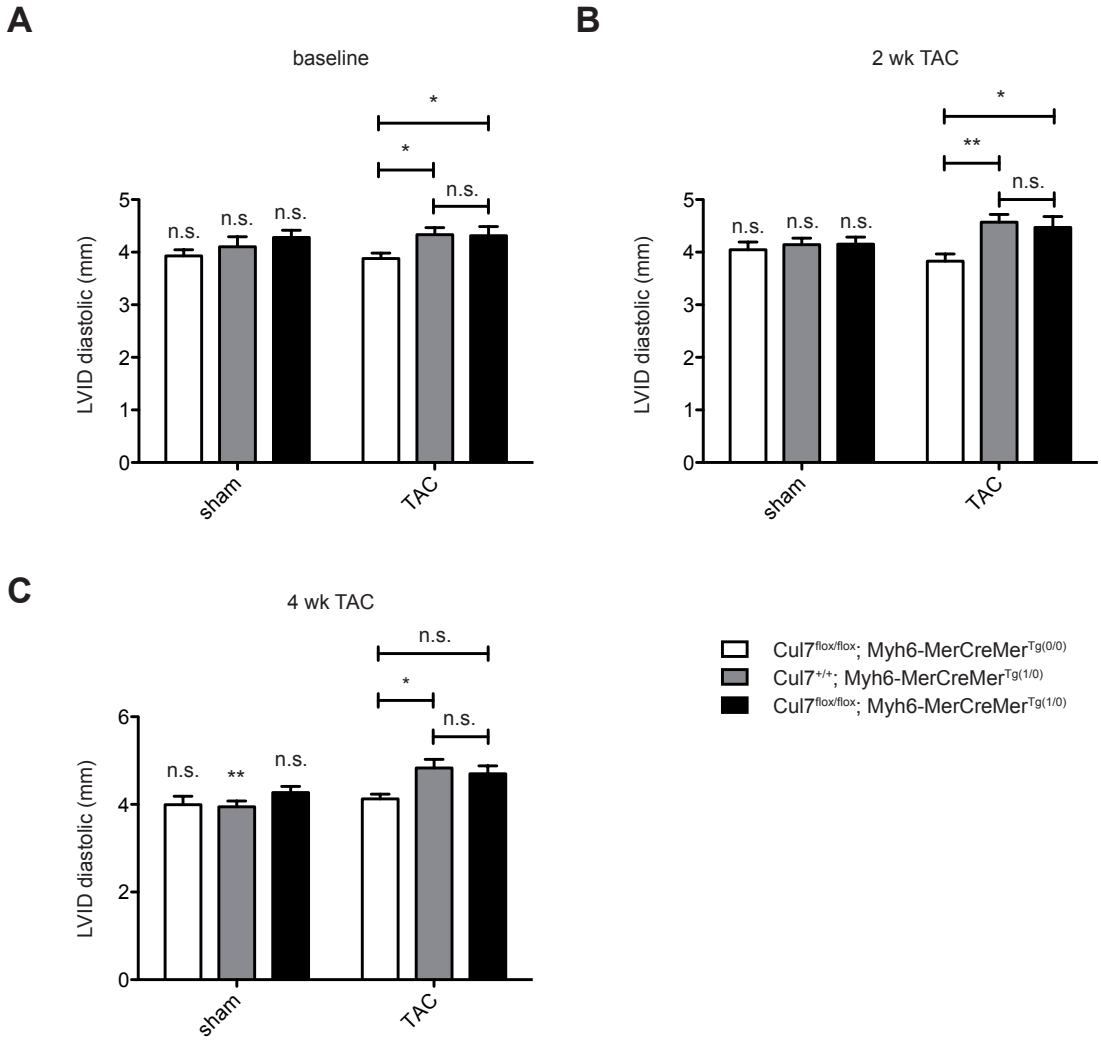

Figure 27: Left ventricular end-diastolic inner diameter (LVID, diastolic) under conditions of increased afterload.

Echocardiographic assessment of left ventricular end-diastolic inner diameter (LVID, diastolic) after transverse aortic constriction (TAC) and respective sham period at baseline (Fig. 27 A), after two weeks of transverse aortic constriction (Fig. 27 B) and after 4 weeks of aortic constriction (Fig. 27 C). Sham animals are shown in lanes 1-3, TAC animals in lanes 4-5, respectively. N=7-9. Statistics: ANOVA, *: $p<0.05$, **: $p<0.01$.

Left ventricular end-systolic inner diameter (LVID, systolic) at baseline did not show any difference between the sham and TAC group for comparison of isogenetic animals. Within the TAC group, there was an increase in LVID, systolic in Cul7$^{+/+}$; Myh6-MerCreMer$^{Tg(1/0)}$ and Cul7$^{flox/flox}$; Myh6-MerCreMer$^{Tg(1/0)}$ animals compared to Cul7$^{flox/flox}$; Myh6-

MerCreMer$^{Tg(0/0)}$ controls, that reached significance. Between Cul7$^{+/+}$; Myh6-MerCreMer$^{Tg(1/0)}$ and Cul7$^{flox/flox}$; Myh6-MerCreMer$^{Tg(1/0)}$ there was no difference detectable (Fig 28 A). After 2 weeks of TAC LVID, systolic was markedly increased in Cul7$^{+/+}$; Myh6-MerCreMer$^{Tg(1/0)}$ and Cul7$^{flox/flox}$; Myh6-MerCreMer$^{Tg(1/0)}$ mice, when compared to respective sham operated animals, whereas there was no difference for Cul7$^{flox/flox}$; Myh6-MerCreMer$^{Tg(0/0)}$ controls. Within the TAC group after 2 weeks the Cul7$^{+/+}$; Myh6-MerCreMer$^{Tg(1/0)}$ and Cul7$^{flox/flox}$; Myh6-MerCreMer$^{Tg(1/0)}$ mice displayed an significantly increased LVID, systolic when compared to Cul7$^{flox/flox}$; Myh6-MerCreMer$^{Tg(0/0)}$ controls (Fig. 28 B). This constellation was similar after 4 weeks of TAC (Fig. 28 C).

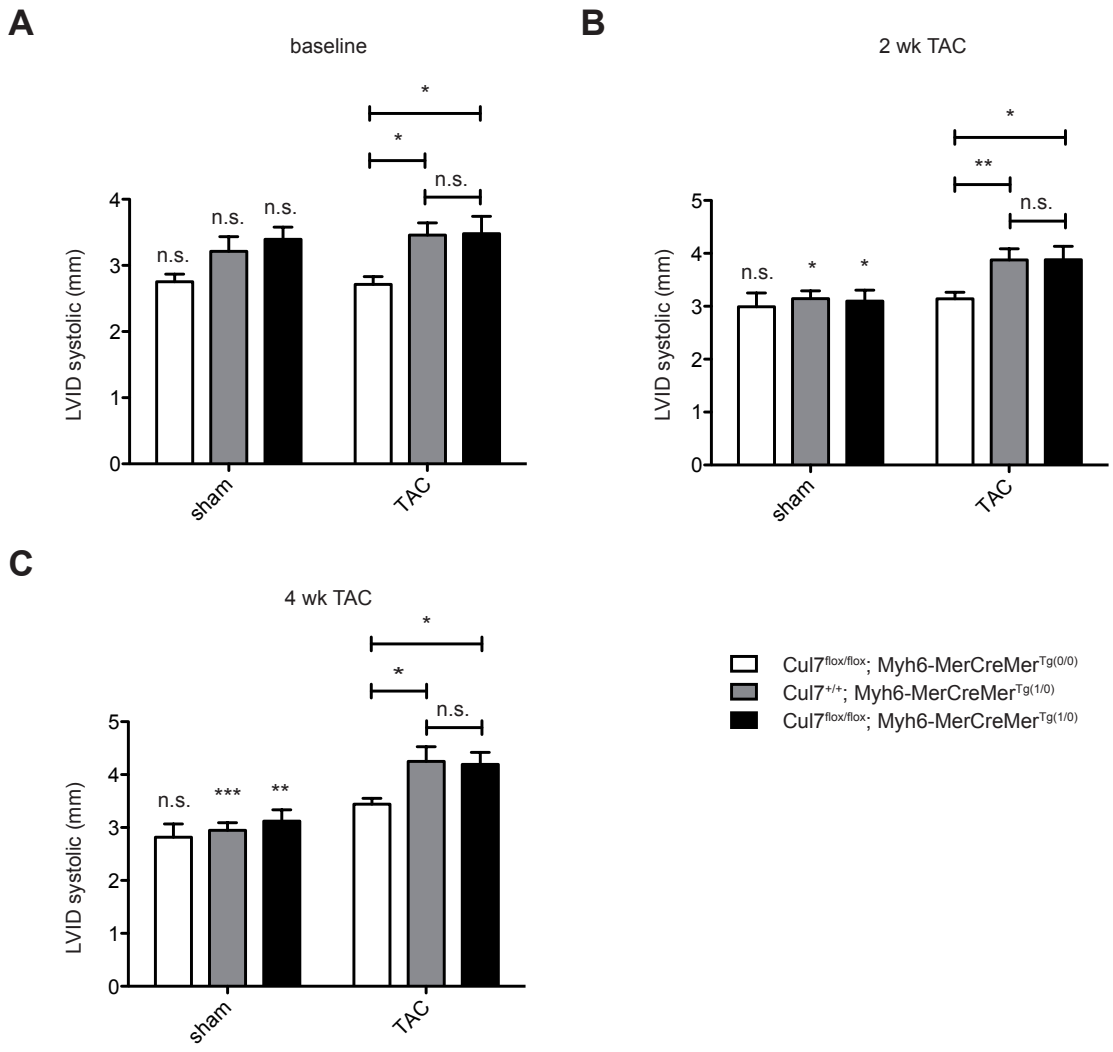

Figure 28: Left ventricular end-systolic inner diameter (LVID, systolic) under conditions of increased afterload.

Echocardiographic assessment of left ventricular end-systolic inner diameter (LVID, systolic) after transverse aortic constriction (TAC) and respective sham period at baseline (Fig. 28 A), after two weeks of transverse aortic constriction (Fig. 28 B) and after 4 weeks of aortic constriction (Fig. 28 C). Sham animals are shown in lanes 1-3, TAC animals in lanes 4-5, respectively. N=7-9. Statistics: ANOVA, *: $p<0.05$, **: $p<0.01$.

Taken together, increased afterload by transverse aortic constriction caused depression of cardiac function at both time points, 2 and 4 weeks, evidenced by decreased ejection fraction and fractional shortening as well as increased end-diastolic and end-systolic inner diameters of the ventricle. Cardiomyocyte-specific depletion of CUL7 under conditions of increased afterload was not sufficient to induce an improvement of cardiac function or an

amelioration of cardiac dysfunction when comparing Cul7$^{flox/flox}$; Myh6-MerCreMer$^{Tg(1/0)}$ mice with Cul7$^{+/+}$; Myh6-MerCreMer$^{Tg(1/0)}$ controls, as observed under basal conditions.

6.12. Left ventricular fibrosis under conditions of increased afterload

To investigate fibrosis under conditions of increased afterload, animals were subjected to transverse aortic constriction for 4 weeks and heart sections stained with Sirius Red / Fast Green. 4 weeks of transverse aortic constriction resulted in a significant increase of left ventricular fibrosis in both the Cul7$^{flox/flox}$; Myh6-MerCreMer$^{Tg(0/0)}$ and Cul7$^{+/+}$; Myh6-MerCreMer$^{Tg(1/0)}$ animals, with 1.3 % ± 0.7 % and 5.0 % ± 3.3 % for sham and TAC in Cul7$^{flox/flox}$; Myh6-MerCreMer$^{Tg(0/0)}$ animals ($p<0.05$) and 8.8 % ± 3.9 % and 12.4 % ± 2.9 % in Cul7$^{+/+}$; Myh6-MerCreMer$^{Tg(1/0)}$ mice ($p<0.05$), respectively. In Cul7$^{flox/flox}$; Myh6-MerCreMer$^{Tg(1/0)}$ mice, interstitial cardiac fibrosis was not significantly increased with 7.2 % ± 5.1 % for sham operated mice and 8.7 % ± 3.1 % in the TAC group. Additionally, as observed under basal conditions, Cul7$^{+/+}$; Myh6-MerCreMer$^{Tg(1/0)}$ (12.4 % ± 2.9 %, $p<0.001$) and Cul7$^{flox/flox}$; Myh6-MerCreMer$^{Tg(1/0)}$ animals (8.7 % ± 3.1 %, $p<0.05$) showed higher levels of left ventricular fibrosis, when compared to Cul7$^{flox/flox}$; Myh6-MerCreMer$^{Tg(0/0)}$ controls (5.0 % ± 3.3 %). Most remarkably, Cul7$^{flox/flox}$; Myh6-MerCreMer$^{Tg(1/0)}$ mice developed reduced left ventricular fibrosis in comparison to Cul7$^{+/+}$; Myh6-MerCreMer$^{Tg(1/0)}$ controls (8.7 % ± 3.1 % vs. 12.4 % ± 2.9 %, $p<0.05$), reflecting a reduction of left ventricular fibrosis of 29.8 % (Fig. 29 B).

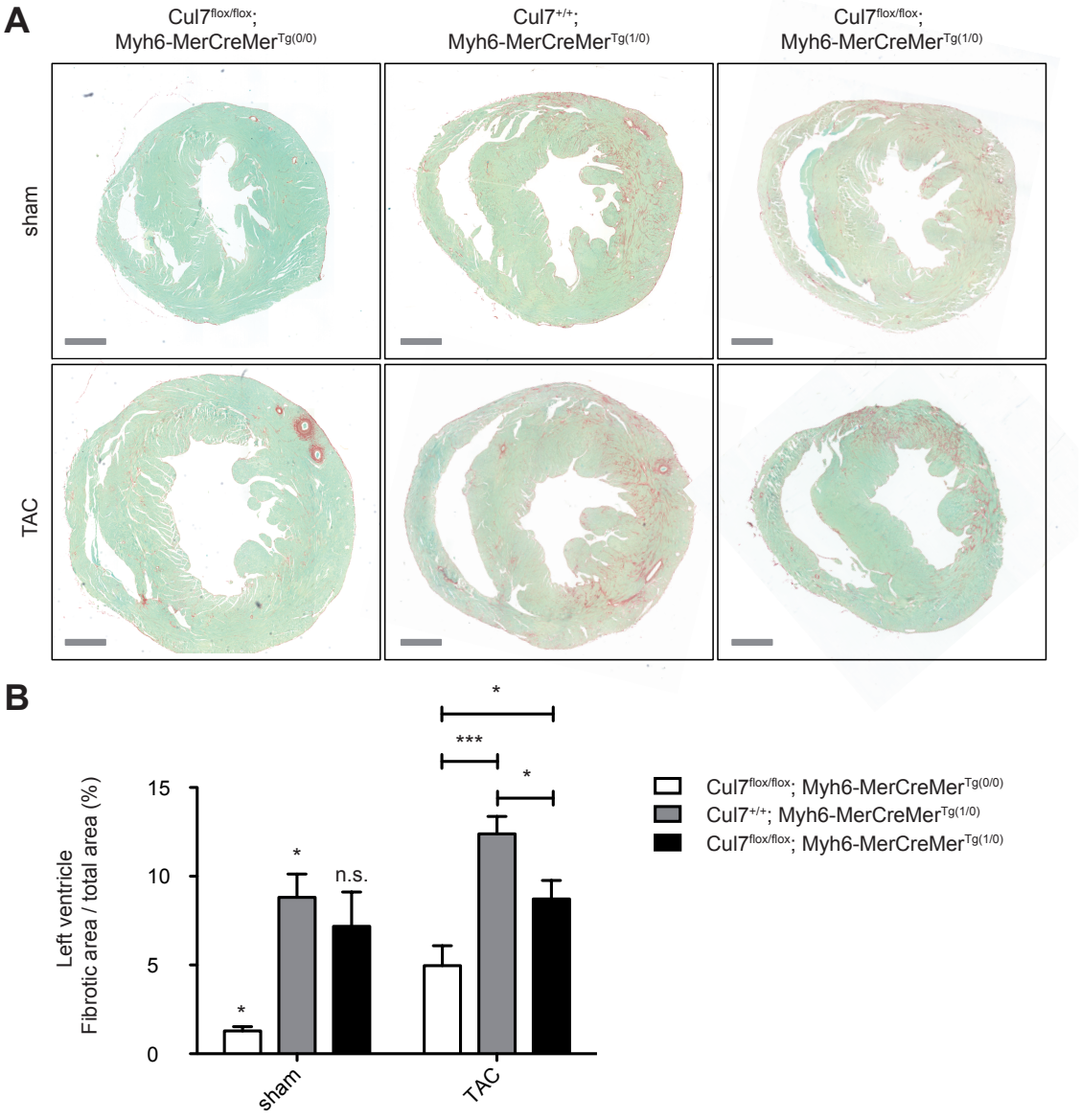

Figure 29: Left ventricular fibrosis under conditions of increased afterload.

Left ventricular interstitial fibrosis assessed by Sirius red / Fast green staining of murine hearts after 4 weeks of transverse aortic constriction (TAC) (Fig. 29 A, lower panel) and respective sham period (Fig. 29 A, top panel). Quantification of interstitial fibrosis in sham animals (Fig. 29 B, lanes 1-3) and TAC animals (Fig. 29 B, lanes 4-6). N=7-9. Representative pictures shown. Statistics: ANOVA, *: p<0.05, **: p<0.01, ***: p<0.001. Scale bar: 1 mm.

6.13. Cross sectional area under conditions of increased afterload

To elucidate effects of the cardiomyocyte-specific depletion of CUL7 on CM size under conditions of increased afterload, mice were subjected to 4 weeks of TAC and heart sections were stained using the wheat germ agglutinin assay followed by analysis of CM cross-sectional area (CSA). After 4 weeks of transverse aortic constriction, CSA was significantly increased in $Cul7^{flox/flox}$; $Myh6\text{-}MerCreMer^{Tg(0/0)}$ (468 μm^2 ± 68 μm^2 vs. 617 μm^2 ± 95 μm^2, $p<0.01$) , $Cul7^{+/+}$; $Myh6\text{-}MerCreMer^{Tg(1/0)}$ (433 μm^2 ± 83 μm^2 vs. 609 μm^2 ± 120 μm^2 ±, $p<0.001$) and $Cul7^{flox/flox}$; $Myh6\text{-}MerCreMer^{Tg(1/0)}$ animals (499 μm^2 ± 117 μm^2 vs. 609 μm^2 ± 138 , $p<0.05$) in comparison to their respective sham-operated controls (Fig. 30 B). Within the mice subjected to TAC-operation, there was no difference in CSA detectable for the different genotypes.

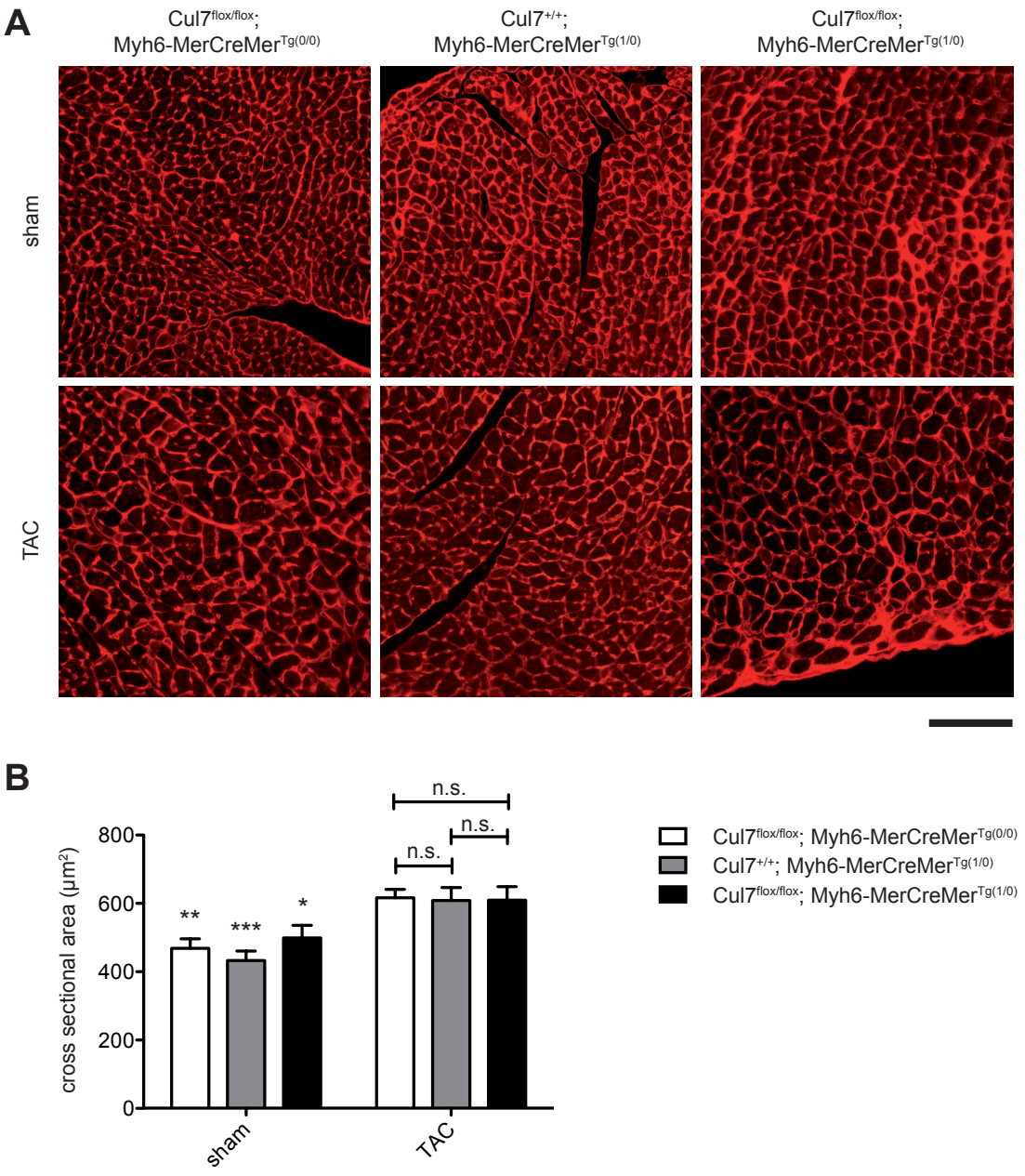

Figure 30: Cross sectional area under conditions of increased afterload.

Cross sectional area (CSA) of cardiomyocytes assessed by WGA staining of murine hearts after 4 weeks of transverse aortic constriction (TAC) (Fig. 30 A, lower panel) and respective sham period (Fig. 30 A, top panel). Quantification of CSA in sham animals (Fig. 30 B, lanes 1-3) and TAC animals (Fig. 30 B, lanes 4-6). N=3-8. Representative pictures displayed. Statistics: ANOVA, *: p<0.05, **: p<0.01, ***: p<0.001. Scale bar: 100 µm.

In conclusion, cardiomyocyte-specific CUL7 depletion did not lead to cellular cardiomyocyte hypertrophy as observed under basal conditions. Most remarkably, CM-specific CUL7 depletion resulted in a significant attenuation of left ventricular fibrosis and thereby cardiac remodeling under conditions of increased afterload in $Cul7^{flox/flox}$; Myh6-$MerCreMer^{Tg(1/0)}$ mice when compared to $Cul7^{+/+}$; Myh6-$MerCreMer^{Tg(1/0)}$ controls, as similarly observed to a smaller extent under basal conditions.

6.14. CUL7 in neonatal rat cardiomyocytes (NRCM)

To investigate the pathophysiological effect of CUL7 in cardiomyocytes in vitro, neonatal rat cardiomyocytes (NRCMs) were depleted of CUL7 via treatment with siRNA and the effects in response to phenylephrine-induced hypertrophy were studied. After treatment of NRCMs with siRNA directed against *Cul7*, the mRNA abundance was significantly reduced to 37 % ± 24 %, when compared to scramble treated cells (100 % ± 43 %; $p<0.05$) (Fig. 31 B). After treatment with phenylephrine (PE) mock-, scramble- and *Cul7* siRNA treated cells displayed a marked increase in cellular area (1164 μm^2 ± 121 μm^2, 1324 μm^2 ± 216 μm^2 and 1097 μm^2 ±185 μm^2), when compared to basal conditions (468 μm^2 ± 45 μm^2, 541 μm^2 ± 54 μm^2 and 491 μm^2 ± 101 μm^2, $p<0.001$) (Fig. 31 C). Remarkably, *Cul7* siRNA treated cells showed a significant reduction in cell area after PE treatment when compared with mock- or scramble-treated controls ($p<0.01$) (Fig. 31 C). The number of surviving cells was not statistically different between the mock, scramble and siRNA treated groups under basal (249 ± 184, 243 ± 112 and 265 ± 126) or PE conditions (346 ± 226, 488 ± 357 and 308 ± 136), respectively (Fig. 31 D).

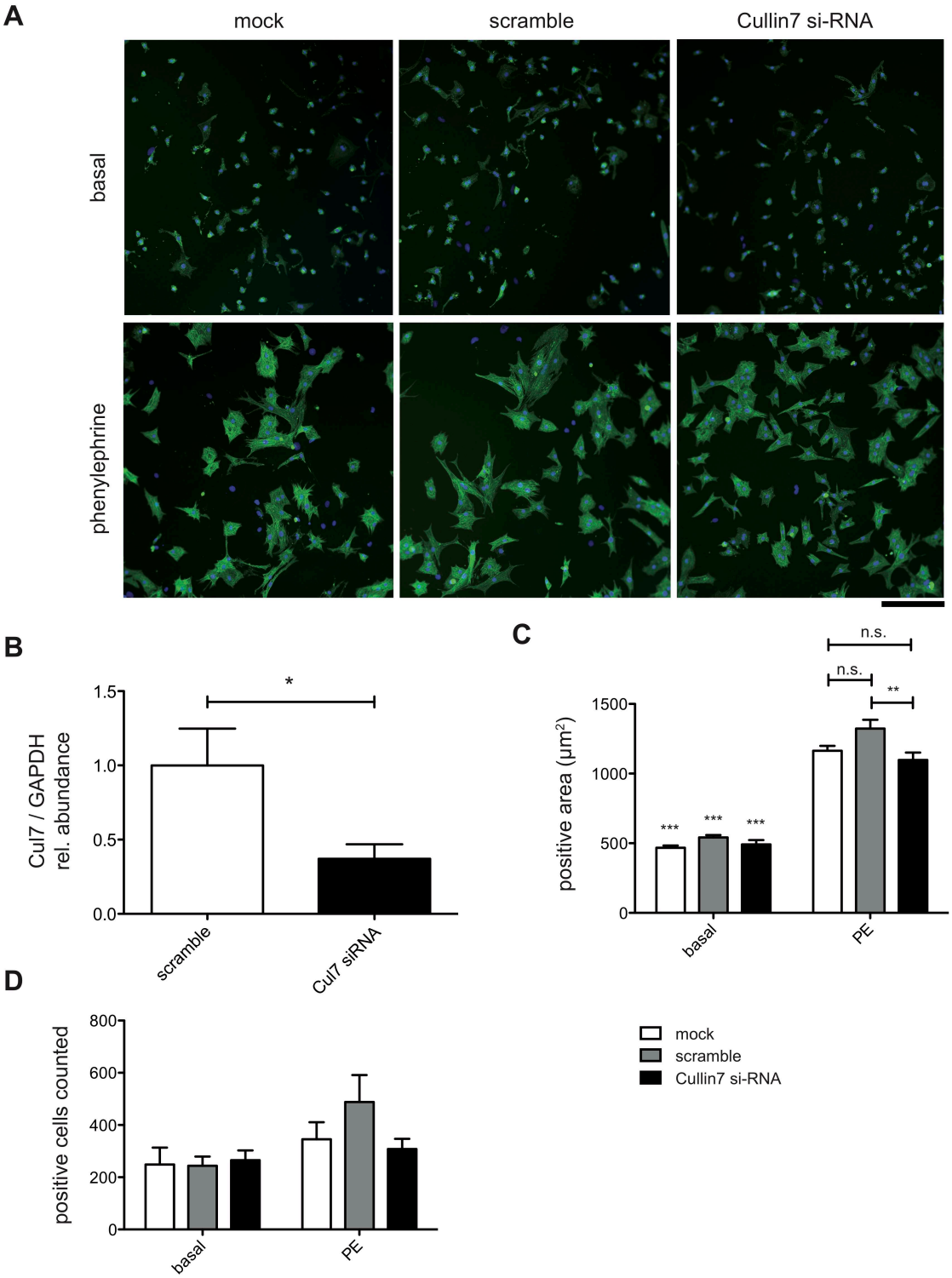

Figure 31: Cardiomyocyte hypertrophy under phenylephrine stimulation.

Immunofluorescence microscopy of NRCM after depletion of CUL7 by siRNA and stimulation with phenylephrine (Fig. 31 A, lower panel) or respective basal conditions (Fig. 31 A, top panel). Abundance of *Cul7* mRNA after

treatment of NRCM with siRNA vs. respective scramble RNA; N=3-6 (Fig. 31 B). Positive cross sectional area of NRCMs after stimulation with phenylephrine; N=8-12 (Fig. 31 C, lanes 4-6) and respective basal condition; N=8-12 (Fig. 31 C, lanes 1-3). Positive cell count of NRCM after stimulation with phenylephrine; N=8-12 (Fig. 31 D, lanes 4-6) and respective basal conditions; N=8-12 (Fig. 31 D, lanes 1-3). Representative pictures displayed. Statistics: ANOVA. *: $p<0.05$, **: $p<0.01$, ***: $p<0.001$. Scale bar: 250 µm.

7. Discussion

Cullin7 protein expression in different murine tissues and detection of a putative muscle-specific isoform.

When analyzing the expression pattern of the Cullin7 protein in different types of murine tissue, we were able to show robust expression throughout pancreas, lung, liver, kidney, adipose tissue, testis, brain and spleen. This is in concordance with findings from Huber et al. in 2005 where the described similar levels of RNA via Northern Blot analysis for kidney, lung, liver and brain, with an exception for the pancreas, in which they found a more pronounced expression in comparison to the before mentioned types of tissue (Huber et al. 2005). Additionally, we investigated the expression pattern of CUL7 in different types of muscle tissue. Interestingly, we found robust expression of the protein in cardiac and smooth muscle tissue, but only a weak expression of CUL7 in protein samples derived from skeletal muscle, when analyzing the signal intensity at the expected running height of the CUL7 at approximately 190 kDa in immunoblot analysis. Unexpectedly for both, in cardiac muscle and even more pronounced in skeletal muscle, there was a second protein band at the running height of 150 kDa, which was not detectable in the other types of tissue investigated. If taking this band into account, the CUL7 abundance in skeletal muscle observed in our protein expression studies was in significant concordance with earlier findings of Huber et al., with skeletal muscle being among the tissues showing the highest CUL7 expression. Furthermore, we were able to demonstrate expression of this second protein band in the purified cardiomyocyte cell fraction of the murine heart, whereas the non-cardiomyocytes cell fraction did not reveal expression of this additional band. BLAST analysis of the epitope of the CUL7 antibody used in the immunoblot analysis did not reveal any predicted targets at this running height, or more specifically the molecular weight of 150 kDa, in cardiac or skeletal muscle or any other of the investigated tissues. Thus these findings raise evidence for the existence of a by now not described isoform of CUL7. This isoform may have a limited expression pattern for striated types of muscle tissue, as its expression was only observed in skeletal muscle and cardiomyocytes. Database research of the expression of human CUL7 revealed the existence of two protein-coding transcripts, one with the length of 5504 bp (Transcript ID: ENST00000535468) and the other with 5254 bp (Transcript ID: ENST00000265348), resulting in a 1782 aa and 1698 aa long protein, respectively (www.ensembl.org.). The alteration between those two isoforms is located at the N-terminus of the Cullin7 protein, with exons one and two being longer in the long

version of the protein. Interestingly, Okazaki et al found a predicted protein-coding sequence of the *Cul7* gene, when investigating mouse cDNA libraries for human KIAA homologous genes in 2004 (Okazaki 2004). They reported on a predicted protein-coding cDNA sequence, which was identical with the *Cul7* cDNA, except an N-terminal truncation of 928 bps corresponding to a loss of 182 aa. Most interestingly, this truncated version of the CUL7 still comprises all relevant functional domains of the known Cullin7 protein and thus may be the homolog of an N-terminally truncated second isoform of CUL7 in murine tissue, as observed in humans. To elucidate this point more clearly, mass spectrometry analysis would be necessary, to clearly show the presence of a truncated Cullin7 protein in striated types of murine muscle tissue.

CUL7 depletion mediates an improvement of cardiac function after tamoxifen-treatment.

Furthermore, we elucidated the impact of the cardiomyocyte-specific CUL7 deletion on the phenotype of mice under basal conditions. Morphological phenotype of the animals was unchanged after CUL7 depletion. Additionally, we evaluated cardiac performance after CUL7 depletion. Two weeks after the induction of the Cre-mediated recombination, we observed a decrease in ejection fraction and fractional shortening in Cre-carrying animals when compared to non Cre-carrying animals. This is in concordance with findings from Hall et al in 2011, where they described a transient reduction of cardiac function in Cre-carrying animals after injection of tamoxifen when compared to non-Cre carrying animals. Cre-carrying animals did not show any differences in cardiac functional parameters at baseline before injection of tamoxifen when compared to non-Cre carrying animals, nor did tamoxifen injection alone alter cardiac function in animals not carrying the Cre-allele (Hall et al. 2011). After six weeks of CUL7 deletion, CUL7 depleted animals showed an improved cardiac function when compared to their respective Cre-carrying control group, the $Cul7^{+/+}$; Myh6-$MerCreMer^{Tg(1/0)}$ animals. Furthermore, they did not display a reduction of ejection fraction or fractional shortening in comparison to non-Cre carrying controls, $Cul7^{flox/flox}$. At the same time point, $Cul7^{+/+}$; Myh6-$MerCreMer^{Tg(1/0)}$ still displayed significantly impaired cardiac function in comparison to the latter group. After two more weeks, those differences have vanished. In light of those findings cardiomyocyte-specific CUL7 depletion was able to improve cardiac function under basal, unchallenged conditions, although this improvement of cardiac function could also be interpreted as an amelioration of cardiac dysfunction, that

was induced by tamoxifen treatment of the Cre-carrying animals as described by Hall and coworkers (Hall et al. 2011). This improvement of cardiac function / amelioration of dysfunction in Cul7$^{flox/flox}$; Myh6-MerCreMer$^{Tg(1/0)}$ animals was further underlined by lower end-systolic left ventricular volumes when compared to respective Cre-carrying control group, which displayed more dilation of the ventricle and similar values as their non Cre-carrying controls. Similar effects were observed on diastolic function. Left ventricular wall thickness as an indicator of cardiac hypertrophy and contractility did not show significant alterations in Cul7$^{flox/flox}$; Myh6-MerCreMer$^{Tg(1/0)}$ animals when compared to their respective control groups, but displayed a trend towards an increase of left ventricular wall thickness, mainly in the systole, when compared to Cre-carrying controls, Cul7$^{+/+}$; Myh6-MerCreMer$^{Tg(1/0)}$. This is in considerable concordance with our previous findings, underlining an improvement of cardiac function / amelioration of cardiac dysfunction, in this case, evident as dilation of the ventricle and decrease in posterior wall thickness, pointing towards a situation similar to failing hearts, displaying eccentric hypertrophic reactions (van Berlo et al. 2013).

CUL7 depletion leads to cardiomyocyte hypertrophy under basal conditions.

We subsequently investigated the influence of cardiomyocyte-specific CUL7 depletion on hypertrophy of the cardiomyocyte on a cellular level. We were able to show, that the cross-sectional area of left ventricular sections from CUL7 depleted hearts of Cul7$^{flox/flox}$; Myh6-MerCreMer$^{Tg(1/0)}$ animals displayed an increased cross-sectional area when compared to respective controls under basal, unchallenged conditions. In contradiction to this, Nakajima et al observed a reduction of hypertrophy in hearts of mice expressing a dominant negative mutant of CUL7 under the control of the alpha-MHC promoter after subjecting those animals to myocardial infarction by occlusion of the left anterior descending artery in 2004. Additionally, they observed induction of DNA-synthesis in cardiomyocytes in the interventricular septum of those mice, pointing towards a re-entry of otherwise post-mitotic cardiomyocytes into the cell cycle, thereby leading to a compensation of lost CM due to myocardial infarction, finally resulting in a reduced necessity of compensatory hypertrophy of remnant CM to maintain cardiac function (Nakajima et al. 2004). Furthermore, the increase of the cross-sectional area was more pronounced in the septum of the hearts of the Cul7$^{flox/flox}$; Myh6-MerCreMer$^{Tg(1/0)}$ animals, while the increase of CSA observed in the lateral wall was developed to a fewer extent. This differences in location of hypertrophy can

have different underlying mechanisms. Werfel et al showed in 2014, that the Myh6-MerCreMer$^{Tg(1/0)}$ construct is not equally activated throughout the left ventricle. Therefore, they crossed Myh6-MerCreMer$^{Tg(1/0)}$ animals with ROSA26-LacZ reporter mice and observed increased expression of LacZ in the lateral walls of those animals, underlining the asymmetric distribution of the activity of the Myh6-MerCreMer$^{Tg(1/0)}$ construct (Werfel et al. 2014). This may lead to an increased hypertrophic response in the septum of affected hearts due to compensatory effects of a higher detraction of the cardiomyocytes and thus contractility of the lateral wall of the left ventricle. Another explanation for the occurrence of asymmetric hypertrophy of the left ventricle with a pronunciation of the septum would be an impairment of the ubiquitin-proteasome system. Impairment of the UPS has been linked to the development of hypertrophic cardiomyopathy, leading to pronounced hypertrophy of the septum (Schlossarek et al. 2011). On the other hand, the precise regulation of the activity of the UPS in the heart has been shown to be critical for the development of pathological conditions and therefore has to be regulated in a strict manner (Predmore et al. 2010). One major point for the regulation of the UPS is posttranslational modification by phosphorylation / de-phosphorylation as demonstrated by Zong et al in 2006, where they reported on the pivotal role of phosphorylation in regulation of the cardiac proteasome. Here, they were able to identify two key players, namely PKA and protein phosphatase 2A (PP2A) (Zong et al. 2006). By influencing signaling cascades in the cardiomyocyte, disturbance of function of the CRL7 may affect those strictly controlled phosphorylation-mediated regulation networks and thus impair proper function of the ubiquitin-proteasome system in the heart, finally leading to its malfunction and cardiomyopathy. Additionally, there is the possibility of the existence of a by now not described proteolytic target of the CRL7 in the heart, thereby causing an accumulation of this substrate protein upon depletion of CUL7, finally leading to cellular stress and a surcharge of the remaining degradation machinery. One example for a similar mechanism is the familial hypertrophic cardiomyopathy (FHC), which is known to be caused by mutations of structural sarcomeric proteins leading to a surcharge of the UPS and thereby inhibition of its proper function (Sarikas et al. 2005). Furthermore, we were able to show that CUL7 plays an important role in insulin signaling and thereby energy homeostasis, thus having a possible influence on cardiac ATP levels, which itself play an important role in the highly energy dependent UPS machinery (Scheufele et al. 2014).

CUL7 depletion ameliorates interstitial cardiac fibrosis in unchallenged conditions.

Subsequently, we investigated the influence of cardiomyocyte-specific CUL7 depletion on cardiac left ventricular interstitial fibrosis under basal, unchallenged conditions. We found, that CUL7 depleted hearts of Cul7$^{flox/flox}$; Myh6-MerCreMer$^{Tg(1/0)}$ animals displayed an amelioration of cardiac interstitial fibrosis by trend when compared to the respective Cre-carrying control group, Cul7$^{+/+}$; Myh6-MerCreMer$^{Tg(1/0)}$. In addition to that, we observed an increase of fibrotic area in both Cre-carrying groups, Cul7$^{flox/flox}$; Myh6-MerCreMer$^{Tg(1/0)}$ and Cul7$^{+/+}$; Myh6-MerCreMer$^{Tg(1/0)}$, when compared to non Cre-carrying Cul7$^{flox/flox}$; Myh6-MerCreMer$^{Tg(0/0)}$ animals. A possible underlying mechanism for this could be a Cre-mediated loss of cardiomyocytes due to Cre-toxicity resulting in remodeling of the myocardium and development of interstitial reparative fibrosis in the heart (van Berlo et al. 2013). Similar results were observed by Lexow et al. in 2013, as they reported on focal cardiac fibrosis in Myh6-MerCreMer$^{Tg(1/0)}$ animals in a Tβ4shRNA^{flox} × Myh6-MerCreMer$^{Tg(1/0)}$ transgene strain that was independent of the presence or absence of the Tβ4shRNA^{flox} allele. This was accompanied by increased expression of pro-inflammatory cytokines and hypertrophy markers (Lexow et al. 2013). Thus, the reduction of cardiac fibrosis observed in Cul7$^{flox/flox}$; Myh6-MerCreMer$^{Tg(1/0)}$ may likely result from a reduction of cardiomyocyte loss, less remodeling and thus less interstitial reparative fibrosis.

CUL7 depletion leads to activation of the Akt signaling pathway in cardiomyocytes.

Additionally, we investigated the impact of cardiomyocyte-specific CUL7 depletion on IRS-1 dependent signaling pathways. Here, we found a 1.5 fold up-regulation of the Akt signaling pathway in cardiomyocytes isolated from the hearts of Cul7$^{flox/flox}$; Myh6-MerCreMer$^{Tg(1/0)}$ animals. This is in considerable concordance with previous findings of our group, in which we investigated the influence of heterozygosity of *Cul7* or *Fbxw8* on IRS-1 dependent signaling in skeletal muscle tissue (M. gastrocnemius) in vivo. For both, the *Cul7*$^{+/-}$ and *Fbxw8*$^{+/-}$ we found a 1.5 – 2-fold increased activation of the Akt signaling pathway in skeletal muscle tissue when compared to respective *Cul7*$^{+/+}$ and *Fbxw8*$^{+/+}$ controls under basal conditions. This effect was even more pronounced by intraperitoneal injection of insulin with a 2.5 – 3-fold increase of Akt signaling evidenced by p-Akt / t-Akt ratio in Cul7$^{+/-}$ and Fbxw8$^{+/-}$ when compared to wild-type controls (Scheufele et al. 2014).

No influence of CUL7 depletion on cardiac phenotype after transverse aortic constriction.

In addition to this, we investigated the effect of cardiomyocyte-specific CUL7 depletion on the phenotype of the mice under conditions of increased afterload. We observed a significant increase of heart weight / tibia length, ventricular weight / tibia length and atrial weight / tibia length ratios when comparing animals subjected to 4 weeks of transverse aortic constriction with sham operated controls for $Cul7^{flox/flox}$; $Myh6\text{-}MerCreMer^{Tg(1/0)}$, $Cul7^{+/+}$; $Myh6\text{-}MerCreMer^{Tg(1/0)}$ and $Cul7^{flox/flox}$; $Myh6\text{-}MerCreMer^{Tg(0/0)}$ animals. There were no significant differences detectable between the respective groups under conditions of increased afterload, with exception of an increased atrial weight / tibia length ratio in $Cul7^{flox/flox}$; $Myh6\text{-}MerCreMer^{Tg(1/0)}$ mice when compared to $Cul7^{flox/flox}$; $Myh6\text{-}MerCreMer^{Tg(0/0)}$ controls. Increased atrial weight / tibia length ratios may reflect more severe impairment of cardiac function. On the other hand, while TAC increased the lung weight / tibia length ratio in comparison to sham-operated mice in all genotypes, lung weight / tibia length ratio was equally increased in $Cul7^{flox/flox}$; $Myh6\text{-}MerCreMer^{Tg(1/0)}$ and $Cul7^{+/+}$; $Myh6\text{-}MerCreMer^{Tg(1/0)}$ mice when compared to $Cul7^{flox/flox}$; $Myh6\text{-}MerCreMer^{Tg(0/0)}$ controls, reflecting an impaired cardiac function in those Cre-carrying animals and the transition towards heart failure, whereas the non Cre-carrying animals were still in a phase of compensation (van Berlo et al. 2013). The presence or absence of the CUL7 protein did not change transition to heart failure. More likely the Cre-induced cardiomyopathy and remodeling status of the heart may depict a disposition towards the development of heart failure and may reduce the ability of the heart to maintain the status of compensation of cardiac function.

No beneficial effect of CUL7 depletion on cardiac function under conditions of increased afterload.

Next, we investigated the effect of cardiomyocyte-specific CUL7 depletion on cardiac function under conditions of increased afterload. As observed under basal conditions, cardiac function, assessed by ejection fraction and fractional shortening, was initially decreased in both the $Cul7^{flox/flox}$; $Myh6\text{-}MerCreMer^{Tg(1/0)}$ and $Cul7^{+/+}$; $Myh6\text{-}MerCreMer^{Tg(1/0)}$ animals, when compared to non Cre-carrying controls, $Cul7^{flox/flox}$; $Myh6\text{-}MerCreMer^{Tg(0/0)}$. After two weeks of aortic constriction, $Cul7^{flox/flox}$; $Myh6\text{-}MerCreMer^{Tg(1/0)}$ animals did not show improved EF and FS as observed under unchallenged conditions when compared to $Cul7^{+/+}$; $Myh6\text{-}MerCreMer^{Tg(1/0)}$ controls, but even a further decrease in cardiac functional

parameters. After 4 weeks of increased afterload, cardiac function showed a more severe impairment in the TAC group when compared to respective sham-operated animals and in comparison to 2 weeks of aortic constriction, as expected. Depletion of CUL7 did not improve or deteriorate cardiac function when compared to Cre-carrying controls. Further, assessment of cardiac function showed an increased end-diastolic left ventricular inner diameter in both the Cul7$^{flox/flox}$; Myh6-MerCreMer$^{Tg(1/0)}$ and Cul7$^{+/+}$; Myh6-MerCreMer$^{Tg(1/0)}$ animals, when compared to Cul7$^{flox/flox}$; Myh6-MerCreMer$^{Tg(0/0)}$ controls, at baseline, after 2 weeks and 4 weeks of transverse aortic constriction. Interestingly, this difference in end-diastolic left ventricular inner diameter vanished in the sham group at the time points of 2 and 4 weeks, whereas it was still prominent in the TAC group. This raises evidence for an even more pronounced cardio-depressive effect of the Cre-enzyme under conditions of increased afterload, with a reduced ability for regeneration of cardiac function after Cre-activation and the tendency towards dilation of the left ventricular. Additionally, we measured the end-systolic left ventricular inner diameter at baseline, after 2 weeks and 4 weeks of TAC. In analogy to the end-diastolic left ventricular inner diameter, end-systolic left ventricular inner diameter was increased in both Cre-carrying animals, Cul7$^{flox/flox}$; Myh6-MerCreMer$^{Tg(1/0)}$ and Cul7$^{+/+}$; Myh6-MerCreMer$^{Tg(1/0)}$, when compared to Cul7$^{flox/flox}$; Myh6-MerCreMer$^{Tg(0/0)}$ controls at baseline for both sham-operated animals and animals subjected to TAC. Similar effects were observed after 2 weeks and 4 weeks of increased afterload. On the other hand, increased end-systolic left ventricular inner diameter normalized after 2 and 4 weeks in the sham group. This underlined an impairment of systolic function in Cre-carrying animals, Cul7$^{flox/flox}$; Myh6-MerCreMer$^{Tg(1/0)}$ and Cul7$^{+/+}$; Myh6-MerCreMer$^{Tg(1/0)}$, that was transient under basal, unchallenged conditions but did not show the ability of regeneration under challenging conditions of increased afterload.

CUL7 depletion is protective against intestinal fibrosis under conditions of increased afterload.

Subsequently, we investigated the development of left ventricular fibrosis under conditions of increased afterload by transverse aortic constriction in cardiomyocyte-specific CUL7 depleted murine hearts and respective controls. In the sham group, we were able to reproduce the results as observed under basal conditions with an increase in left ventricular fibrotic area in both Cre-carrying animals, when compared to non Cre-carrying controls, while the presence of fibrosis was attenuated in Cul7$^{flox/flox}$; Myh6-MerCreMer$^{Tg(1/0)}$ when

compared to Cul7$^{+/+}$; Myh6-MerCreMer$^{Tg(1/0)}$ controls. Four weeks of transverse aortic constriction resulted in a significant increase of left ventricular fibrosis in both the Cul7$^{flox/flox}$; Myh6-MerCreMer$^{Tg(0/0)}$ and Cul7$^{+/+}$; Myh6-MerCreMer$^{Tg(1/0)}$ animals. Interestingly, TAC for 4 weeks did not result in a significant increase in fibrotic area in Cul7$^{flox/flox}$; Myh6-MerCreMer$^{Tg(1/0)}$ mice when compared to sham-operated controls suggesting a protective effect of CUL7 depletion. Most notably, Cul7$^{flox/flox}$; Myh6-MerCreMer$^{Tg(1/0)}$ animals showed a reduction of left ventricular fibrosis by 29.8 % when compared to Cul7$^{+/+}$; Myh6-MerCreMer$^{Tg(1/0)}$ animals after 4 weeks of increased afterload. There have been earlier reports on CUL7 and its role in fibrogenesis by Paradis et al. in 2013, where they described an increased presence of a 6p21.1 amplification, representing the human *Cul7* gene locus, in hepatocellular carcinoma (HCC) on the basis of metabolic syndrome in humans when compared to HCC due of infection with hepatitis C virus. They further report on an increased peri-tumoral liver fibrosis in those individuals carrying the 6p21.1 amplification and a reduced rate of cell proliferation and increased apoptosis in hepatoma cell lines transfected with siRNA directed against *Cul7* (Paradis et al. 2013). Additionally, our group was able to raise evidence for a pivotal role of premature senescence in the development of cardiac fibrosis. Meyer at al. showed that, under conditions of increased ventricular fibrosis, introduced by expression of a transgenic active mutant of the β-1 receptor or by an increment of afterload through TAC, markers of senescence were up-regulated in fibrotic lesions of the heart when compared to unchallenged controls. In concordance to that, mice deficient of key senescence molecules, p53 and p16 were found to be more susceptible to the development of cardiac fibrosis upon pathologic stimuli. On the other hand, cardiac overexpression of CCN1 ameliorated fibrotic response to increased afterload by TAC (Meyer et al. 2016). In 2008 Xu and coworkers reported on murine fibroblasts null for *Cul7* (Cul7$^{-/-}$) displaying poor growth rates and a phenotype similar to that observed in senescent cells with an enlarged and flat morphology in culture, despite activation of pro-growth pathways Akt and Erk1/2. In addition to that, *Cul7*$^{-/-}$ murine embryonic fibroblasts showed increased staining intensity of senescence-associated β-galactosidase activity (SA-β-gal) when compared to *Cul7*$^{+/+}$ controls, which was found to be further increased during passage of the cells to up to 60 %, whereas *Cul7*$^{+/+}$ cells showed a maximum β-galactosidase positivity of 8 % (Xu et al. 2008). Thus, reduction of cardiac fibrosis observed in Cul7$^{flox/flox}$; Myh6-MerCreMer$^{Tg(1/0)}$ mice after 4 weeks of increased afterload may be mediated by induction of a senescent phenotype in the heart, which is having its origin in senescent cardiomyocytes. Here, the development a senescence-associated secretory phenotype (SASP), and thus influence on the surrounding interstitial cells, like fibroblasts by the

induction of senescence in a paracrine manner may be an underlying mechanism. This was described by Acosta et al in 2013, where the showed induction of paracrine senescence of normal cells in vitro and in vivo mediated via the SASP (Acosta et al. 2013).

CUL7 depletion did not enhance TAC mediated cardiomyocyte hypertrophy.

In addition to that, we studied the effect of cardiomyocyte-specific depletion of CUL7 on cardiac hypertrophy under conditions of increased afterload by transverse aortic constriction. We found that for $Cul7^{flox/flox}$; Myh6-$MerCreMer^{Tg(0/0)}$, $Cul7^{+/+}$; Myh6-$MerCreMer^{Tg(1/0)}$ and $Cul7^{flox/flox}$; Myh6-$MerCreMer^{Tg(1/0)}$ animals, CSA was significantly increased after a period of 4 weeks of transverse aortic banding. On the other hand, depletion of CUL7 in cardiomyocytes of $Cul7^{flox/flox}$; Myh6-$MerCreMer^{Tg(1/0)}$ animals did not result in increased CSA under conditions of increased afterload, when compared to respective $Cul7^{flox/flox}$; Myh6-$MerCreMer^{Tg(0/0)}$ and $Cul7^{+/+}$; Myh6-$MerCreMer^{Tg(1/0)}$ control animals of the TAC group. This differential impact of depletion of CUL7 on hypertrophy of cardiomyocytes could be caused by the different signaling pathways, that are predominantly activated during conditions of physiological cardiac hypertrophy (induced by repeated exercise stimulation e.g. swimming or running) and pathological hypertrophy (induced by pathological stimulation of the heart e.g. volume overload or increased afterload). Central signaling pathways involved in the development of physiological hypertrophy of the heart are the IGF-1 signaling pathway and the growth hormone pathway, both activating PI3K isoform p110α, which further leads to activation of Akt by PDK1. This finally results in phosphorylation and activation of mTOR, a key player in the regulation of protein synthesis and biogenesis of ribosomes (Dorn et al. 2005). Shioi et al showed, that cardiomyocyte-specific expression of a constitutively active mutant of PI3K resulted in the development of increased heart size with the absence of cardiac fibrosis, apoptosis, activation of fetal genes and functional impairment and thus mimicking parameters of physiological cardiac hypertrophy. This was mediated by an increased activation of the Akt signaling pathway, while activation levels of Erk1/2 were not altered. Furthermore, the expression of a dominant negative mutant of PI3K resulted in a reduced heart size (Shioi et al. 2000). The importance of PI3K/Akt signaling in the development of physiological hypertrophy was further underlined by McMullen et al, as they demonstrated, that expression of a cardiomyocyte-specific dominant negative mutant of PI3K was able to prevent development of cardiac hypertrophy induced by exercise (e.g. swimming), whereas its expression did not prevent hypertrophy

due the pathological stimulus of increased afterload by aortic banding. Furthermore, its expression led to severe cardiac dilatation and functional impairment after aortic banding, underlining the protective effect of the Akt pathway under pathological conditions (McMullen et al. 2003). On the other hand, Erk1/2 is known to be an important signaling pathway involved in the development of concentric hypertrophy, a form of cardiac hypertrophy observed under pathological conditions, arising from increased afterload (e.g. hypertension, aortic valve disease or aortic stenosis). This initially leads to compensation of the compromised cardiac function, but finally results in decompensation, dilatation and ultimately heart failure. Bueno et al. demonstrated, that cardiomyocyte directed expression of an active mutant of MEK1, leading to activation of Erk1/2, but not JNK and p38, resulted in the development of concentric hypertrophy and an increase in cardiac function, both characteristics of the phenotype of mice subjected to increased afterload (Bueno et al. 2000). Further important signaling pathways in the development of pathological hypertrophy are Calcineurin-NFAT and Ca^{2+}/Cam II signaling pathways, both known to be activated upon afterload increment leading to hypertrophy. It has been shown, that expression of an activated Calcineurin or NFAT mutant in vivo resulted in cardiac hypertrophy, and treatment with Cyclosporin A was able to abrogate this effect (Molkentin et al. 1998). Additionally, Bueno et al showed that Calcineurin Aβ-deficient mice displayed a reduction of cardiac hypertrophy in response to pressure overload, isoproterenol or angiotensin II infusion (Bueno et al. 2002). Furthermore, NFATc3-null mice displayed attenuated cardiac hypertrophy in response to increased afterload and Ang-II infusion (Wilkins et al. 2002). Similar effects were observed with deletion of NFATc2, they major transcript of the NFAT genes, which resulted in an attenuation of afterload induced hypertrophy by transverse aortic constriction, whereas exercise-induced physiological cardiac growth was not affected (Bourajjaj et al. 2008). Additionally, calcium / calmodulin-dependent protein kinase II (CaMKII) plays an important role in afterload induced cardiac hypertrophy, as it has been demonstrated, that depletion of the predominant cardiac isoform CaMKII δ, resulted in attenuation of cardiac growth in response to pressure overload (Backs et al. 2009). Thus, activation of Akt signaling by depletion of CUL7 in cardiomyocytes as observed in our study was able to cause cardiac hypertrophy evidenced by increased CSA under basal conditions, but may not have been sufficient to further increase hypertrophic response under conditions of increased afterload, in which other signaling pathways (e.g. Erk1/2, Calcineurin-NFAT and Ca^{2+}/Cam II) play a more dominant role for cardiac growth than the Akt signaling pathway. Otherwise, as evidenced by the reduced cardiac fibrosis observed in $Cul7^{flox/flox}$; Myh6-$MerCreMer^{Tg(1/0)}$ animals when compared to respective control mice, activation of Akt

by CUL7 depletion under conditions of increased afterload may have executed a protective effect on cardiomyocytes resulting in reduced cardiomyocyte loss and apoptosis, finally leading to attenuated reparative cardiac fibrosis and remodeling.

CUL7 depletion protects NRCMs against pathological hypertrophy induced by PE in vitro.

To further investigate the impact of CUL7 depletion in cardiomyocytes on the hypertrophic response in vitro, we transfected isolated neonatal rat cardiomyocytes with a pool of siRNA directed against *Cul7*. After 48 hours, cells were stimulated with 50 mM (R)-(-)-phenylephrine hydrochloride (PE), fixed with PFA and stained using an antibody directed against α-actinin and DAPI as described above, followed by analysis of the positive stained area. Treatment of PE-induced an increase in cellular area in mock-, scramble- and siRNA-treated cells, which was highly significant when compared to cells under basal conditions in all three groups. Interestingly, neonatal rat cardiomyocytes (NRCMs) depleted of CUL7 showed an attenuation of cellular hypertrophy when compared to cells treated with negative scramble control. This effect could be mediated via the activation of the class I A PI3K downstream pathway, having its origin at IRS-1 dependent receptor tyrosine kinases, e.g. IGF-1 or insulin. Class I A PI3K subtypes (PI3Kα, PI3Kβ and PI3Kδ) have been shown to play a key role in physiological cardiac growth, as overexpression of the IGF1 receptor in the heart resulted in physiological hypertrophy, an effect that could be further enhanced by exercise stimuli (McMullen et al. 2004). Furthermore, co-expression of a dominant negative PI3Kα mutant (the cardio- dominant class I A PI3K subtype) attenuated physiological hypertrophy (McMullen et al. 2004). Most notably, overexpression of IGF1R, thereby increasing class I A PI3K signaling, blunted pathological hypertrophy (McMullen et al. 2004). On the other hand, class I B PI3K has been shown to be involved in the development of pathological hypertrophy and to be activated via the Gβγ subunit of G-protein coupled receptors, that are pivotal players of hypertrophic response in the heart and are activated by agents as α-receptor agonists, β-receptor agonists, Angiotensin II and Endothelin-1 (Oudit et al. 2009). There are randomized trials and meta-analysis suggesting a benefit from exercise training leading to physiological cardiac growth via the class I A PI3K pathway under conditions of impaired heart function resulting in reduced hospitalization due to heart failure and reduced mortality (O'Connor et al. 2009, Davies et al. 2010). In addition to that, Yang et al showed that oligodeoxynucleotides containing CpG motifs (CpG-ODN) were able

to counteract the development of pathological hypertrophy and improve cardiac function by activation of the class I A PI3K pathway. They demonstrated that activation of the PI3Kα pathway via treatment with CpG-ODN C274 resulted in an attenuation of cellular hypertrophy of NRCMs under the pro-hypertrophic stimulation with isoproterenol and silencing of PI3Kα via siRNA was able to abrogate this effect. Additionally, they showed that treatment of mice with C274 was able to attenuate the pathological effects of isoproterenol treatment in vivo, with improved cardiac function, reduced pathological hypertrophy and fetal gene expression, alongside with increased Akt phosphorylation and reduced fibrosis of the ventricle due to less reparative remodeling (Yang et al. 2013). These findings are in considerable concordance with our observations of reduced cellular hypertrophy of CUL7 depleted NRCMs after stimulation of PE and further support the moderating beneficial effect of cardiomyocyte-specific CUL7 depletion on cardiac fibrosis under conditions of increased afterload in vivo, both mediated via activation of protective class I A PI3K signaling.

8. Figure legend

Figure 28: Left ventricular end-systolic inner diameter (LVID, systolic) under conditions of increased afterload.

Figure 29: Left ventricular fibrosis under conditions of increased afterload.

Figure 30: Cross sectional area under conditions of increased afterload.

Figure 31: Cardiomyocyte hypertrophy under phenylephrine stimulation.

9. Item list

Items and chemicals referred to in the method section if not indicated differently.

(R)-(-)-Phenylephrine hydrochloride (Sigma, Cat. No. P6126)

1.5 ml Micro Tubes (Sarstedt, Ref. 72.706.400)

100 μm Cell Strainer (BD falcon, 100 μm pore size)

24 x 50 mm coverslip (Roth, Cat. No. 1871)

30% Acrylamid + 0.8 Bis (Bio Rad, Ref. No. 1610156)

4',6-diamindino-2-phenylindole dihydrochloride (DAPI) (Sigma, Cat. No. D9542)

5 X siRNA Buffer (Thermo Scientific, Cat. No. B-002000-UB-100)

96 well plate (IBDI, Cat. No. 89606)

Acetic Acid 100 % (Roth, Serial No. 6755.2)

Agarose (Roth, Serial no. 3810.3)

Anti-alpha-actinin antibody (Sigma, Cat. No. A7811, Clone EA-53)

Antipain Dihydrochlorid (Roth, Serial No. 2933.1)

APS Ammoniumperoxodisulfat (Roth, Serial No. 9592.3)

Aquatex (Merck, Cat. No. 1.08562.0050)

BDM (500 mM) (Sigma, Cat. No. B0753)

Benzonase® Nuclease (Sigma, Serial No. E1014-5KU)

Bio-Rad Protein Assay Dye Reagent Concentrate (BIO RAD, Bio-Rad Cat.No. 500-0006)

Bluing Reagent (ThermoScientific, Cat. No. 7301)

BrdU (Sigma, Cat. No. B5002-1G)

Bromophenol Blue Sodium Salt (Roth, Serial No. A512.1)

BSA (AppliChem, Cat.No. A6588.0100)

CaCl2 (Sigma, Ref. No. 449709-10G)

Cell Scraper 2-Posit. Blade 25 (Sarstedt, Ref. 83.1830)

Cell Strainer Falcon® 100µm (Corning, Ref. No. 352360)

Cell Strainer filter 0.22 µm pore (Corning, Cat. No. 430624)

Cell Strainer with 40 µm pores (BD, Cat. No. 352340)

Clarifier 2 (ThermoScientific, Cat. No. 7402)

Collagenase Type 2 (280 U/mg) (Worthington, Ref. No. LS004174)

CryoPure Tube 1.8ml (Sarstedt, Ref. 72.379)

Deoxynucleoside Triphosphate Set (Sigma, Cat. No. 000000011969064001)

DEPEX (Serva, Cat. No. 18243)

DeVisionG 2.0 software program (Decon Science Tec GmbH)

Difco Trypsin 250 (BD, Cat. No. 212540-100G)

Direct Red 80 (Sigma, Cat. No. 365548-5G)

DNase (Sigma, Cat. No. DN-25-100MG)

DTT (Roth, Serial No. 6908.3)

EDTA (Roth, Serial No. 8043.4)

EGTA (Roth, Serial No. 3054.1)

Electrophoresis power supply EPS-301 (GE Healthcare Life Science, Serial no. 18-1130-01)

Eosin Y Solution aqueous (Sigma, Cat. No. HT110216-500ml)

Eppendorf centrifuge 5417R (Eppendorf AG, Serial no. 5407YJ028399)

Erlenmeyer flask (Fisherbrand, Serial no. FB 33132)

Ethanol ≥99.5 %, Ph.Eur (Roth, Serial no. 5054.5)

Ethidiumbromid (Roth, Serial No. 2218.1)

Fast Green FCF (Sigma, Cat. No. F7252-5G)

FastStart SYBR Green Master (Roche, Cat. No. 04913922001)

FCS (PAN Biotech, Cat. No. 3302-P282905)

Fujifilm LAS 4000 multipurpose CCD camera system (GE Healthcare Life sciences, Product code: 28-9558-10)

Gel comb 14 well 1.0mm (PeqLab, Serial no. 40-0911-14C)

Gel tray Mini M (PeqLab, Serial No 40-0911-UVT)

Gibco™ DPBS, no calcium, no magnesium (life technologies, Serial No. 14190-144)

Glucose (Merck, Cat. No. 8342)

Glucose 5 % (Sigma, Cat. No. G7528)

Glycerol ROTIPURAN® ≥99.5 % (Roth, Serial No. 3783.4)

Glycin (Roth, Cat. No. 200-272-2)

Goat anti-mouse IgG (H+L), Alexa 488 (Invitrogen, Cat. No. A11029)

HCl 37% (Roth, Serial No. 4625.2)

Hematoxylin 2 solution (ThermoScientific, Cat. No. 7231)

HEPES (AppliChem, Cat. No. A1069,1000)

Hepes Buffer 1 M (Sigma, Cat. No. H0887)

Isopropanol (Roth, Cat. No. 200-272-27343.2)

KCl (Sigma, Cat. No. P4504)

KH_2PO_4 (Sigma, Cat. No. P5379)

$KHCO_3$ (Sigma, Cat. No. P9144)

Laminin (BD Bioscience, Cat. No. 354232, 1mg)

Leupeptin Hemisulfat (Roth, Serial No. CN33.1)

L-Glutamine (200 mM) (Pan Biotech, Cat. No. P04-80100)

Lipofectamine 2000 (Invitrogen, Cat. No. 11668-027)

MEM (Gibco, Cat. No. 21575)

Methanol (Sigma, Serial No. 322415-18L)

$MgSO_4$ x $7H_2O$ (Sigma, Cat. No. M9397)

MicroAmp® Fast 96-Well Reaction Plate (applied biosystems, life technologies, Prod. No. 4346907)

Microwave (Panasonic, Serial no. NN-E245W)

Miglyol® 812 (Caesar & Loretz GmbH, Cat. No. 3274-250 ml)

Mini-PROTEAN® Tetra Cell (Bio Rad, Ref No. 1658001)

Mini-PROTEAN® Tetra Cell Casting Stand (BIO RAD, Ref. No. 1658050)

Mouth pipette (BD, Cat. No. 357550)

MultiGauge Software (Fujifilm)

Na_2HPO_4 (Sigma, Cat. No. S0876)

Na_2HPO_4 x $7H_2O$ (Merck, Cat. No. K33946475716)

Na_3VO_4 (Sigma, Cat. No. 450243)

NaCl (Sigma, Cat. No. S9625)

$NaHCO_3$ (Sigma, Cat. No. S5761)

Omifix-F1 1ml syringe (Braun, Cat. No. 9161406)

Omnifix® F Solo (Braun, Cat. No. 9161406V)

ON-TARGET plus Non-targeting Pool (Thermo Scientific, Cat. No. D-001810-10-20)

ON-TARGET plus SMART pool (Thermo Scientific, Cat. No. L-05471-01-0005)

Optical adhesive Covers (applied biosystems, Prod. No. 4360954)

OptiMEM I serum reduced medium (Invitrogen, Cat. No. 31985-047)

PAN Trypsin (PAN, Cat. No. P10-025025P)

Pap Pen (Sigma, Cat. No. Z377821-1EA)

PBS (PAN Biotech, Cat. No. P04-36500)

Penicillin/Streptomycin (Pan Biotech, Cat. No. P06-07100)

peqGOLD TriFast Reagent (PEQLAB, Prod. No. 30-2020)

Perfusion system (Julabo, type 13, pump type EC-BRÜ-PU; Amersham Bioscience, type P1)

Phenol Red (Sigma, Cat. No. P5530)

Pierce ® ECL 2 Western Blotting Substrate (Thermo Scientific, Prod 80196)

Piric acid-saturated solution 1.3 % (Sigma, Cat. No. P6744-1GA)

PMSF (Roth, Serial No. 6367.1)

Polylysin (Sigma, Cat. No. P6407-5MG)

Precision Plus Protein™ Standards (BIO RAD, Cat. No.: 161-0373)

Prot/Elec Tips (Bio Rad, Ref No 2239915)

Proteinase K 10mg/ml (AppliChem, A3830,0100)

PUFFERAN® ≥99 % TRIS Hydrochlorid (Roth, Serial No. 9090.4)

PVDF Immobilon® Transfer Membranes Immobilon®-P (Millipore, Cat. No.: IPVH00010)

Quick-Load® 100 bp DNA ladder (New England Biolabs GmbH, Serial no. NEB #N3270)

RNase free H_2O (Dharmacon. GE lifesciences, Ref. No. B-003000-WB-100)

RNase free water (life technologies, Gibco, Cat. No. 10977-035)

RNaseOUT™ Ribonuclease Inhibitor (lifetechnologies, Ref. No. 10777-019)

Roti® Phenol/Chloroform/Isoamyl alcohol, (Roth, Serial no. A156.2

SafeSeal Micro tube 2 ml (Sarstedt, Ref. 72.695.400)

SafeSeal tube 0.5ml (Sarsted, Cat. No. 72.704)

SDS (Roth, Serial No. CN30.3)

Sealing tape (Sarstedt Cat.-no. 95.1995)

Sterican® Insulin G 26 x 1/2" / ø 0.45 x 12 mm cannula (Braun, Cat. No. 4665457)

SuperScript® II Reverse Transcriptase (lifetechnologies, Ref. No. 18064-022)

SYTOX® Green dye (Life Technologies / Molecular Probes, Cat. No. S7020)

Tamoxifen (Sigma, Cat. No. T5648-1G)

Taq Buffer (GenScript, Cat. No. B0005)

Taq DNA Polymerase (Genscript, Cat no. E00007)

Taurine (Sigma, Cat. No. T0625)

TEMED (BIO RAD, Bio-Rad Cat.No.1610801)

Thermomixer compact" (Eppendorf AG, Serial no. 5350YI832147)

Tri Sodium citrate (dihydrate) (Roth, Cat. No. 3580.1)

Triton™ X-100 (Sigma, Serial No. T8787-50ML)

Trypan Blue (AppliChem, Cat. No. A0668,0025)

Tube 15ml, 120x17mm, PP (Sarstedt, Ref. 62.554.001)

Tube 50ml, 114x28mm, PP (Sarstedt, Ref. 62.548.004)

Tween 20 (AppliChem, Cat. No. A4974,0250)

TWEEN® (Roth, Serial No. 9127.1)

UV transilluminator MD-25/HD-25 (Wealtec, serial no. 1142003)

Vevo 770 ultrasonic machine (VisualSonics FUJIFILM)

Vitamin B12 (Sigma, Cat. No. V-2876-100MG)

WGA, Alexa Fluor® 647 conjugate (Life Technologies / Molecular Probes, Cat. No. W32466)

Xylol (Roth, Cat. No. 9713.3)

10. Acknowledgments

First of all, I want to thank Prof. Dr. Dr. Stefan Engelhardt for giving me the opportunity to graduate at the IPT and for learning basic science techniques as well as developing as a researcher.

Next, I want to thank PD Dr. Antonio Sarikas for mentoring my work and accompanying me along the way of this dissertation at all times.

Additionally, I want to thank Kathleen Meyer, Melanie Anger and Dr. Thomas Hartmann for great teamwork within our research group.

I also want to express my special gratitude to my all my colleagues within the institution for building a great team and helping each other at any time and topic.

Furthermore, I want to thank Kornelija Sakac for performing mouse surgery and echocardiography.

Additionally, I thank Sabine Brummer, Lucia Koblitz and Urszula Kremser for assistance with cell culture and histopathological experiments.

I also want to thank Dr. Katrin Domes for providing Myh6-MerCreMerTg$^{(1/0)}$ mice and assistance with crossing of the mice.

Furthermore, I want to thank Prof. Dr. James DeCaprio and coworkers for providing Cullin7$^{flox/flox}$ mice.

In addition to that, I want to thank Dr. Vanessa Philippi for critical prove of animal experiments and handling.

Next, I want to thank Mehmet Durmaz and Selahattin Sahiner for assistance with mouse breeding and keeping.

Last but not least, I want to express my gratitude to my family and friends without whose support this work would have been impossible.

11. References

Acosta, J. C., A. Banito, T. Wuestefeld, A. Georgilis, P. Janich, J. P. Morton, D. Athineos, T. W. Kang, F. Lasitschka, M. Andrulis, G. Pascual, K. J. Morris, S. Khan, H. Jin, G. Dharmalingam, A. P. Snijders, T. Carroll, D. Capper, C. Pritchard, G. J. Inman, T. Longerich, O. J. Sansom, S. A. Benitah, L. Zender and J. Gil (2013). "A complex secretory program orchestrated by the inflammasome controls paracrine senescence." Nat Cell Biol **15**(8): 978-990.

Ali, S. H., J. S. Kasper, T. Arai and J. A. DeCaprio (2004). "Cul7/p185/p193 Binding to Simian Virus 40 Large T Antigen Has a Role in Cellular Transformation." Journal of Virology **78**(6): 2749-2757.

Antos, C. L., T. A. McKinsey, N. Frey, W. Kutschke, J. McAnally, J. M. Shelton, J. A. Richardson, J. A. Hill and E. N. Olson (2002). "Activated glycogen synthase-3 beta suppresses cardiac hypertrophy in vivo." Proc Natl Acad Sci U S A **99**(2): 907-912.

Arai, T., J. S. Kasper, J. R. Skaar, S. H. Ali, C. Takahashi and J. A. DeCaprio (2003). "Targeted disruption of p185/Cul7 gene results in abnormal vascular morphogenesis." Proc Natl Acad Sci U S A **100**(17): 9855-9860.

Backs, J., T. Backs, S. Neef, M. M. Kreusser, L. H. Lehmann, D. M. Patrick, C. E. Grueter, X. Qi, J. A. Richardson, J. A. Hill, H. A. Katus, R. Bassel-Duby, L. S. Maier and E. N. Olson (2009). "The delta isoform of CaM kinase II is required for pathological cardiac hypertrophy and remodeling after pressure overload." Proc Natl Acad Sci U S A **106**(7): 2342-2347.

Bassermann, F., R. Eichner and M. Pagano (2014). "The ubiquitin proteasome system - implications for cell cycle control and the targeted treatment of cancer." Biochim Biophys Acta **1843**(1): 150-162.

Belke, D. D., S. Betuing, M. J. Tuttle, C. Graveleau, M. E. Young, M. Pham, D. Zhang, R. C. Cooksey, D. A. McClain, S. E. Litwin, H. Taegtmeyer, D. Severson, C. R. Kahn and E. D. Abel (2002). "Insulin signaling coordinately regulates cardiac size, metabolism, and contractile protein isoform expression." J Clin Invest **109**(5): 629-639.

Bhattacharyya, S., H. Yu, C. Mim and A. Matouschek (2014). "Regulated protein turnover: snapshots of the proteasome in action." Nat Rev Mol Cell Biol **15**(2): 122-133.

Bourajjaj, M., A. S. Armand, P. A. da Costa Martins, B. Weijts, R. van der Nagel, S. Heeneman, X. H. Wehrens and L. J. De Windt (2008). "NFATc2 is a necessary mediator of calcineurin-dependent cardiac hypertrophy and heart failure." J Biol Chem **283**(32): 22295-22303.

Brouillard, P., L. M. Boon, J. B. Mulliken, O. Enjolras, M. Ghassibe, M. L. Warman, O. T. Tan, B. R. Olsen and M. Vikkula (2002). "Mutations in a novel factor, glomulin, are responsible for glomuvenous malformations ("glomangiomas")." Am J Hum Genet **70**(4): 866-874.

Bueno, O. F., L. J. De Windt, K. M. Tymitz, S. A. Witt, T. R. Kimball, R. Klevitsky, T. E. Hewett, S. P. Jones, D. J. Lefer, C. F. Peng, R. N. Kitsis and J. D. Molkentin (2000). "The MEK1-ERK1/2 signaling pathway promotes compensated cardiac hypertrophy in transgenic mice." EMBO J **19**(23): 6341-6350.

Bueno, O. F., B. J. Wilkins, K. M. Tymitz, B. J. Glascock, T. F. Kimball, J. N. Lorenz and J. D. Molkentin (2002). "Impaired cardiac hypertrophic response in Calcineurin Abeta -deficient mice." Proc Natl Acad Sci U S A **99**(7): 4586-4591.

Davies, E. J., T. Moxham, K. Rees, S. Singh, A. J. Coats, S. Ebrahim, F. Lough and R. S. Taylor (2010). "Exercise training for systolic heart failure: Cochrane systematic review and meta-analysis." Eur J Heart Fail **12**(7): 706-715.

DeBosch, B., I. Treskov, T. S. Lupu, C. Weinheimer, A. Kovacs, M. Courtois and A. J. Muslin (2006). "Akt1 is required for physiological cardiac growth." Circulation **113**(17): 2097-2104.

Delaughter, M. C., G. E. Taffet, M. L. Fiorotto, M. L. Entman and R. J. Schwartz (1999). "Local insulin-like growth factor I expression induces physiologic, then pathologic, cardiac hypertrophy in transgenic mice." FASEB J **13**(14): 1923-1929.

Dias, D. C., G. Dolios, R. Wang and Z. Q. Pan (2002). "CUL7: A DOC domain-containing cullin selectively binds Skp1.Fbx29 to form an SCF-like complex." Proc Natl Acad Sci U S A **99**(26): 16601-16606.

Dorn, G. W., 2nd and T. Force (2005). "Protein kinase cascades in the regulation of cardiac hypertrophy." J Clin Invest **115**(3): 527-537.

Glennon, P. E., S. Kaddoura, E. M. Sale, G. J. Sale, S. J. Fuller and P. H. Sugden (1996). "Depletion of Mitogen-Activated Protein Kinase Using an Antisense Oligodeoxynucleotide Approach Downregulates the Phenylephrine-Induced Hypertrophic Response in Rat Cardiac Myocytes." Circulation Research **78**(6): 954-961.

Hall, M. E., G. Smith, J. E. Hall and D. E. Stec (2011). "Systolic dysfunction in cardiac-specific ligand-inducible MerCreMer transgenic mice." Am J Physiol Heart Circ Physiol **301**(1): H253-260.

Haq, S., G. Choukroun, Z. B. Kang, H. Ranu, T. Matsui, A. Rosenzweig, J. D. Molkentin, A. Alessandrini, J. Woodgett, R. Hajjar, A. Michael and T. Force (2000). "Glycogen Synthase Kinase-3β Is a Negative Regulator of Cardiomyocyte Hypertrophy." The Journal of Cell Biology **151**(1): 117-130.

Harrington, L. S., G. M. Findlay and R. F. Lamb (2005). "Restraining PI3K: mTOR signalling goes back to the membrane." Trends Biochem Sci **30**(1): 35-42.

Hassink, R. J., H. Nakajima, H. O. Nakajima, P. A. Doevendans and L. J. Field (2009). "Expression of a transgene encoding mutant p193/CUL7 preserves cardiac function and limits infarct expansion after myocardial infarction." Heart **95**(14): 1159-1164.

Heineke, J. and J. D. Molkentin (2006). "Regulation of cardiac hypertrophy by intracellular signalling pathways." Nat Rev Mol Cell Biol **7**(8): 589-600.

Hershko, A. and A. Ciechanover (1998). "The ubiquitin system." Annu Rev Biochem **67**: 425-479.

Hu, P., D. Zhang, L. Swenson, G. Chakrabarti, E. D. Abel and S. E. Litwin (2003). "Minimally invasive aortic banding in mice: effects of altered cardiomyocyte insulin signaling during pressure overload." Am J Physiol Heart Circ Physiol **285**(3): H1261-1269.

Huber, C., D. Dias-Santagata, A. Glaser, J. O'Sullivan, R. Brauner, K. Wu, X. Xu, K. Pearce, R. Wang, M. L. Uzielli, N. Dagoneau, W. Chemaitilly, A. Superti-Furga, H. Dos Santos, A. Megarbane, G. Morin, G. Gillessen-Kaesbach, R. Hennekam, I. Van der Burgt, G. C. Black, P. E. Clayton, A. Read, M. Le Merrer, P. J. Scambler, A. Munnich, Z. Q. Pan, R. Winter and V. Cormier-Daire (2005). "Identification of mutations in CUL7 in 3-M syndrome." Nat Genet **37**(10): 1119-1124.

Kaustov, L., J. Lukin, A. Lemak, S. Duan, M. Ho, R. Doherty, L. Z. Penn and C. H. Arrowsmith (2007). "The conserved CPH domains of Cul7 and PARC are protein-protein interaction modules that bind the tetramerization domain of p53." J Biol Chem **282**(15): 11300-11307.

Kim, J., A. R. Wende, S. Sena, H. A. Theobald, J. Soto, C. Sloan, B. E. Wayment, S. E. Litwin, M. Holzenberger, D. LeRoith and E. D. Abel (2008). "Insulin-like growth factor I receptor signaling is required for exercise-induced cardiac hypertrophy." Mol Endocrinol **22**(11): 2531-2543.

Kong, C., D. Samovski, P. Srikanth, M. J. Wainszelbaum, A. J. Charron, J. Liu, J. J. Lange, P. I. Chen, Z. Q. Pan, X. Su and P. D. Stahl (2012). "Ubiquitination and degradation of the hominoid-specific oncoprotein TBC1D3 is mediated by CUL7 E3 ligase." PLoS One **7**(9): e46485.

Lexow, J., T. Poggioli, P. Sarathchandra, M. P. Santini and N. Rosenthal (2013). "Cardiac fibrosis in mice expressing an inducible myocardial-specific Cre driver." Dis Model Mech **6**(6): 1470-1476.

Lu, Z., Y. P. Jiang, W. Wang, X. H. Xu, R. T. Mathias, E. Entcheva, L. M. Ballou, I. S. Cohen and R. Z. Lin (2009). "Loss of cardiac phosphoinositide 3-kinase p110 alpha results in contractile dysfunction." Circulation **120**(4): 318-325.

Luo, J., J. R. McMullen, C. L. Sobkiw, L. Zhang, A. L. Dorfman, M. C. Sherwood, M. N. Logsdon, J. W. Horner, R. A. DePinho, S. Izumo and L. C. Cantley (2005). "Class IA phosphoinositide 3-kinase regulates heart size and physiological cardiac hypertrophy." Mol Cell Biol **25**(21): 9491-9502.

McMullen, J. R., T. Shioi, W. Y. Huang, L. Zhang, O. Tarnavski, E. Bisping, M. Schinke, S. Kong, M. C. Sherwood, J. Brown, L. Riggi, P. M. Kang and S. Izumo (2004). "The insulin-like growth factor 1 receptor induces physiological heart growth via the phosphoinositide 3-kinase(p110alpha) pathway." J Biol Chem **279**(6): 4782-4793.

McMullen, J. R., T. Shioi, L. Zhang, O. Tarnavski, M. C. Sherwood, P. M. Kang and S. Izumo (2003). "Phosphoinositide 3-kinase(p110alpha) plays a critical role for the induction of physiological, but not pathological, cardiac hypertrophy." Proc Natl Acad Sci U S A **100**(21): 12355-12360.

Meyer, K., B. Hodwin, D. Ramanujam, S. Engelhardt and A. Sarikas (2016). "Essential Role for Premature Senescence of Myofibroblasts in Myocardial Fibrosis." J Am Coll Cardiol **67**(17): 2018-2028.

Mieulet, V. and R. F. Lamb (2008). "Shooting the messenger: CULLIN' insulin signaling with Fbw8." Dev Cell **14**(6): 816-817.

Molkentin, J. D., J. R. Lu, C. L. Antos, B. Markham, J. Richardson, J. Robbins, S. R. Grant and E. N. Olson (1998). "A calcineurin-dependent transcriptional pathway for cardiac hypertrophy." Cell **93**(2): 215-228.

Nakajima, H., H. O. Nakajima, S. C. Tsai and L. J. Field (2004). "Expression of mutant p193 and p53 permits cardiomyocyte cell cycle reentry after myocardial infarction in transgenic mice." Circ Res **94**(12): 1606-1614.

Nicol, R. L., N. Frey, G. Pearson, M. Cobb, J. Richardson and E. N. Olson (2001). "Activated MEK5 induces serial assembly of sarcomeres and eccentric cardiac hypertrophy." EMBO J **20**(11): 2757-2767.

O'Connor, C. M., D. J. Whellan, K. L. Lee, S. J. Keteyian, L. S. Cooper, S. J. Ellis, E. S. Leifer, W. E. Kraus, D. W. Kitzman, J. A. Blumenthal, D. S. Rendall, N. H. Miller, J. L. Fleg, K. A. Schulman, R. S. McKelvie, F. Zannad, I. L. Pina and H.-A. Investigators (2009). "Efficacy and safety of exercise training in patients with chronic heart failure: HF-ACTION randomized controlled trial." JAMA **301**(14): 1439-1450.

Okazaki, N. (2004). "Prediction of the Coding Sequences of Mouse Homologues of KIAA Gene: IV. The Complete Nucleotide Sequences of 500 Mouse KIAA-homologous cDNAs Identified by Screening of Terminal Sequences of cDNA Clones Randomly Sampled from Size-Fractionated Libraries." DNA Research **11**(3): 205-218.

Oudit, G. Y. and J. M. Penninger (2009). "Cardiac regulation by phosphoinositide 3-kinases and PTEN." Cardiovasc Res **82**(2): 250-260.

Oudit, G. Y., H. Sun, B. G. Kerfant, M. A. Crackower, J. M. Penninger and P. H. Backx (2004). "The role of phosphoinositide-3 kinase and PTEN in cardiovascular physiology and disease." J Mol Cell Cardiol **37**(2): 449-471.

Paradis, V., M. Albuquerque, M. Mebarki, L. Hernandez, S. Zalinski, S. Quentin, J. Belghiti, J. Soulier and P. Bedossa (2013). "Cullin7: a new gene involved in liver carcinogenesis related to metabolic syndrome." Gut **62**(6): 911-919.

Pasumarthi, K. B. S., S. C. Tsai and L. J. Field (2001). "Coexpression of Mutant p53 and p193 Renders Embryonic Stem Cell-Derived Cardiomyocytes Responsive to the Growth-Promoting Activities of Adenoviral E1A." Circulation Research **88**(10): 1004-1011.

Patrick, G. N., B. Bingol, H. A. Weld and E. M. Schuman (2003). "Ubiquitin-Mediated Proteasome Activity Is Required for Agonist-Induced Endocytosis of GluRs." Current Biology **13**(23): 2073-2081.

Predmore, J. M., P. Wang, F. Davis, S. Bartolone, M. V. Westfall, D. B. Dyke, F. Pagani, S. R. Powell and S. M. Day (2010). "Ubiquitin proteasome dysfunction in human hypertrophic and dilated cardiomyopathies." Circulation **121**(8): 997-1004.

Reiss, K., W. Cheng, A. Ferber, J. Kajstura, P. Li, B. S. Li, G. Olivetti, C. J. Homcy, R. Baserga and P. Anversa (1996). "Overexpression of insulin-like growth factor-1 in the heart is coupled with myocyte proliferation in transgenic mice." Proceedings of the National Academy of Sciences of the United States of America **93**(16): 8630-8635.

Sarikas, A., L. Carrier, C. Schenke, D. Doll, J. Flavigny, K. S. Lindenberg, T. Eschenhagen and O. Zolk (2005). "Impairment of the ubiquitin-proteasome system by truncated cardiac myosin binding protein C mutants." Cardiovasc Res **66**(1): 33-44.

Sarikas, A., T. Hartmann and Z. Q. Pan (2011). "The cullin protein family." Genome Biol **12**(4): 220.

Sarikas, A., X. Xu, L. J. Field and Z. Q. Pan (2008). "The cullin7 E3 ubiquitin ligase: a novel player in growth control." Cell Cycle **7**(20): 3154-3161.

Scheufele, F., B. Wolf, M. Kruse, T. Hartmann, J. Lempart, S. Muehlich, A. F. Pfeiffer, L. J. Field, M. J. Charron, Z. Q. Pan, S. Engelhardt and A. Sarikas (2014). "Evidence for a regulatory role of Cullin-RING E3 ubiquitin ligase 7 in insulin signaling." Cell Signal **26**(2): 233-239.

Schlossarek, S., G. Mearini and L. Carrier (2011). "Cardiac myosin-binding protein C in hypertrophic cardiomyopathy: mechanisms and therapeutic opportunities." J Mol Cell Cardiol **50**(4): 613-620.

Shaul, Y. D. and R. Seger (2007). "The MEK/ERK cascade: from signaling specificity to diverse functions." Biochim Biophys Acta **1773**(8): 1213-1226.

Shioi, T., P. M. Kang, P. S. Douglas, J. Hampe, C. M. Yballe, J. Lawitts, L. C. Cantley and S. Izumo (2000). "The conserved phosphoinositide 3-kinase pathway determines heart size in mice." EMBO J **19**(11): 2537-2548.

Shioi, T., J. R. McMullen, P. M. Kang, P. S. Douglas, T. Obata, T. F. Franke, L. C. Cantley and S. Izumo (2002). "Akt/protein kinase B promotes organ growth in transgenic mice." Mol Cell Biol **22**(8): 2799-2809.

Shiojima, I. and K. Walsh (2006). "Regulation of cardiac growth and coronary angiogenesis by the Akt/PKB signaling pathway." Genes Dev **20**(24): 3347-3365.

Skaar, J. R., L. Florens, T. Tsutsumi, T. Arai, A. Tron, S. K. Swanson, M. P. Washburn and J. A. DeCaprio (2007). "PARC and CUL7 form atypical cullin RING ligase complexes." Cancer Res **67**(5): 2006-2014.

Skurk, C., Y. Izumiya, H. Maatz, P. Razeghi, I. Shiojima, M. Sandri, K. Sato, L. Zeng, S. Schiekofer, D. Pimentel, S. Lecker, H. Taegtmeyer, A. L. Goldberg and K. Walsh (2005). "The FOXO3a transcription factor regulates cardiac myocyte size downstream of AKT signaling." J Biol Chem **280**(21): 20814-20823.

Sutton, J. and L. Lazarus (1976). "Growth hormone in exercise: comparison of physiological and pharmacological stimuli." J Appl Physiol **41**(4): 523-527.

Tsutsumi, T., H. Kuwabara, T. Arai, Y. Xiao and J. A. Decaprio (2008). "Disruption of the Fbxw8 gene results in pre- and postnatal growth retardation in mice." Mol Cell Biol **28**(2): 743-751.

van Berlo, J. H., M. Maillet and J. D. Molkentin (2013). "Signaling effectors underlying pathologic growth and remodeling of the heart." J Clin Invest **123**(1): 37-45.

Wainszelbaum, M. J., J. Liu, C. Kong, P. Srikanth, D. Samovski, X. Su and P. D. Stahl (2012). "TBC1D3, a hominoid-specific gene, delays IRS-1 degradation and promotes insulin signaling by modulating p70 S6 kinase activity." PLoS One **7**(2): e31225.

Werfel, S., A. Jungmann, L. Lehmann, J. Ksienzyk, R. Bekeredjian, Z. Kaya, B. Leuchs, A. Nordheim, J. Backs, S. Engelhardt, H. A. Katus and O. J. Muller (2014). "Rapid and highly efficient inducible cardiac gene knockout in adult mice using AAV-mediated expression of Cre recombinase." Cardiovasc Res **104**(1): 15-23.

Wilkins, B. J., L. J. De Windt, O. F. Bueno, J. C. Braz, B. J. Glascock, T. F. Kimball and J. D. Molkentin (2002). "Targeted Disruption of NFATc3, but Not NFATc4, Reveals an Intrinsic Defect in Calcineurin-Mediated Cardiac Hypertrophic Growth." Molecular and Cellular Biology **22**(21): 7603-7613.

http://www.ensembl.org/. "Homo_sapiens." Retrieved 09.10.2014, 2014, from http://aug2014.archive.ensembl.org/Homo_sapiens/Transcript/Summary?db=core;g=ENSG00000044090;r=6:43037617-43053945;t=ENST00000265348.

Xu, X., A. Sarikas, D. C. Dias-Santagata, G. Dolios, P. J. Lafontant, S. C. Tsai, W. Zhu, H. Nakajima, H. O. Nakajima, L. J. Field, R. Wang and Z. Q. Pan (2008). "The CUL7 E3 ubiquitin ligase targets insulin receptor substrate 1 for ubiquitin-dependent degradation." Mol Cell **30**(4): 403-414.

Yang, L., X. Cai, J. Liu, Z. Jia, J. Jiao, J. Zhang, C. Li, J. Li and X. D. Tang (2013). "CpG-ODN attenuates pathological cardiac hypertrophy and heart failure by activation of PI3Kalpha-Akt signaling." PLoS One **8**(4): e62373.

Yue, T. L., J. L. Gu, C. Wang, A. D. Reith, J. C. Lee, R. C. Mirabile, R. Kreutz, Y. Wang, B. Maleeff, A. A. Parsons and E. H. Ohlstein (2000). "Extracellular signal-regulated kinase plays an essential role in hypertrophic agonists, endothelin-1 and phenylephrine-induced cardiomyocyte hypertrophy." J Biol Chem **275**(48): 37895-37901.

Zebrowska, A., Z. Gasior and J. Langfort (2009). "Serum IGF-I and hormonal responses to incremental exercise in athletes with and without left ventricular hypertrophy." Journal of Sports Science and Medicine **8**(1): 67-76.

Zong, C., A. V. Gomes, O. Drews, X. Li, G. W. Young, B. Berhane, X. Qiao, S. W. French, F. Bardag-Gorce and P. Ping (2006). "Regulation of murine cardiac 20S proteasomes: role of associating partners." Circ Res **99**(4): 372-380.